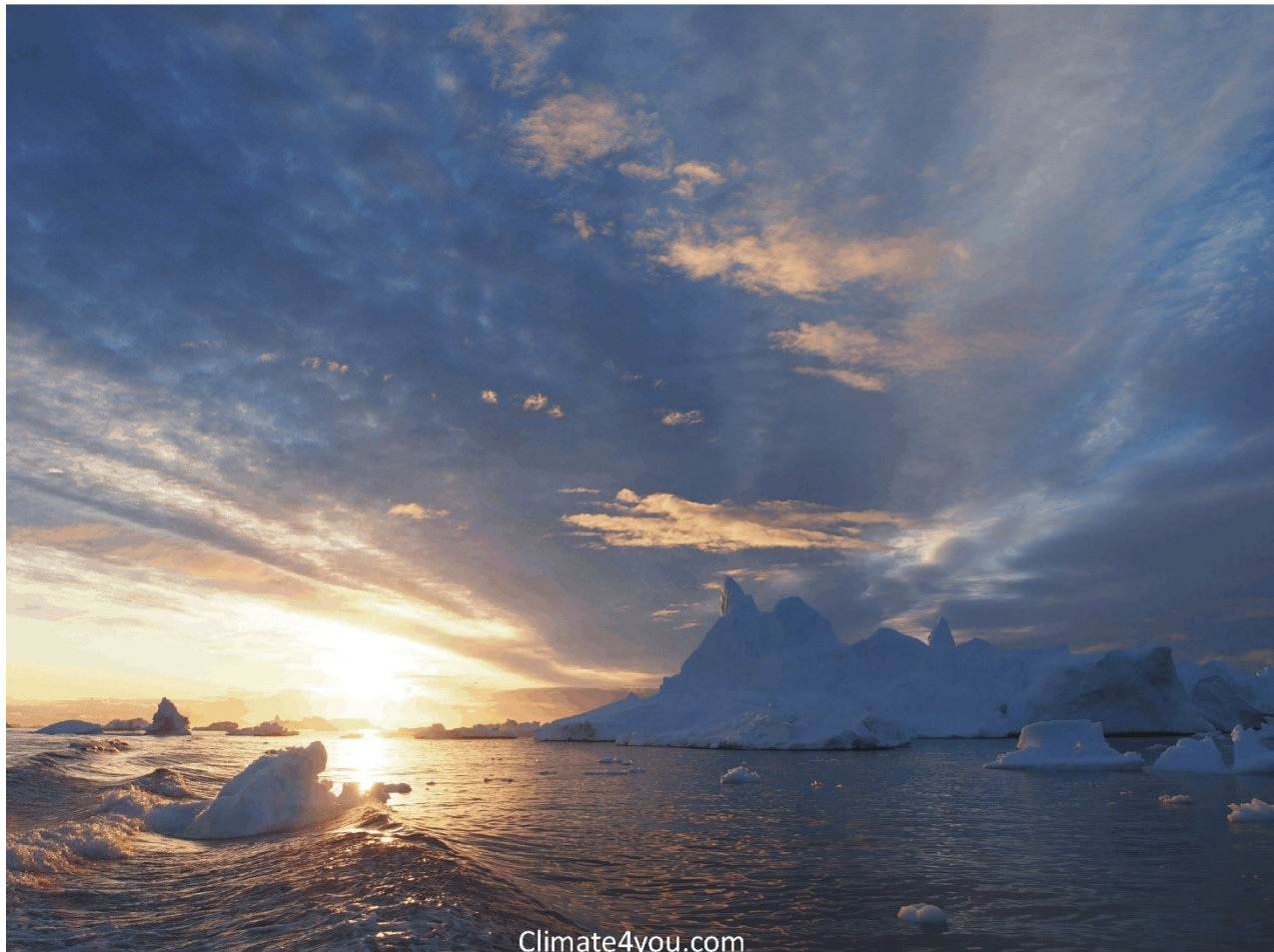


Climate4you update November 2023



1

Summary of observations until November 2023:

- 1: Observed average global air temperature change last 40 years is about $+0.166^{\circ}\text{C}$ per decade. If unchanged, additional average global air temperature increase by year 2100 will be about $+1.26^{\circ}\text{C}$. However, part of the apparent temperature increase reported is due to administrative changes, and the real future increase may therefore be smaller.
- 2: Tide gauges along coasts indicate a typical global sea level increase of about 1-2 mm/yr. Coastal sea level change rate last 100 year has essentially been stable, but with periodic variations. If unchanged, global sea level at coasts will typically increase 8-16 cm by year 2100, although many locations in regions affected by glaciation 20,000 years ago, will experience a relative sea level drop.
- 3: Since 2004 the global oceans above 1900 m depth on average have warmed about 0.07°C . The maximum warming (about 0.2°C , 0-100 m depth) mainly affects oceans near Equator, where the incoming solar radiation is at maximum.
- 4: Sources and sinks for CO_2 are many. However, changes in atmospheric CO_2 follow changes in global air temperature, and changes in global air temperature follow changes in ocean surface temperature.
- 5: There was no perceptible effect on atmospheric CO_2 due to the 2020-21 COVID-related drop in GHG emissions, underlining the fact that natural sinks and sources for atmospheric CO_2 far outweigh human contributions. Therefore, any future reductions in the use of fossil fuels are unlikely to have any significant effect on the amount of atmospheric CO_2 .

Contents:

- Page 3: November 2023 global surface air temperature overview
- Page 4: November 2023 global surface air temperature overview versus November last 10 years
- Page 5: November 2023 global surface air temperature compared to November 2022
- Page 6: Temperature quality class 1: Lower troposphere temperature from satellites
- Page 7: Temperature quality class 2: HadCRUT global surface air temperature
- Page 8: Temperature quality class 3: GISS and NCDC global surface air temperature
- Page 11: Comparing global surface air temperature and satellite-based temperatures
- Page 12: Global air temperature linear trends
- Page 13: Global temperatures: All in one, Quality Class 1, 2 and 3
- Page 15: Global sea surface temperature
- Page 18: Ocean temperature in uppermost 100 m
- Page 20: Pacific Decadal Oscillation (PDO)
- Page 21: North Atlantic heat content uppermost 700 m
- Page 22: North Atlantic temperatures 0-800 m depth along 59N, 30-0W
- Page 23: Global ocean temperature 0-1900 m depth summary
- Page 24: Global ocean net temperature change since 2004 at different depths
- Page 25: La Niña and El Niño episodes, Oceanic Niño Index
- Page 26: Zonal lower troposphere temperatures from satellites
- Page 27: Arctic and Antarctic lower troposphere temperatures from satellites
- Page 28: Arctic and Antarctic surface air temperatures
- Page 31: Long Arctic annual surface air temperature series
- Page 32: Long Antarctic annual surface air temperature series
- Page 33: Temperature over land versus over oceans
- Page 34: Troposphere and stratosphere temperatures from satellites
- Page 35: Sea ice; Arctic and Antarctic
- Page 39: Sea level in general
- Page 40: Global sea level from satellite altimetry
- Page 41: Global sea level from tide gauges (extended Holgate-9)
- Page 42: This month's selected sea level station (tide gauge) with long record
- Page 43: Snow cover; Northern Hemisphere weekly and seasonal
- Page 45: Greenland Ice Sheet net surface mass balance
- Page 46: Atmospheric specific humidity
- Page 47: Atmospheric CO₂
- Page 48: Relation between annual change of atm. CO₂ and La Niña and El Niño episodes
- Page 49: Phase relation between atmospheric CO₂ and global temperature
- Page 50: Global air temperature and atmospheric CO₂
- Page 54: Latest 20-year QC1 global monthly air temperature change
- Page 55: Sunspot activity and QC1 average satellite global air temperature
- Page 56: Sunspot activity and average neutron counts
- Page 57: Sunspot activity, ONI, and change rates of atmospheric CO₂ and specific humidity
- Page 58: Monthly lower troposphere temperature and global cloud cover
- Page 59: Climate and history: *Napoleon's retreat from Moscow 1812*

November 2023 global surface air temperature overview

General: This newsletter contains graphs and diagrams showing a selection of key meteorological variables, updated to the most recent past month, if possible. All temperatures are given in degrees Celsius.

Traditionally, a 30-year reference period is often used by various meteorological institutions for comparison purposes and are supposed to be updated through the end of each decade ending in zero (e.g., 1951-1980, 1961-1990, 1971-2000, etc.). The concept of a normal climate goes back to the first part of the 20th century. At that time, lasting to about 1960, it was generally believed that for all practical purpose's climate could be considered constant, no matter how obvious year-to-year fluctuations might have been. On this basis meteorologist decided to operate with an average or normal climate, defined by a 30-year period, called the normal period, assuming that it was of sufficient length to iron out all intervening variations. In fact, using a 30-yr 'normal' period is truly unfortunate, as observations clearly demonstrate that various global climate parameters (see, e.g., page 20) are influenced by periodic changes of 50-70 years duration. The frequently used 30-yr reference period is roughly half this time interval and is therefore highly unsuited as reference period. In the maps on page 4, showing the geographical pattern of surface air temperature anomalies, the last previous 10 years are therefore used as reference period. This decadal approach corresponds well to the typical memory horizon for many people and is also adopted as reference period by other institutions, e.g., the Danish Meteorological Institute (DMI).

In many diagrams shown in this newsletter the thin line represents the monthly global average value, and the thick line indicate a simple running 37-month average, nearly corresponding to a three-year average.

The year 1979 has been chosen as starting point in many diagrams, as this approximately corresponds to both the beginning of satellite observations and the onset of the late 20th century warming period. However, most of the data series have a longer record length, which may be inspected in greater detail on www.climate4you.com.

November 2023 surface air temperature

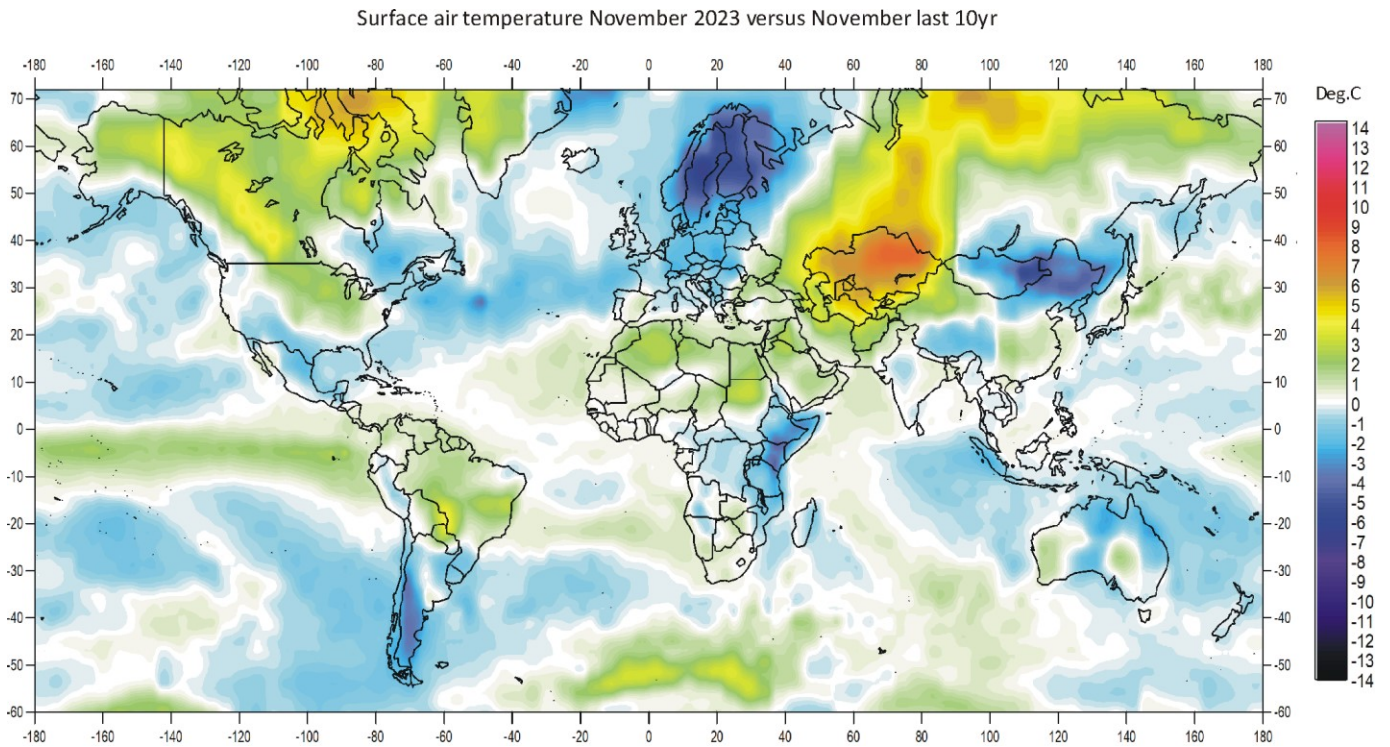
General: For November 2023, the GISS data portal provided AIRS interpolated surface air data, based on satellite observations. According to the GISS and NCDC records, the November global temperature was still high, much like the previous two months. The UAH and RSS lower troposphere satellite series also show the November 2023 temperature anomaly to be high, much like in the two previous months. The AIRS v6 November global average temperature anomaly compared to the last 10 years confirms the above impression (see, diagrams p.4-5). Relatively high temperatures in November were principally limited to Canada, Ukraine, Russia incl. Siberia, and the El Niño region in the Pacific. The atmosphere up to the tropopause has on average warmed (p.34), and much ocean heat released by the present El Niño is now being emitted to space.

The Northern Hemisphere surface temperature anomaly pattern (p.4) was characterised by strong regional contrasts, controlled by the dominant jet stream position. Especially Canada, Ukraine and Russia incl. Siberia were warm relative to the average for the last 10 years. In contrast, much of Europe and northern China were relatively cold. Ocean wise, the North Atlantic region, incl. the Norwegian Sea and the Greenland Sea, was cold. Also, most of the northern Pacific was relatively cold. PDO (p.20) remains negative. Arctic Ocean surface air temperatures were relatively low in the European sector, while the Canada sector was relatively warm.

Near the Equator temperatures were generally above the 10-year average. Especially the part of the Pacific Ocean affected by the ongoing warm El Niño episode display above average surface temperatures, as were also the case for parts of the Atlantic Ocean north of the Equator, especially west of Africa.

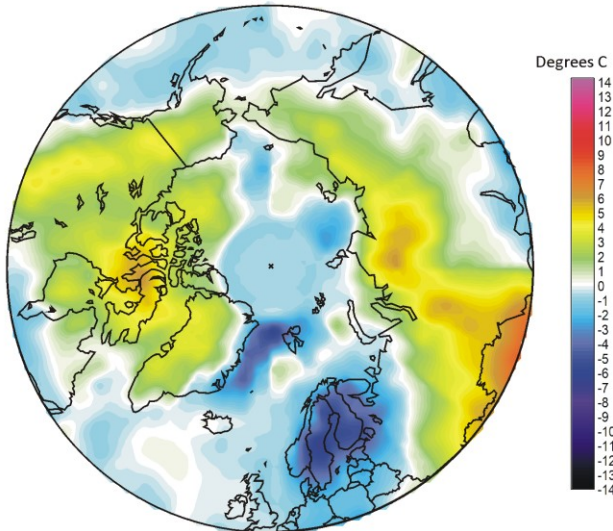
Southern Hemisphere temperatures were near or below the 10-yr average. Most of Australia and New Zealand was relatively cold, as were much of eastern Africa and South America. Finally, most of the Antarctic continent was relatively cold.

November 2023 global surface air temperature overview versus average November last 10 years

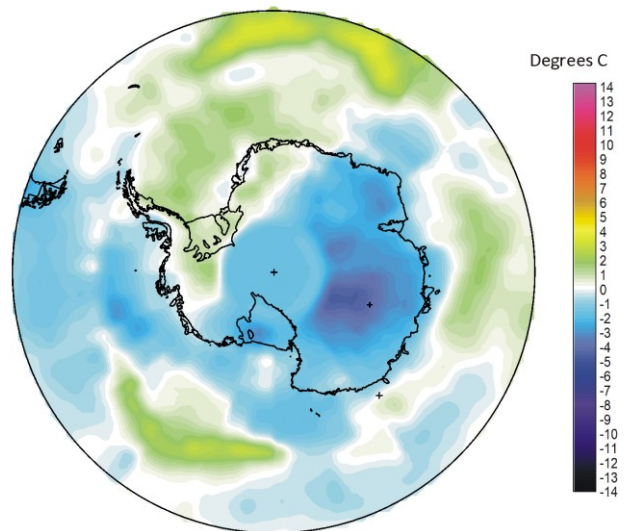


4

Surface air temperature November 2023 versus November last 10 yr

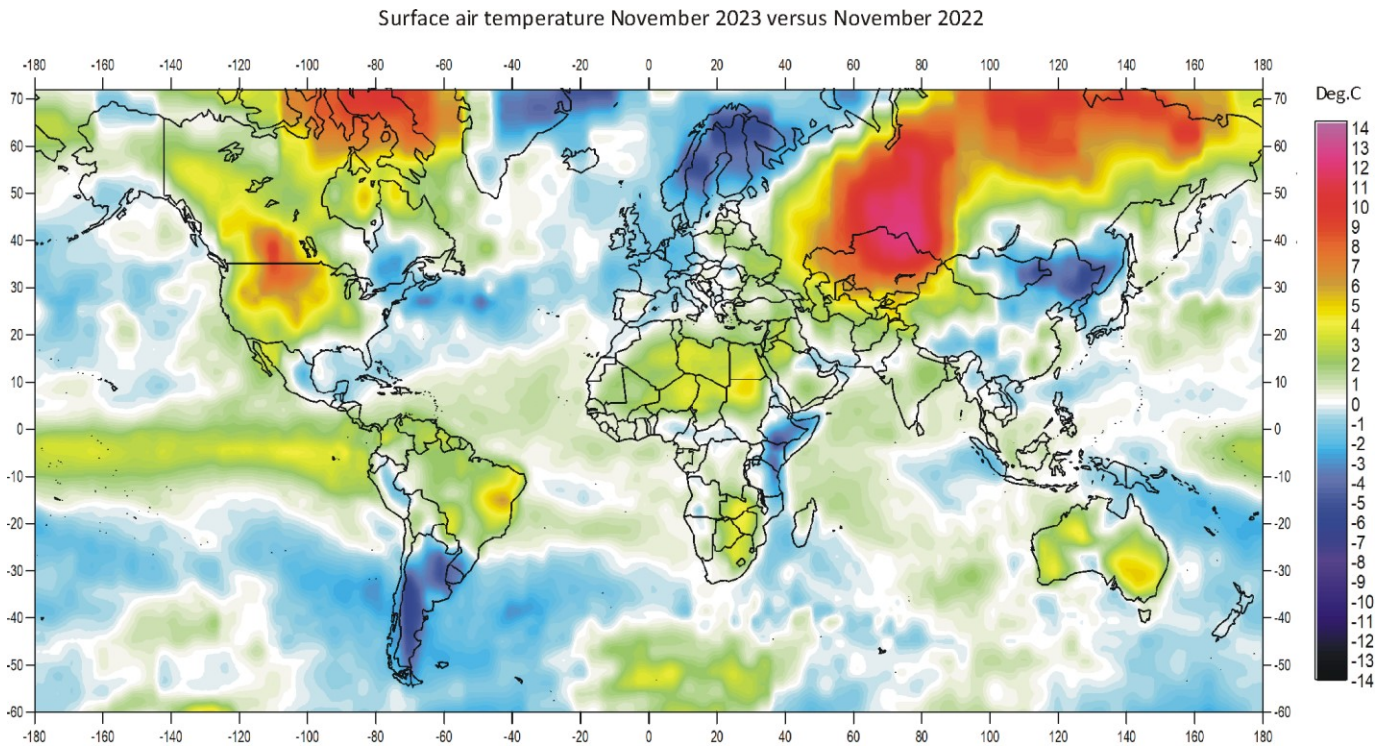


Surface air temperature November 2023 versus November last 10 yr



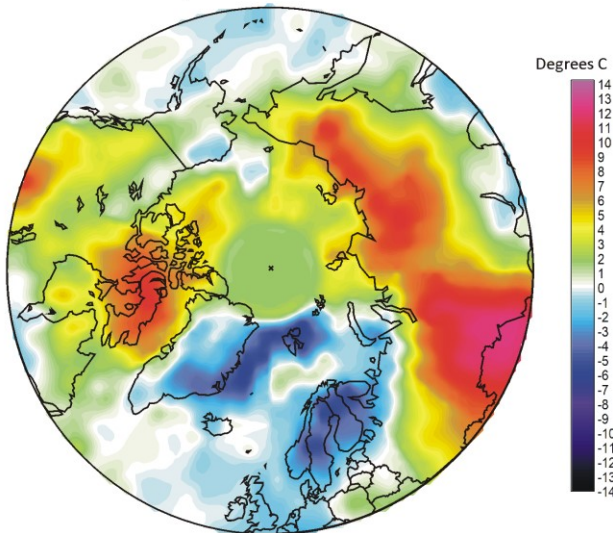
November 2023 surface air temperature compared to the average of November over the last 10 years. Green-yellow-red colours indicate areas with higher temperature than the 10-year average, while blue colours indicate lower than average temperatures. Data source: Remote Sensed Surface Temperature Anomaly, AIRS/Aqua L3 Monthly Standard Physical Retrieval 1-degree x 1-degree V006 (<https://airs.jpl.nasa.gov/>), obtained from the GISS data portal (https://data.giss.nasa.gov/gistemp/maps/index_v4.html).

November 2023 global surface air temperature compared to November 2022

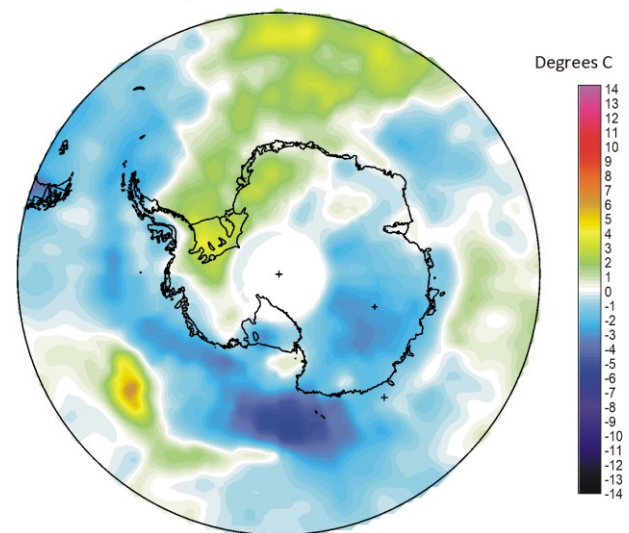


5

Surface air temperature November 2023 versus November 2022

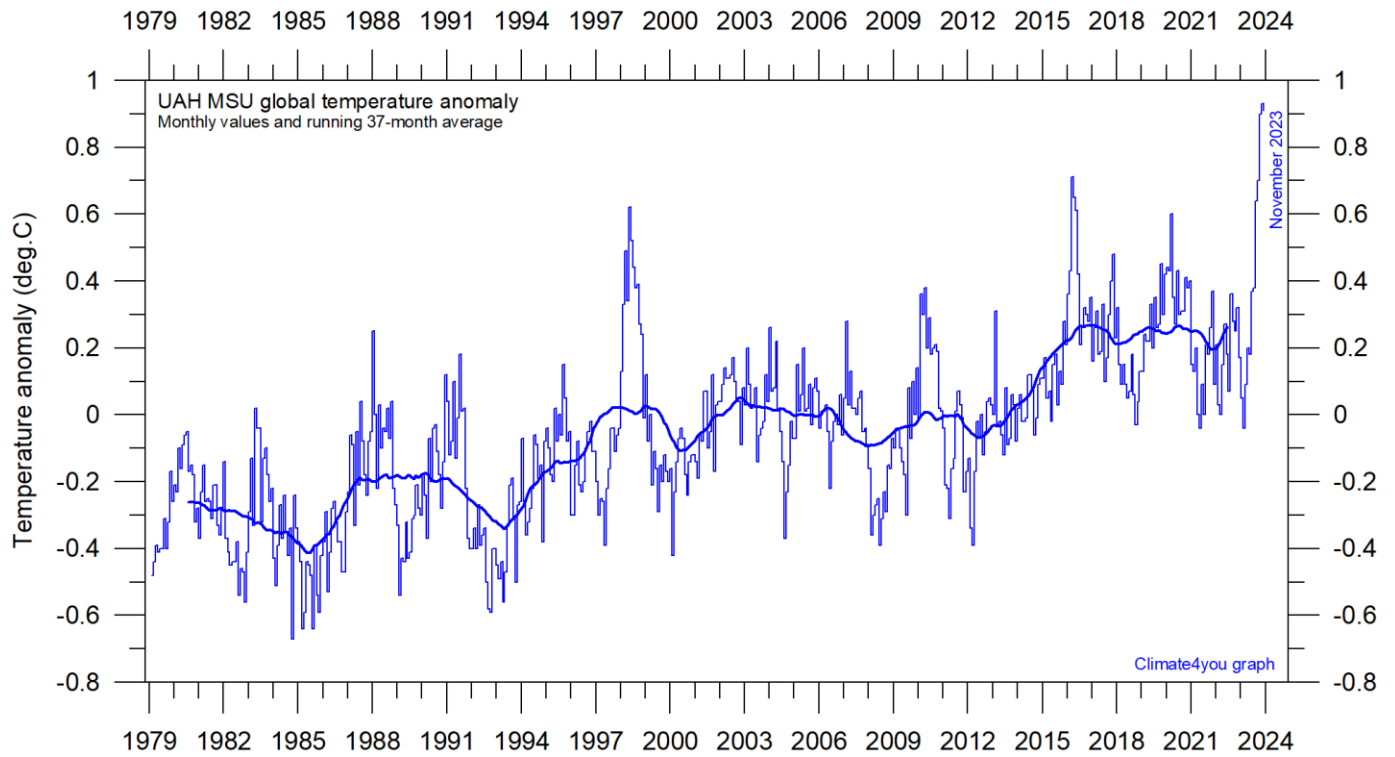


Surface air temperature November 2023 versus November 2022



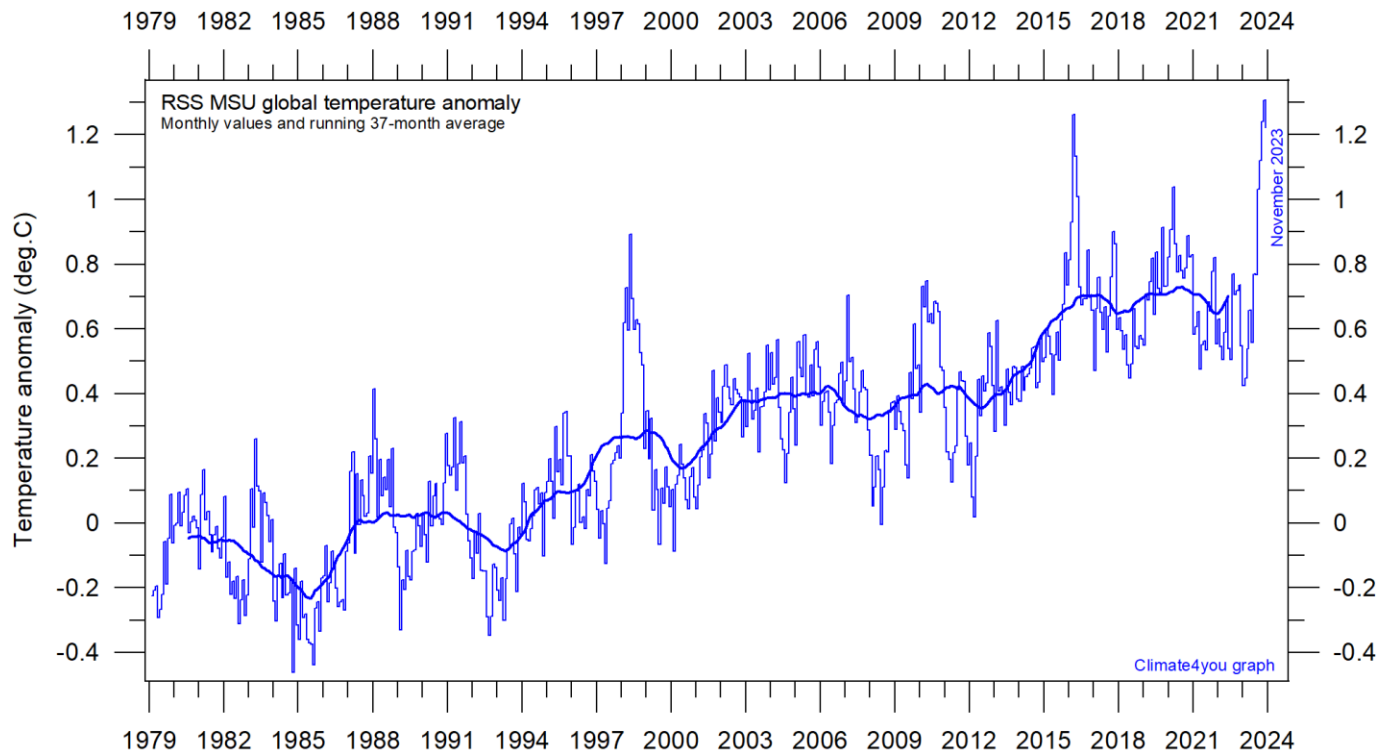
November 2023 surface air temperature compared to November 2022. Green-yellow-red colours indicate regions where the present month was warmer than last year, while blue colours indicate regions where the present month was cooler than last year. Variations in monthly temperature from one year to the next has no tangible climatic importance but may nevertheless be interesting to study. Data source: Remote Sensed Surface Temperature Anomaly, AIRS/Aqua L3 Monthly Standard Physical Retrieval 1-degree x 1-degree V006 (<https://airs.jpl.nasa.gov/>), obtained from the GISS data portal (https://data.giss.nasa.gov/gistemp/maps/index_v4.html).

Temperature quality class 1: Lower troposphere temperature from satellites, updated to November 2023 (see page 9 for definition of classes)



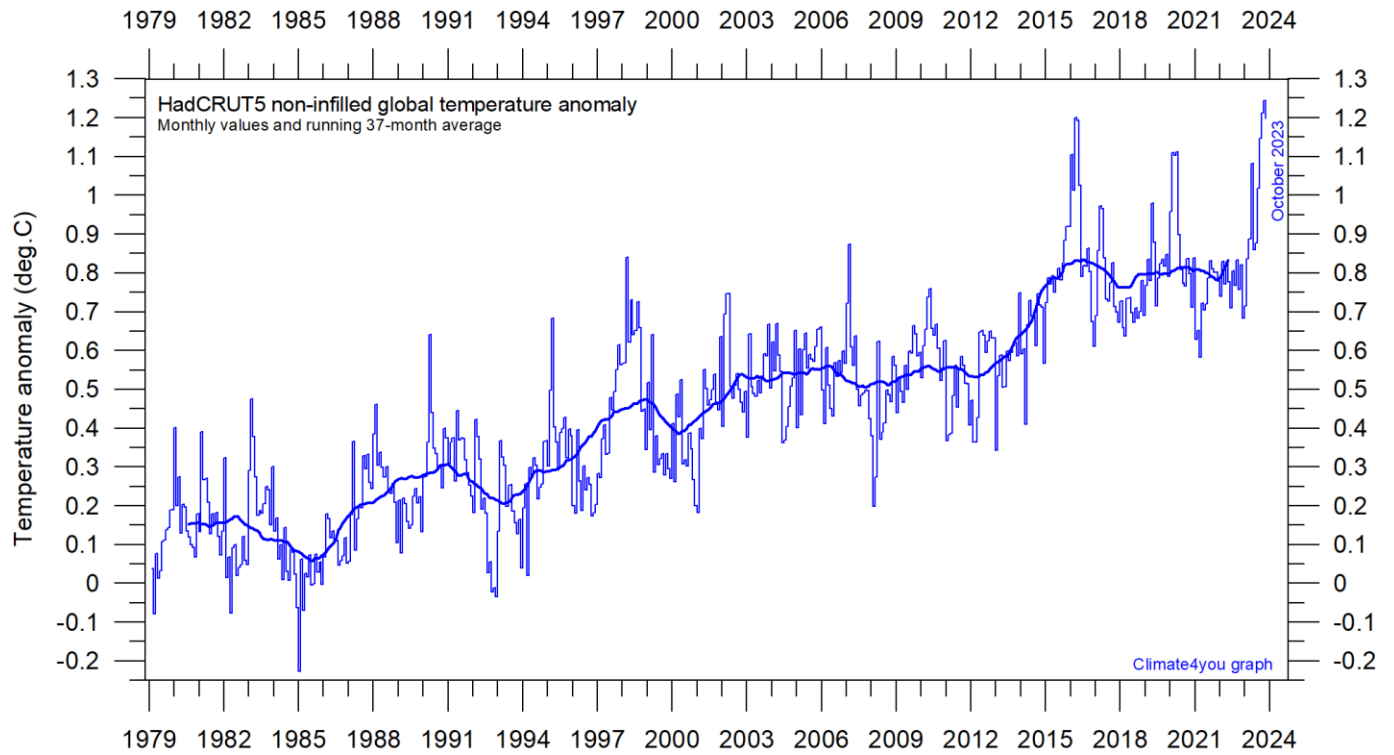
Global monthly average lower troposphere temperature (thin line) since 1979 according to [University of Alabama](#) at Huntsville, USA. The thick line is the simple running 37-month average. Reference period 1991-2020.

6



Global monthly average lower troposphere temperature (thin line) since 1979 according to according to [Remote Sensing Systems](#) (RSS), USA. The thick line is the simple running 37-month average.

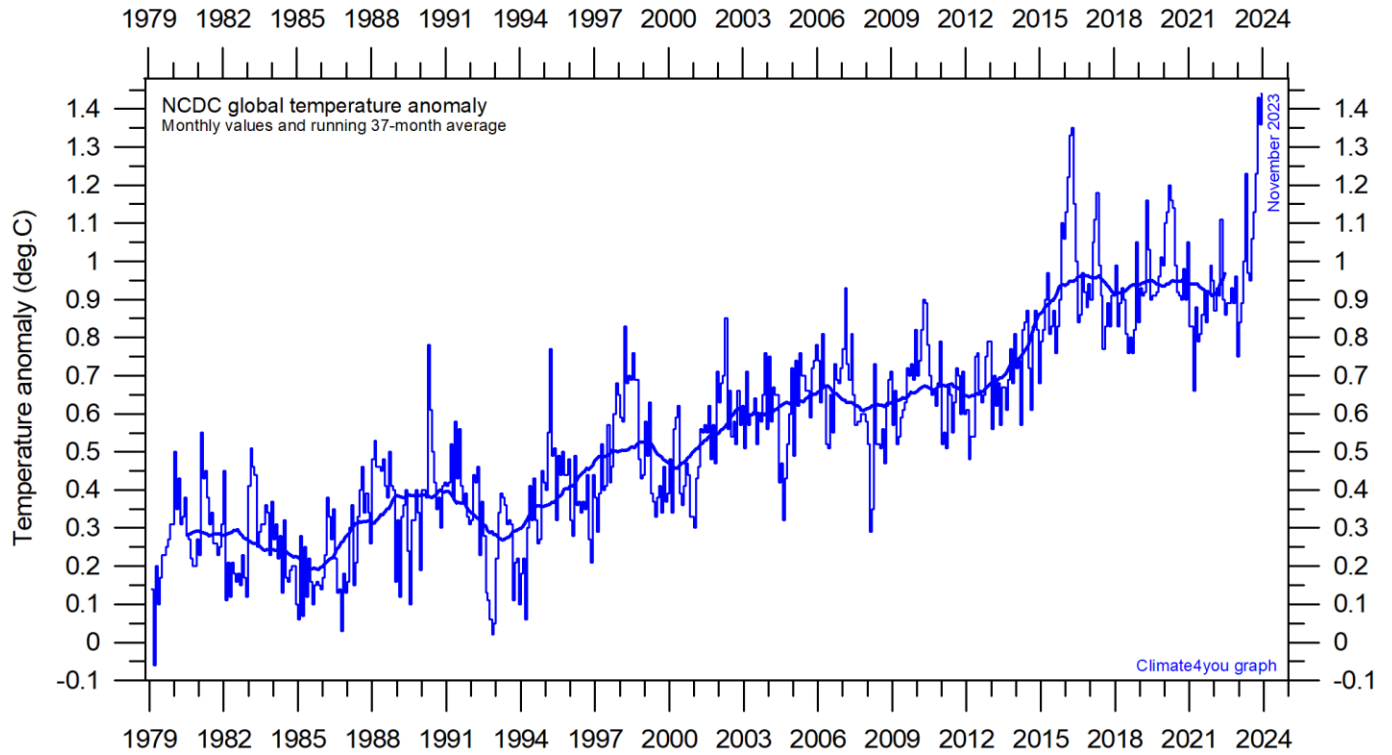
Temperature quality class 2: HadCRUT global surface air temperature, updated to October 2023



7

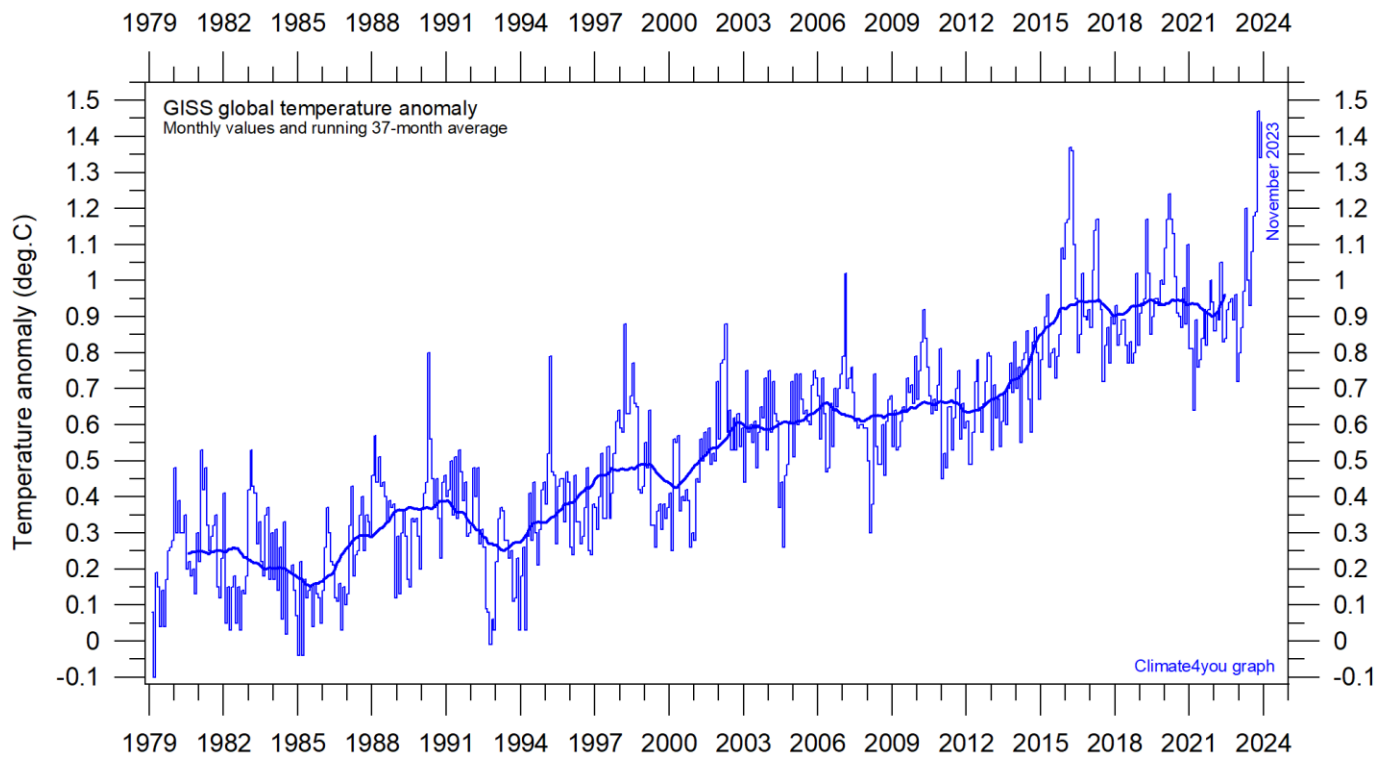
Global monthly average surface air temperature (thin line) since 1979 according to the Hadley Centre for Climate Prediction and Research and the University of East Anglia's [Climatic Research Unit \(CRU\)](#), UK. The thick line is the simple running 37-month average.

Temperature quality class 3: GISS and NCDC global surface air temperature, updated to November 2023



Global monthly average surface air temperature since 1979 according to according to the [National Climatic Data Center](#) (NCDC), USA. The thick line is the simple running 37-month average.

8



Global monthly average surface air temperature (thin line) since 1979 according to according to the [Goddard Institute for Space Studies](#) (GISS), at Columbia University, New York City, USA, using ERSST_v4 ocean surface temperatures. The thick line is the simple running 37-month average.

A note on data record stability and -quality:

The temperature diagrams shown above all have 1979 as starting year. This roughly marks the beginning of the recent episode of global warming, after termination of the previous episode of global cooling from about 1940. In addition, the year 1979 also represents the starting date for the satellite-based global temperature estimates (UAH and RSS). For the three surface air temperature records (HadCRUT, NCDC and GISS), they begin much earlier (in 1850 and 1880, respectively), as can be inspected on www.climate4you.com.

For all three surface air temperature records, but especially NCDC and GISS, administrative changes to anomaly values are quite often introduced, even affecting observations many years back in time. Some changes from the recent past may be due to the delayed addition of new station data or change of station location, while others probably have their origin in changes of the technique implemented to calculate average values from the raw data. It is clearly impossible to evaluate the validity of such administrative changes for the outside user of these records; it is only possible to note that such changes quite often are introduced (see example diagram next page).

In addition, the three surface records represent a blend of sea surface data collected by moving ships or by other means, plus data from land stations of partly unknown quality and unknown degree of representativeness for their region. Many of the land stations also has been moved geographically during their period of operation, instrumentation have been changed, and they are influenced by changes in their near surroundings (vegetation, buildings, etc.). The surface network is inherently heterogeneous (dense over continents but sparse over oceans) and probably contaminated by urbanization surrounding many measurement sites.

The satellite temperature records also have their problems, but these are generally of a more technical nature and probably therefore better correctable. In

addition, the temperature sampling by satellites is more regular and complete on a global basis than that represented by the surface records. It is also important that the sensors on satellites measure temperature directly by microwave radiance (thereby unobstructed by clouds), while most modern surface temperature measurements are indirect, using electronic resistance.

Everybody interested in climate science should gratefully acknowledge the big efforts put into maintaining the different temperature databases referred to in the present newsletter. At the same time, however, it is also important to realise that all temperature records cannot be of equal scientific quality. The simple fact that they to some degree differ shows that they cannot all be correct.

On this background, and for practical reasons, Climate4you therefore operates with three quality classes (1-3) for global temperature records, with 1 representing the highest quality level:

Quality class 1: The satellite records (UAH and RSS).

Quality class 2: The HadCRUT surface record.

Quality class 3: The NCDC and GISS surface records.

The main reason for discriminating between the three surface records is the following:

While both NCDC and GISS often experience quite large administrative changes (see example on p.10), and therefore essentially must be considered as unstable records, the changes introduced to HadCRUT are fewer and smaller. For obvious reasons, as the past does not change, any record undergoing continuing changes cannot describe the past correctly all the time. Frequent and large corrections in a database unavoidably signal a fundamental uncertainty about what is likely to represent the correct values.

You can find more on the issue of lack of temporal stability on www.climate4you.com (go to: *Global Temperature*, and then proceed to *Temporal Stability*).

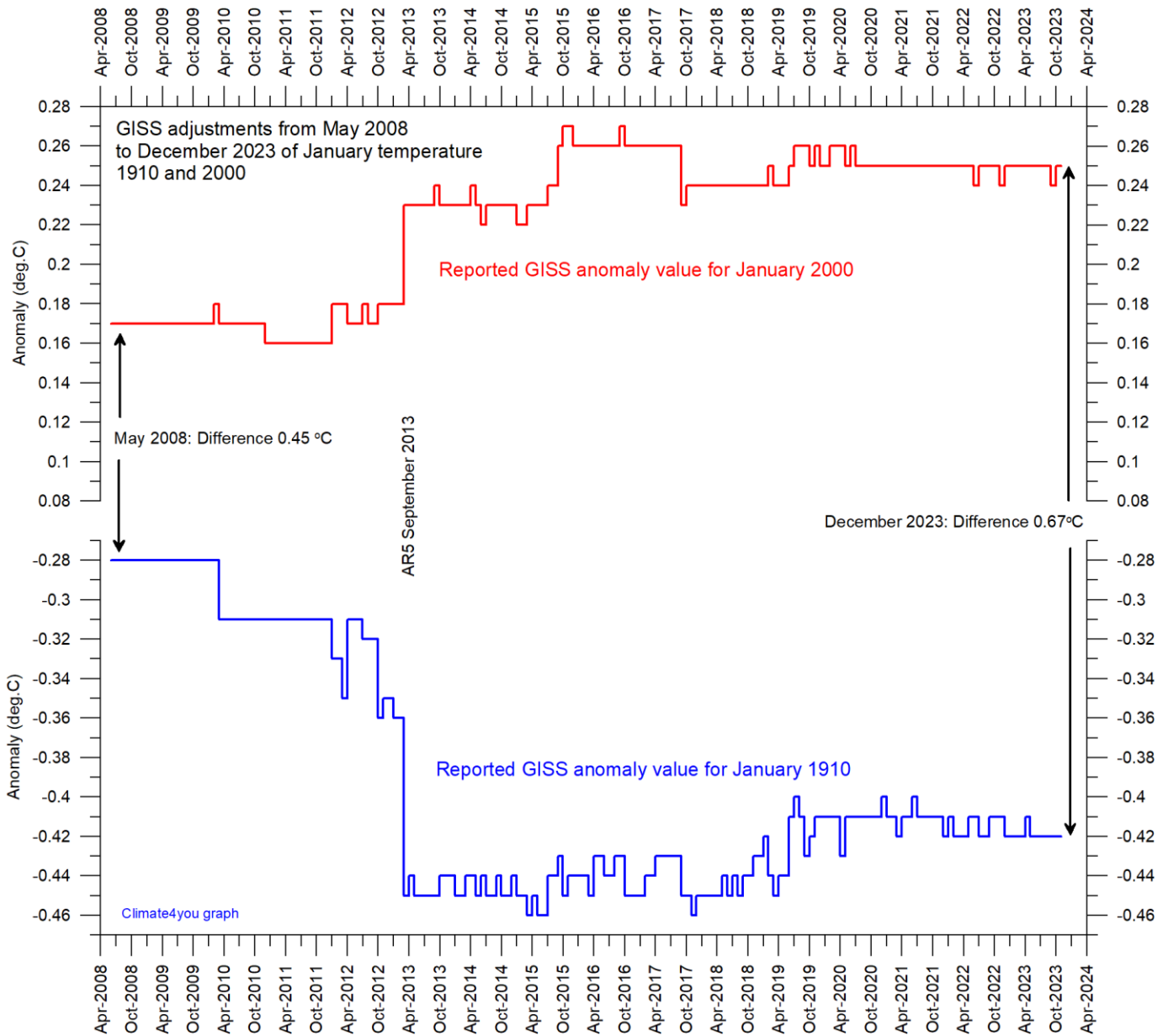
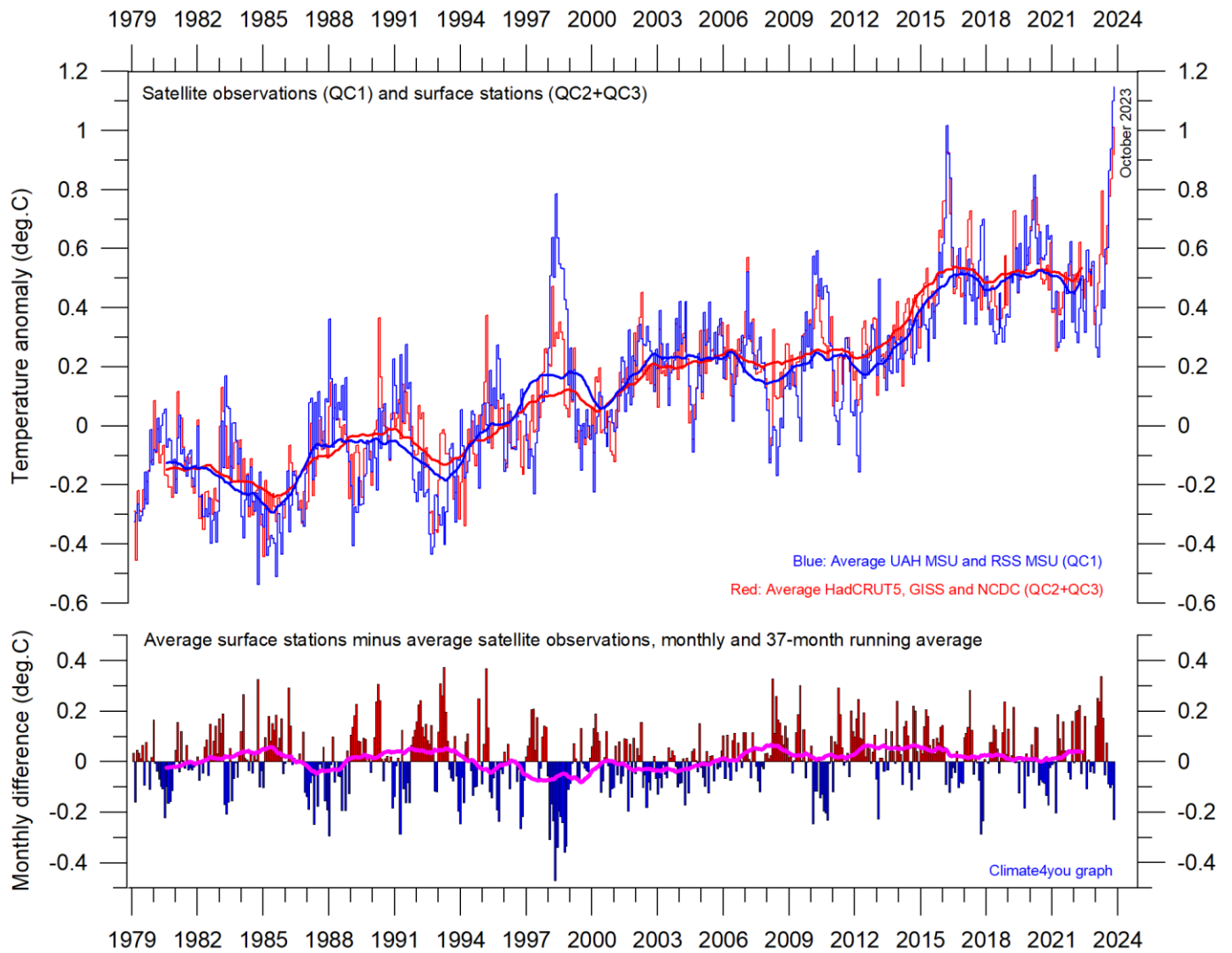


Diagram showing the monthly adjustments made since May 2008 by the [Goddard Institute for Space Studies](#) (GISS), USA, as recorded by published anomaly values for the two months January 1910 and January 2000. AR5 indicates timing of publication of IPCC report AR5 Climate Change 2013: The Physical Science Basis.

The administrative upsurge of the temperature increase from January 1915 to January 2000 has grown from 0.45 (reported May 2008) to 0.67°C (reported December 2023). This represents an about 49% administrative temperature increase over this

period, meaning that a significant part (nearly half) of the apparent global temperature increase from January 1910 to January 2000 (as reported by GISS) is caused by administrative changes of the original data since May 2008.

Comparing global surface air temperature and lower troposphere satellite temperatures; updated to October 2023



11

Plot showing the average of monthly global surface air temperature estimates (HadCRUT5, GISS and NCDC) and satellite-based temperature estimates (RSS MSU and UAH MSU). The thin lines indicate the monthly value, while the thick lines represent the simple running 37-month average, nearly corresponding to a running 3-yr average. The lower panel shows the monthly difference between average surface air temperature and satellite temperatures. As the base period differs for the different temperature estimates, they have all been normalised by comparing to the average value of 30 years from January 1979 to December 2008.

Global air temperature linear trends updated to October 2023

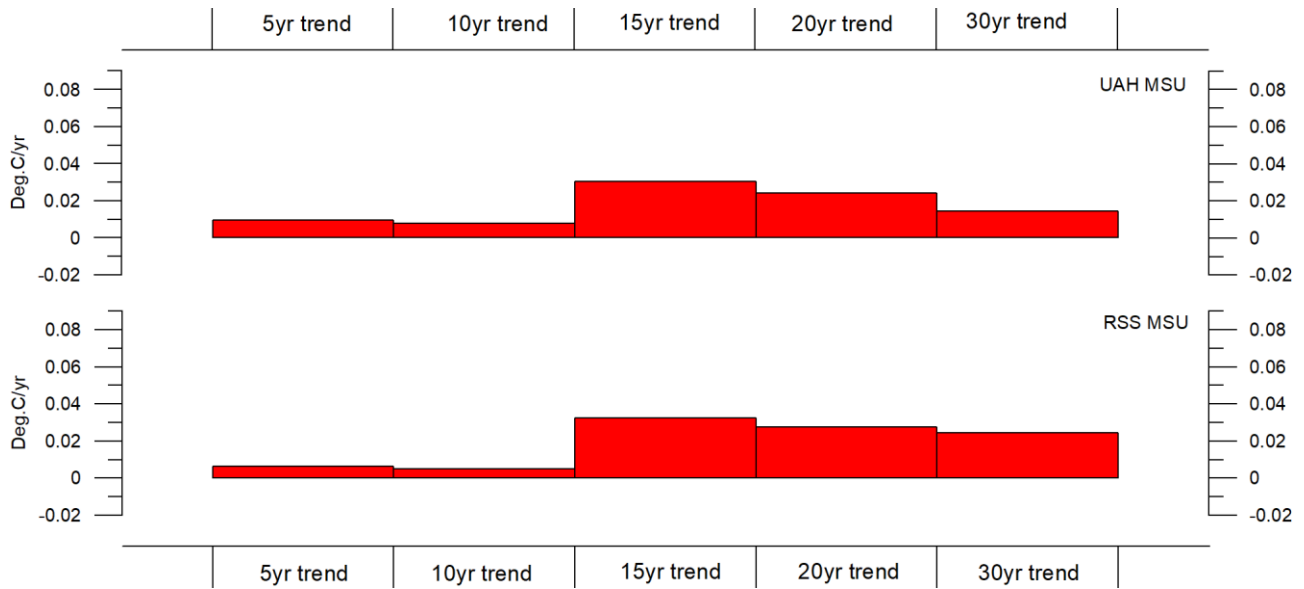


Diagram showing the latest 5, 10, 20 and 30-yr linear annual global temperature trend, calculated as the slope of the linear regression line through the data points, for two satellite-based temperature estimates (UAH MSU and RSS MSU).

12

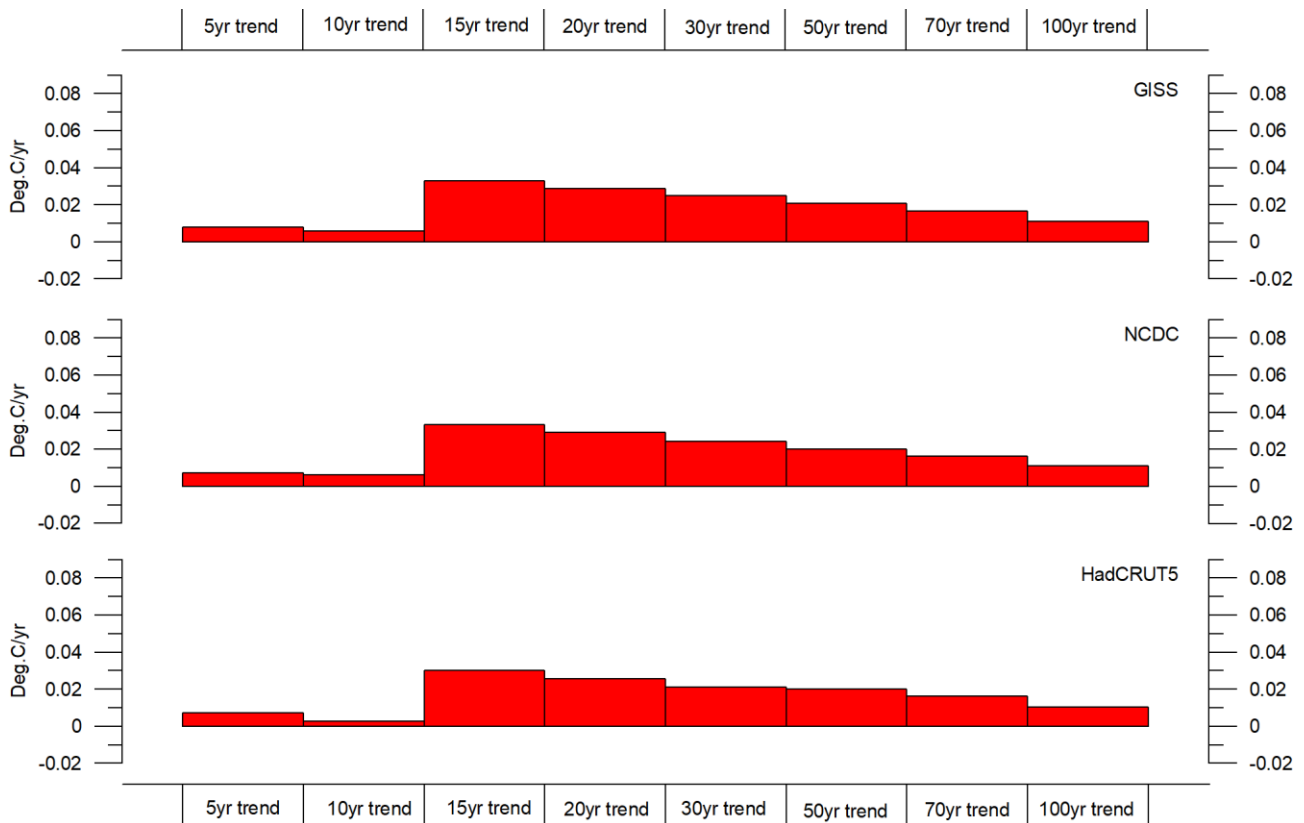
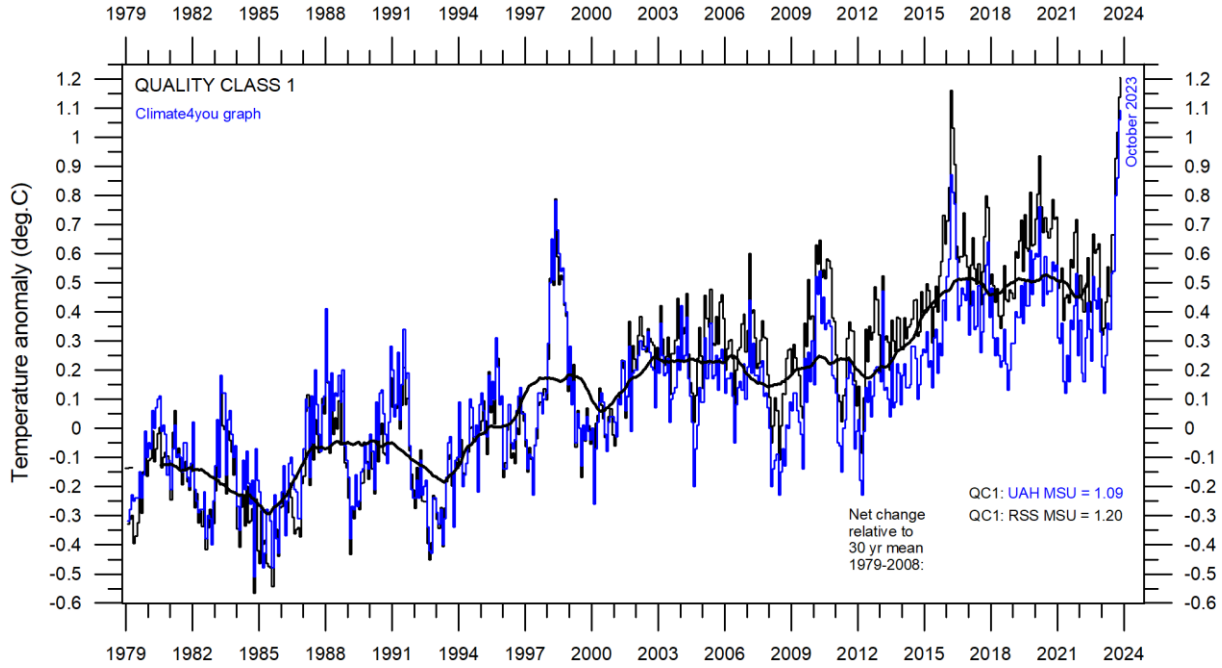


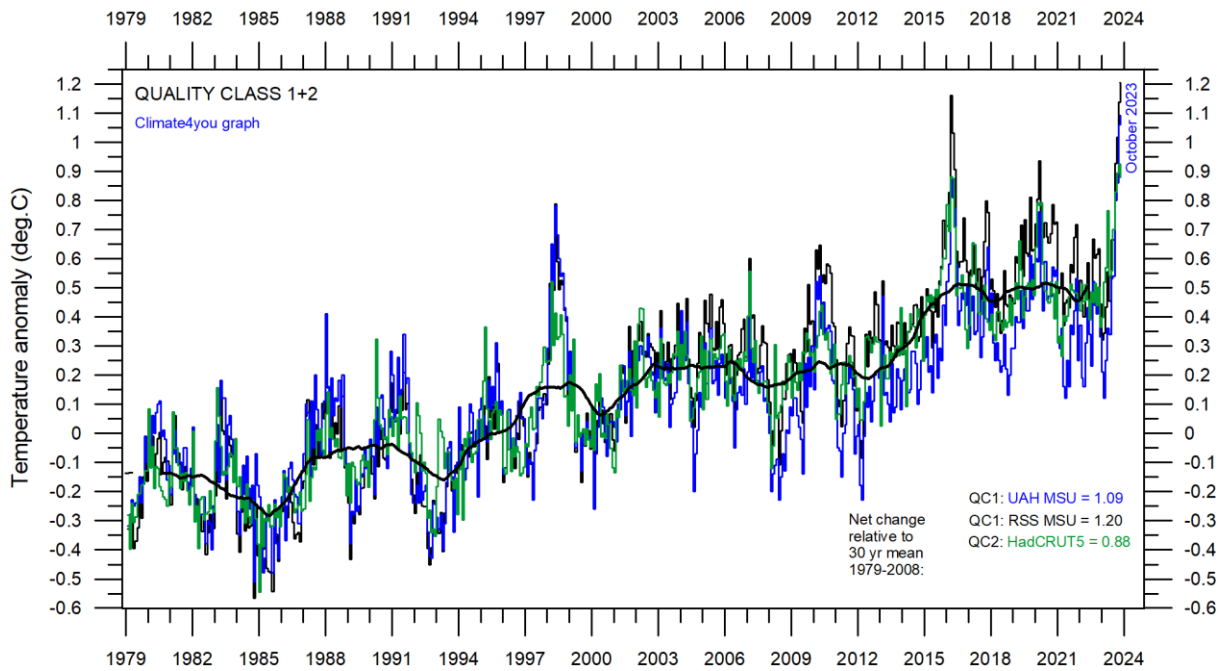
Diagram showing the latest 5, 10, 20, 30, 50, 70 and 100-year linear annual global temperature trend, calculated as the slope of the linear regression line through the data points, for three surface-based temperature estimates (GISS, NCDC and HadCRUT5).

All in one, Quality Class 1, 2 and 3; updated to October 2023

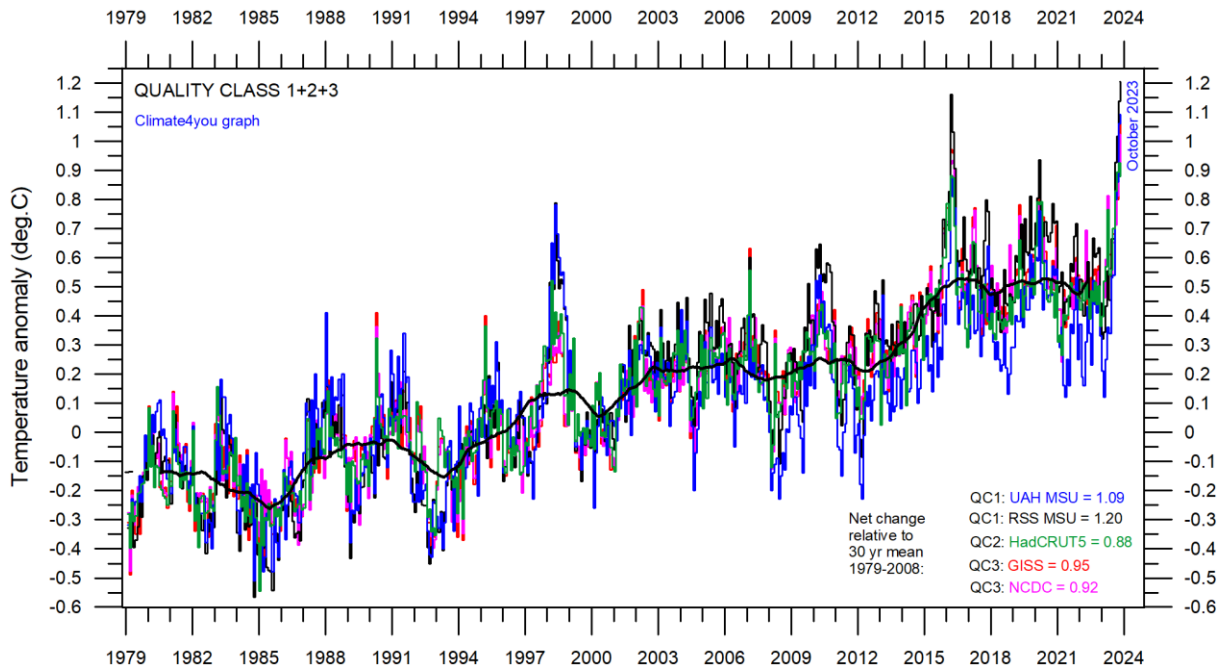


Superimposed plot of Quality Class 1 (UAH and RSS) global monthly temperature estimates. As the base period differs for the individual temperature estimates, they have all been normalised by comparing with the average value of the initial 120 months (30 years) from January 1979 to December 2008. The heavy black line represents the simple running 37 month (c. 3 year) mean of the average of both temperature records. The numbers shown in the lower right corner represent the temperature anomaly relative to the individual 1979-2008 averages.

13



Superimposed plot of Quality Class 1 and 2 (UAH, RSS and HadCRUT) global monthly temperature estimates. As the base period differs for the individual temperature estimates, they have all been normalised by comparing with the average value of the initial 120 months (30 years) from January 1979 to December 2008. The heavy black line represents the simple running 37 month (c. 3 year) mean of the average of all three temperature records. The numbers shown in the lower right corner represent the temperature anomaly relative to the individual 1979-2008 averages.



Superimposed plot of Quality Class 1, 2 and 3 global monthly temperature estimates (UAH, RSS, HadCRUT, GISS and NCDC). As the base period differs for the individual temperature estimates, they have all been normalised by comparing with the average value of the initial 120 months (30 years) from January 1979 to December 2008. The heavy black line represents the simple running 37 month (c. 3 year) mean of the average of all five temperature records. The numbers shown in the lower right corner represent the temperature anomaly relative to the individual 1979-2008 averages.

14 Please see reflections on page 9 relating to the above three quality classes.

Satellite- and surface-based temperature estimates are derived from different types of measurements and comparing them directly as in the above diagrams therefore may be somewhat ambiguous.

However, as both types of estimates often are discussed together in various news media, the above composite diagrams may nevertheless be of some interest.

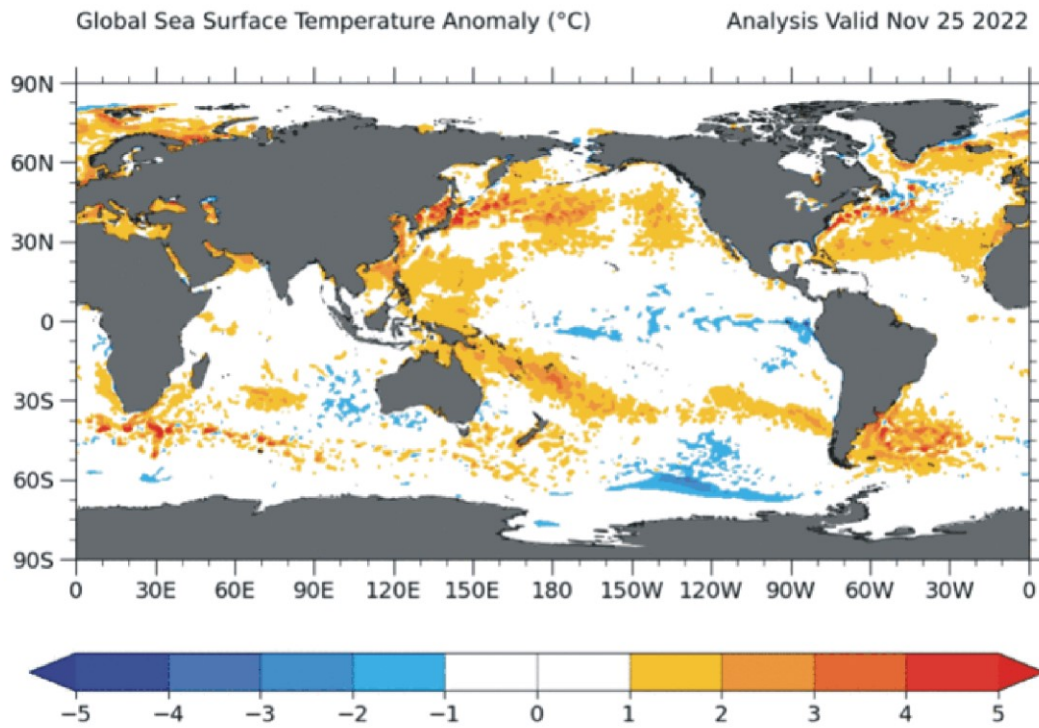
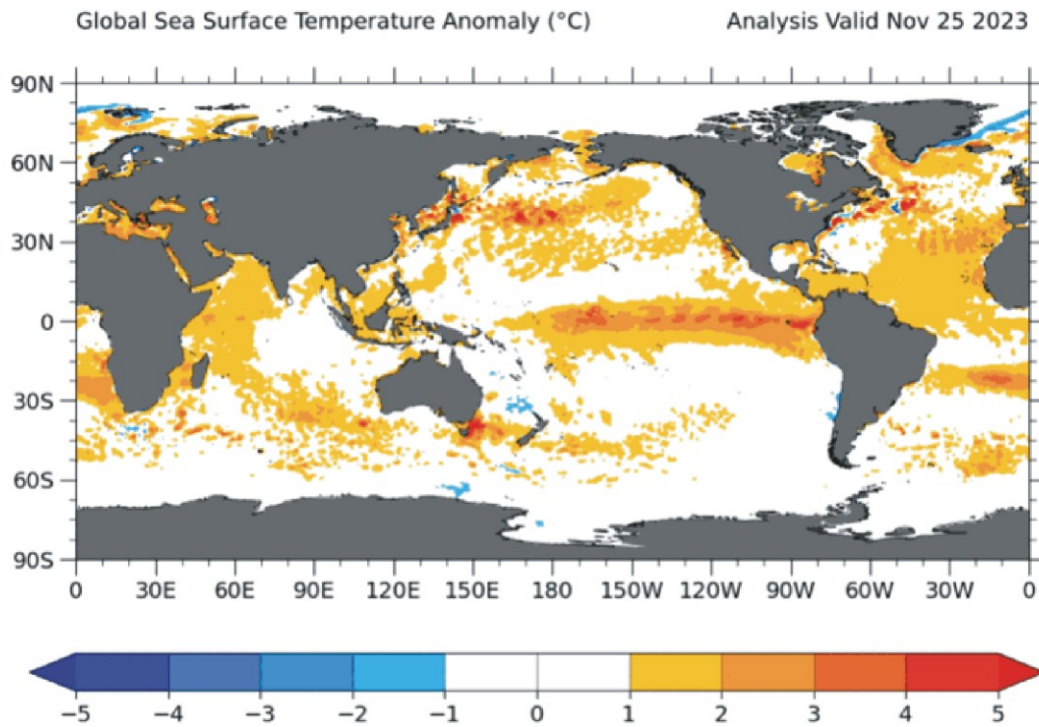
In fact, the different types of temperature estimates appear to agree as to the overall temperature variations on a 2-3-year scale, although on a shorter time scale there are often considerable differences between the individual records. However, since about 2003 the surface records used to be drifting towards higher temperatures than the combined satellite record, but this overall tendency was much removed by the major adjustment of the RSS satellite series in 2015 (see lower diagram on page 6).

The combined records (diagram above) suggest a modest global air temperature increase over the last 30 years, about 0.22°C per decade. It should be noted that the apparent temperature increases since about 2003 at least partly is the result of ongoing administrative adjustments (page 9-10). At the same time, none of the temperature records considered here indicates any overall temperature decrease during the last 20 years.

The present temperature development does not exclude the possibility that global temperatures may begin to increase significantly later. On the other hand, it also remains a possibility that Earth just now is passing an overall temperature peak, and that global temperatures may begin to decrease during the coming 5-10 years.

As always, time will show which of these possibilities is correct.

Global sea surface temperature, updated to November 2023



Plymouth State Weather Center

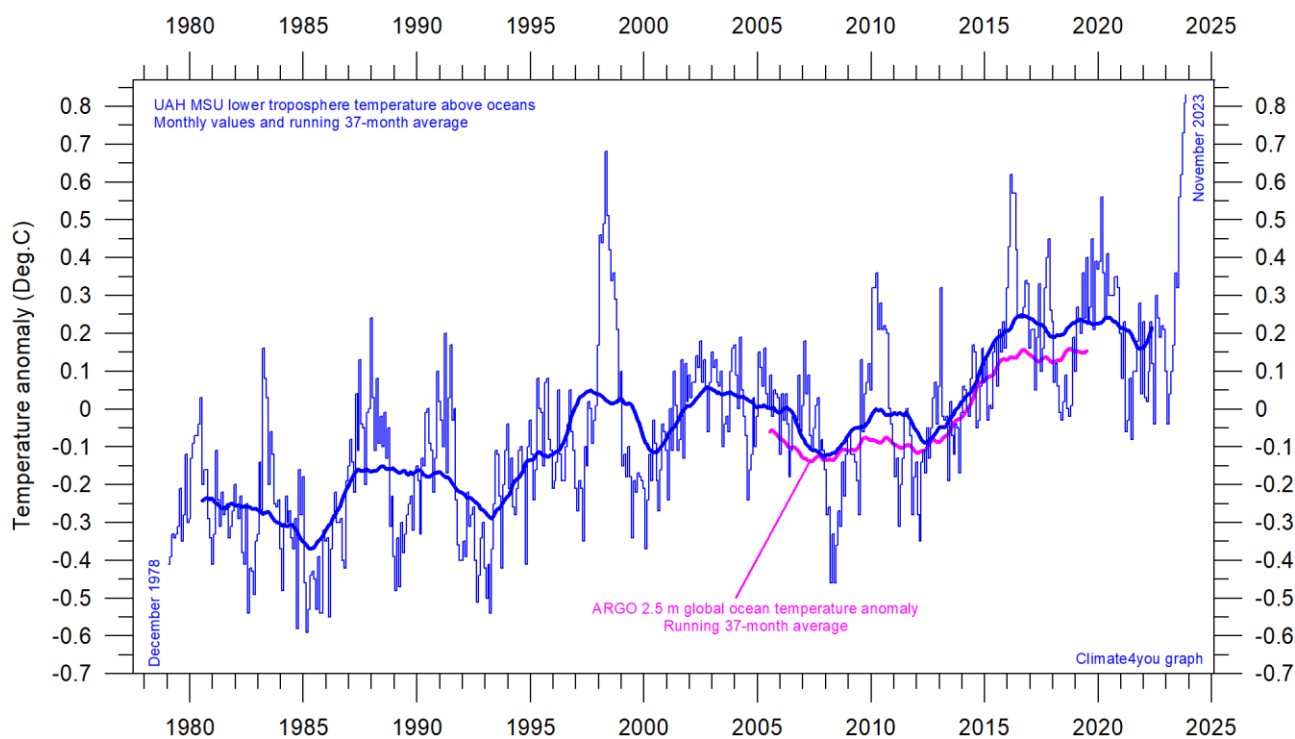
Sea surface temperature anomaly on 25 November 2023 (upper map) and 2022 (lower map). Map source: Plymouth State Weather Center. Reference period: 1977-1991.

Because of the large surface areas near Equator, the temperature of the surface water in these regions is especially important for the global atmospheric temperature (p. 6-8). In fact, no less than 50% of planet Earth's surface area is located within 30°N and 30°S.

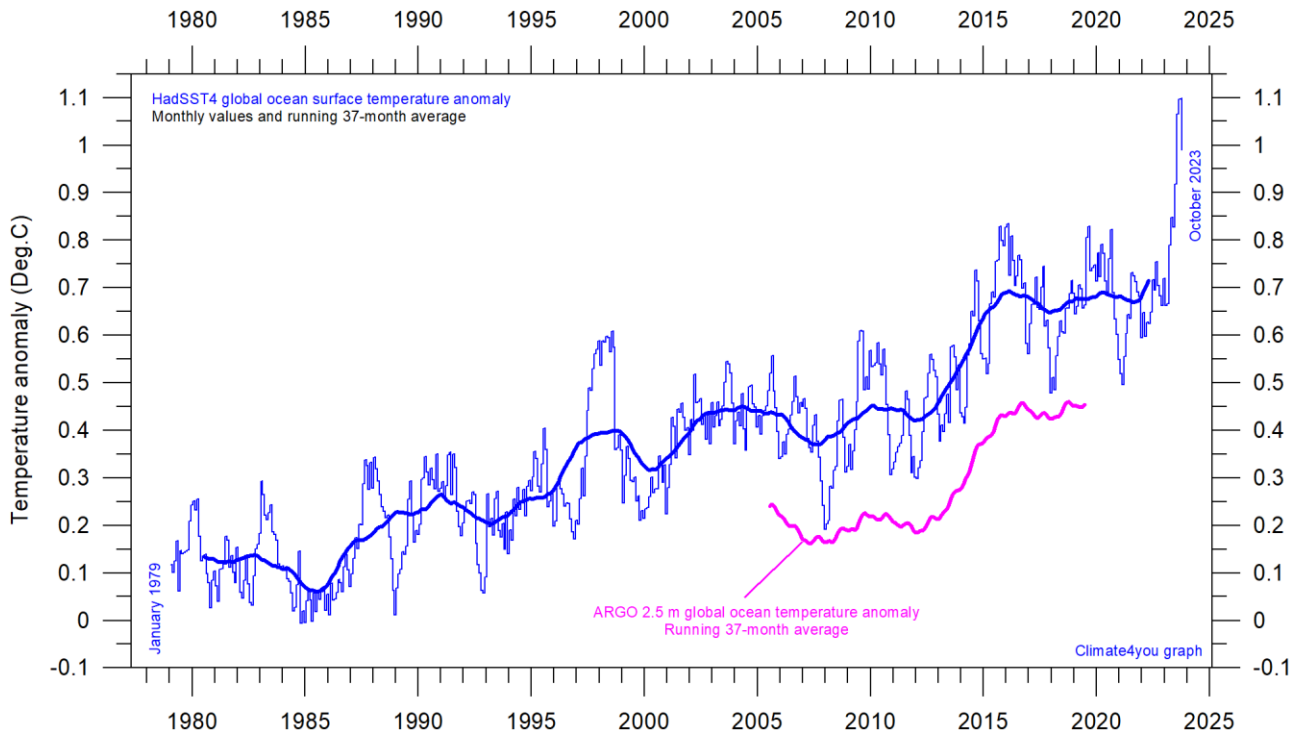
A mixture of relatively warm and cold water presently dominates much of the global ocean surface, but with notable variations from month to month. All such ocean surface temperature changes will be influencing global air temperatures in the months to come. A cold La Niña episode (Pacific Ocean) has recently ended and is now being followed by a warm El Niño episode (maps p.15 and diagram p.25).

The significance of short-term cooling or warming reflected in air temperatures should never be overstated. Whenever Earth experiences cold La Niña or warm El Niño episodes major heat exchanges take place between the Pacific Ocean and the atmosphere above, sooner or later showing up in estimates of the global air temperature.

However, this does not necessarily reflect similar changes in the total heat content of the atmosphere-ocean system. In fact, global net changes can be small and such heat exchanges may mainly reflect redistribution of energy between ocean and atmosphere. What matters is the overall temperature development when seen over several years.

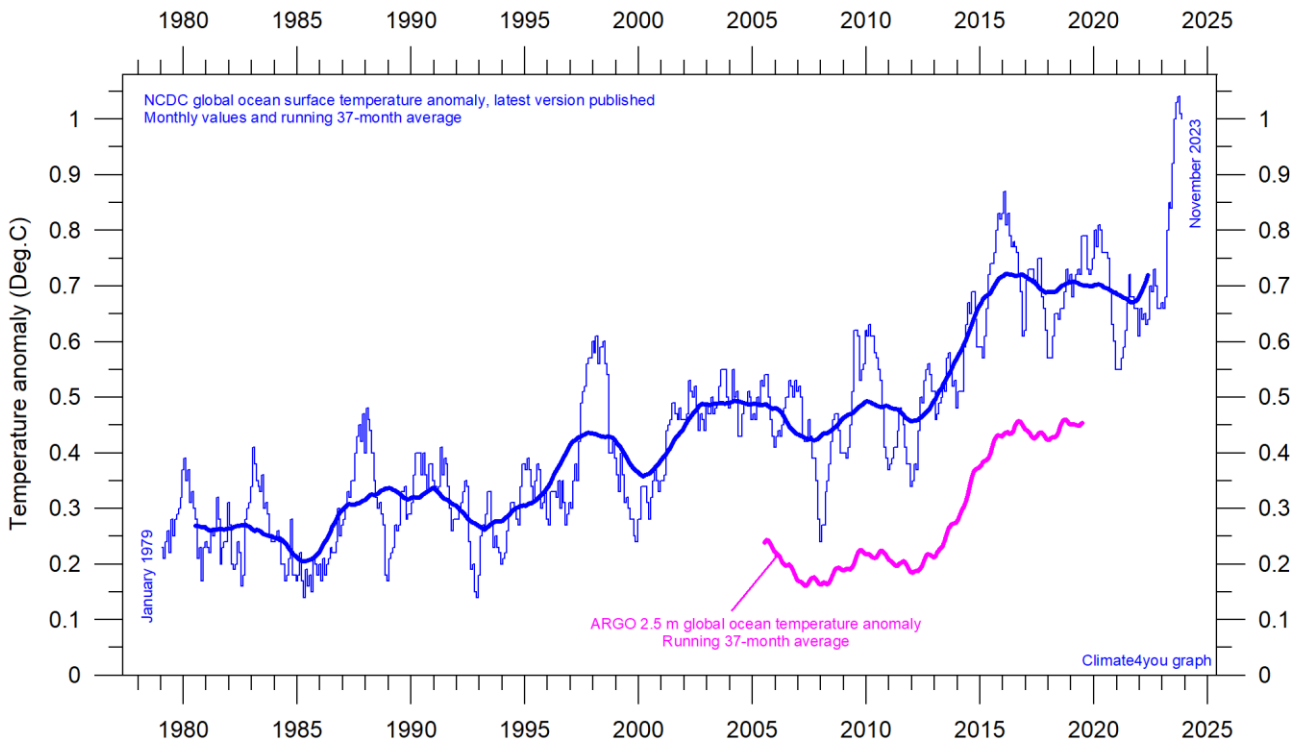


Global monthly average lower troposphere temperature over oceans (thin line) since 1979 according to [University of Alabama](#) at Huntsville, USA. The thick line is the simple running 37-month average. Insert: Argo global ocean temperature anomaly from floats, displaced vertically to make visual comparison easier. UAH reference period: 1991-2020.



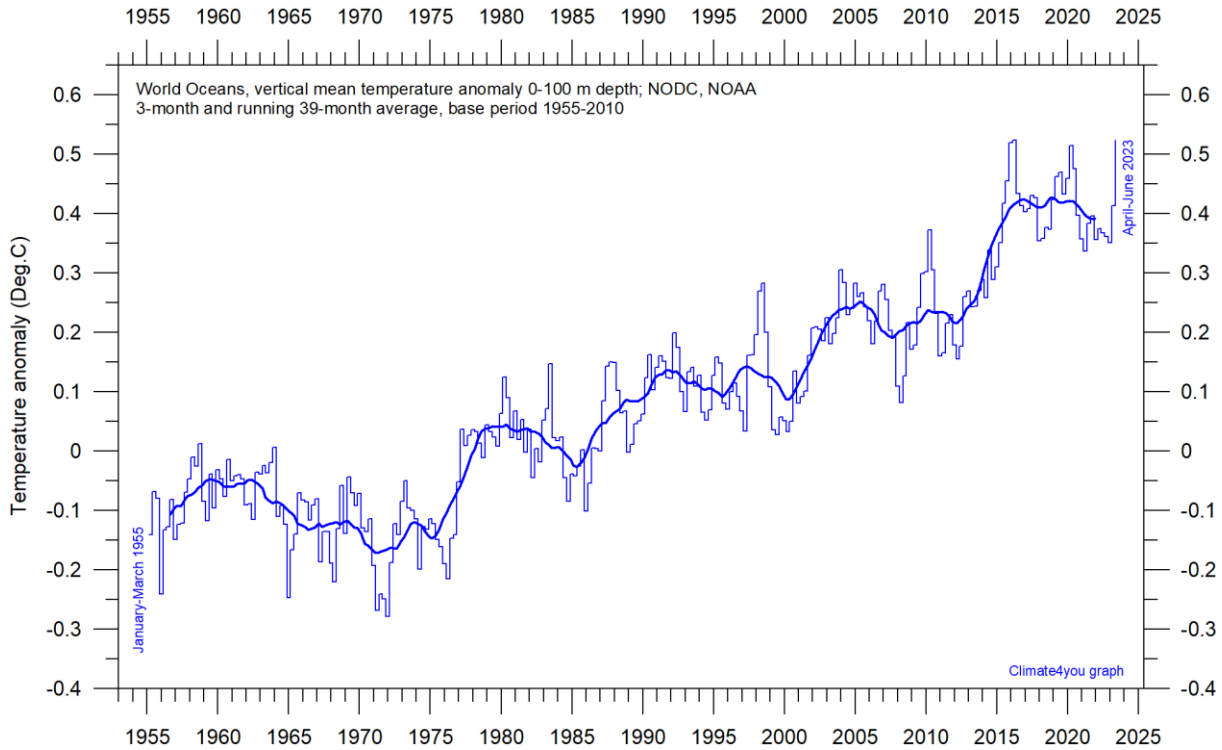
Global monthly average sea surface temperature since 1979 according to University of East Anglia's [Climatic Research Unit \(CRU\)](#), UK. Base period: 1961-1990. The thick line is the simple running 37-month average. Insert: Argo global ocean temperature anomaly from floats, displaced vertically to make visual comparison easier.

17



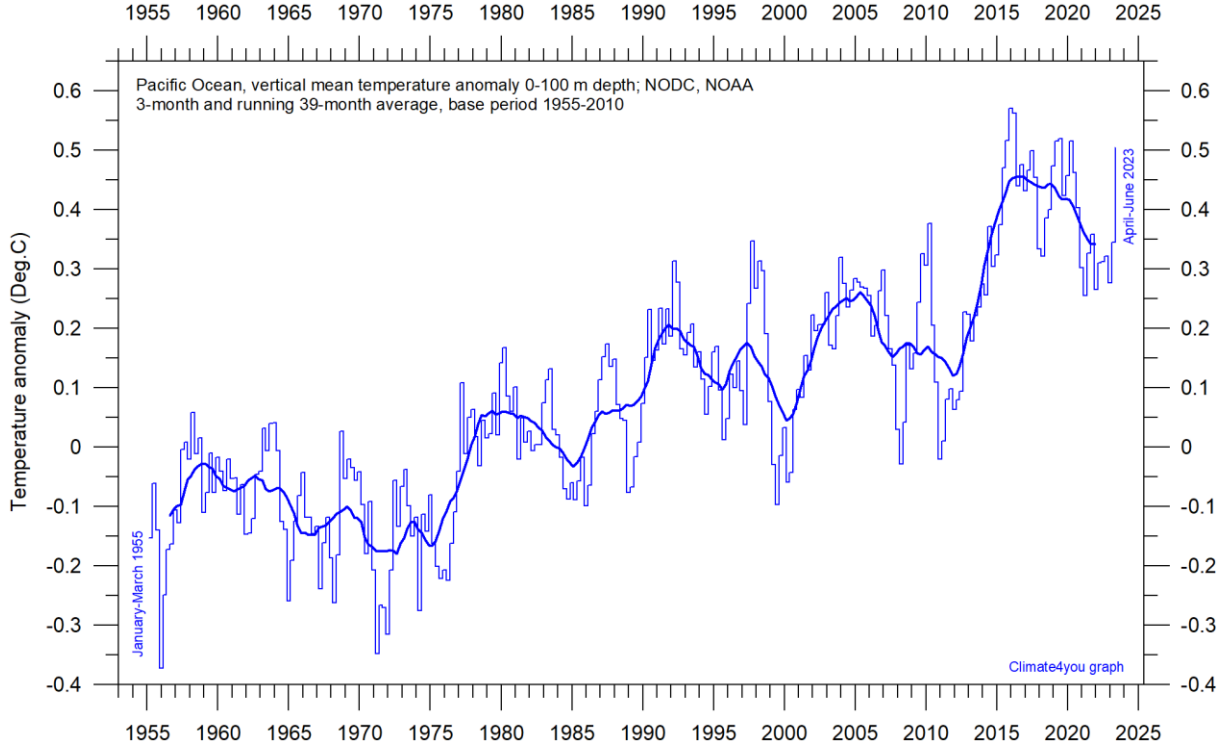
Global monthly average sea surface temperature since 1979 according to the [National Climatic Data Center \(NCDC\)](#), USA. Base period: 1901-2000. The thick line is the simple running 37-month average. Insert: Argo global ocean temperature anomaly from floats, displaced vertically to make visual comparison easier.

Ocean temperature in uppermost 100 m, updated to June 2023

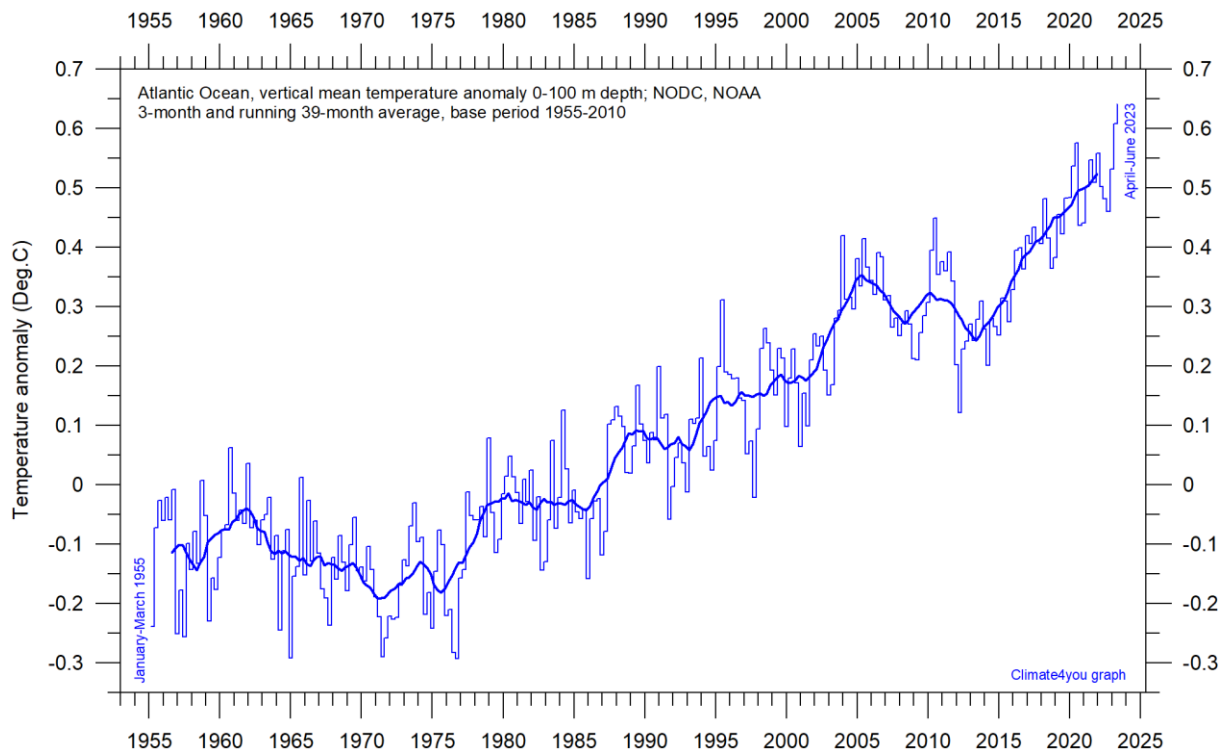


World Oceans vertical average temperature 0-100 m depth since 1955. The thin line indicates 3-month values, and the thick line represents the simple running 39-month (c. 3 year) average. Data source: [NOAA National Oceanographic Data Center](#) (NODC). Base period 1955-2010.

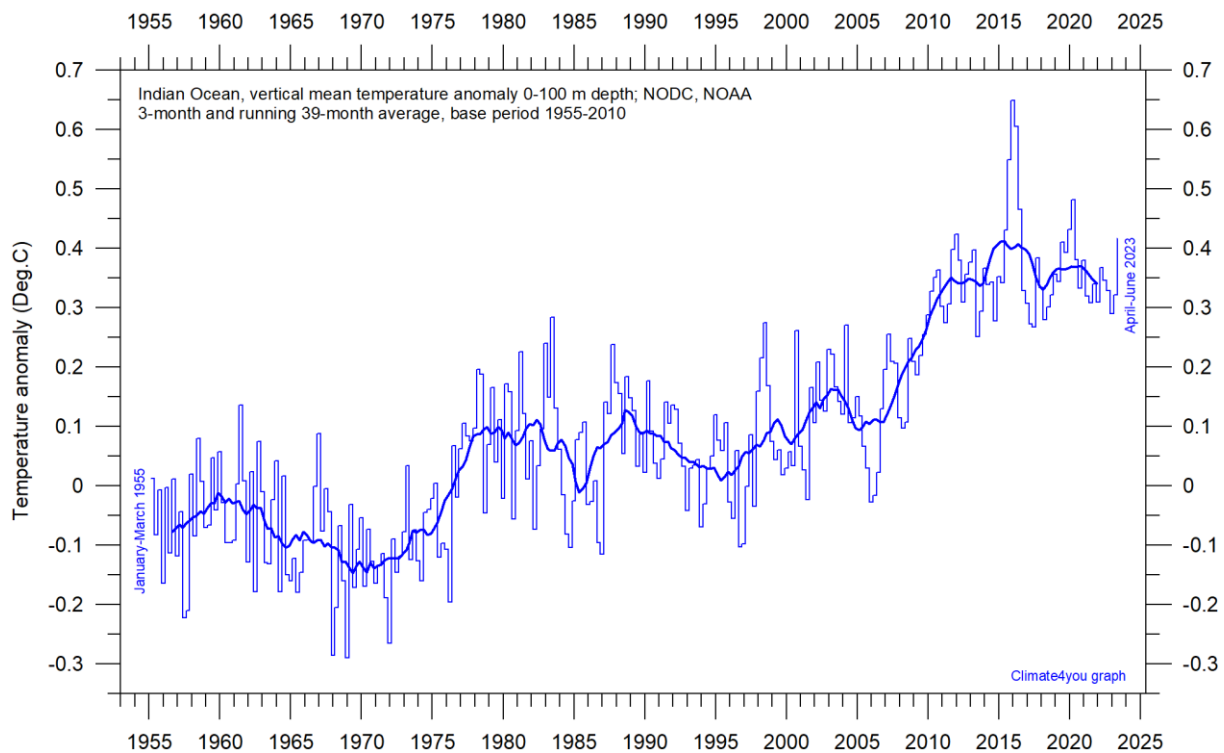
18



Pacific Ocean vertical average temperature 0-100 m depth since 1955. The thin line indicates 3-month values, and the thick line represents the simple running 39-month (c. 3 year) average. Data source: [NOAA National Oceanographic Data Center](#) (NODC). Base period 1955-2010.

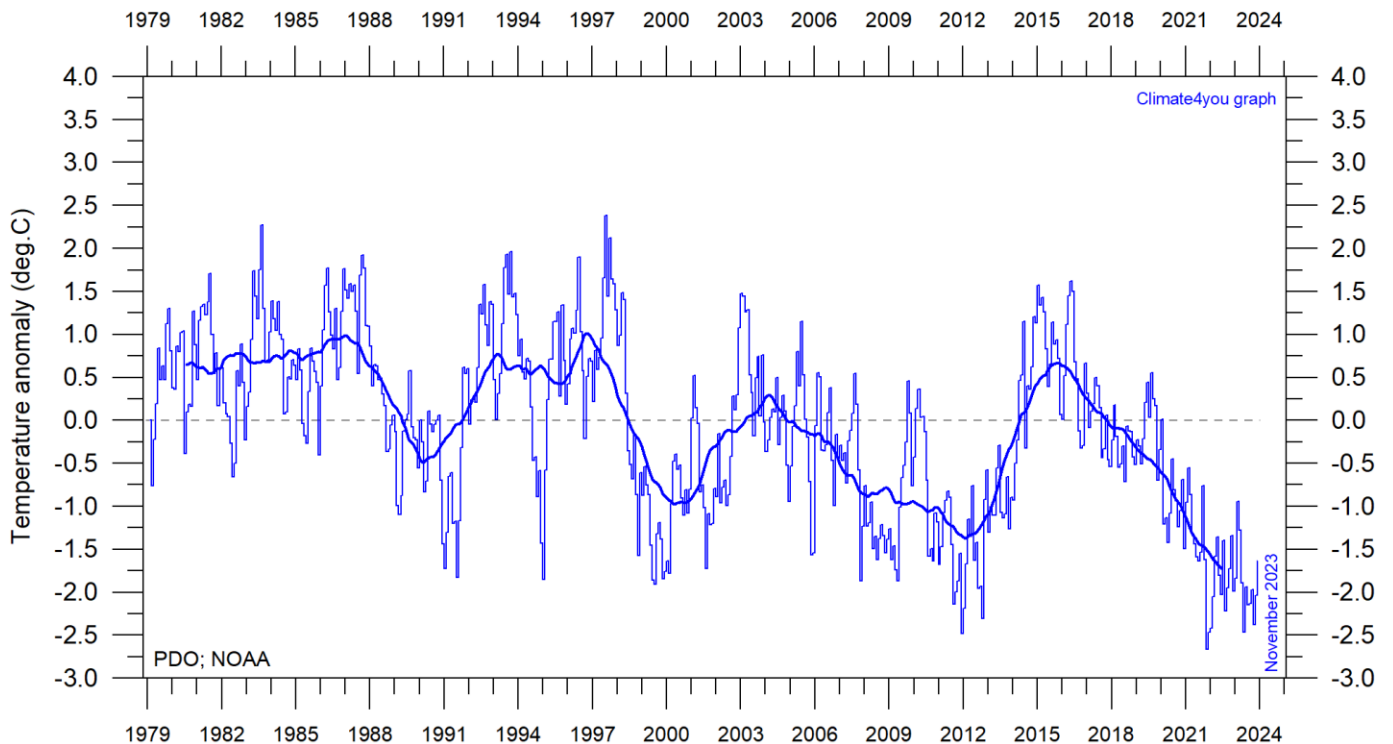


Atlantic Ocean vertical average temperature 0-100 m depth since 1955. The thin line indicates 3-month values, and the thick line represents the simple running 39-month (c. 3 year) average. Data source: [NOAA National Oceanographic Data Center](#) (NODC). Base period 1955-2010.



Indian Ocean vertical average temperature 0-100 m depth since 1955. The thin line indicates 3-month values, and the thick line represents the simple running 39-month (c. 3 year) average. Data source: [NOAA National Oceanographic Data Center](#) (NODC). Base period 1955-2010.

Pacific Decadal Oscillation (PDO), updated to November 2023



20

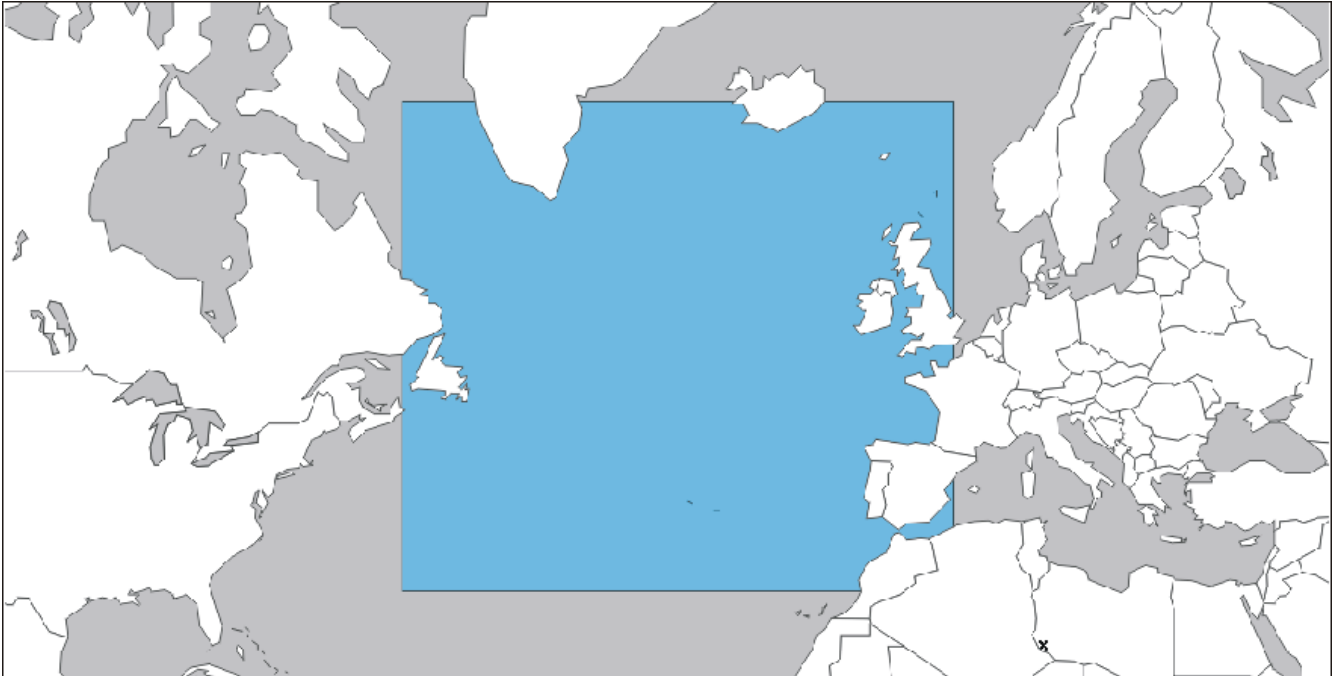
Monthly values of the Pacific Decadal Oscillation (PDO) since January 1979. The PDO is a long-lived El Niño-like pattern of Pacific climate variability, and the data series goes back to January 1854. Base period: 1982-2002. The thin line indicates monthly PDO values, and the thick line is the simple running 37-month average. Data source: [NOAA Physical Science Laboratory](#) (version PDO ERSST V5 plotted above).

The PDO is a long-lived El Niño-like pattern of Pacific climate variability, with data extending back to January 1854. Causes for PDO are not currently known, but even in the absence of a theoretical understanding, PDO climate information improves season-to-season and year-to-year climate forecasts for North America because of its strong tendency for multi-season and multi-year persistence. The PDO also appears to be roughly in phase with global temperature changes. Thus, from a societal impact's perspective, recognition of PDO is important because it shows that "normal" climate conditions can vary over time periods comparable to the length of a human's lifetime.

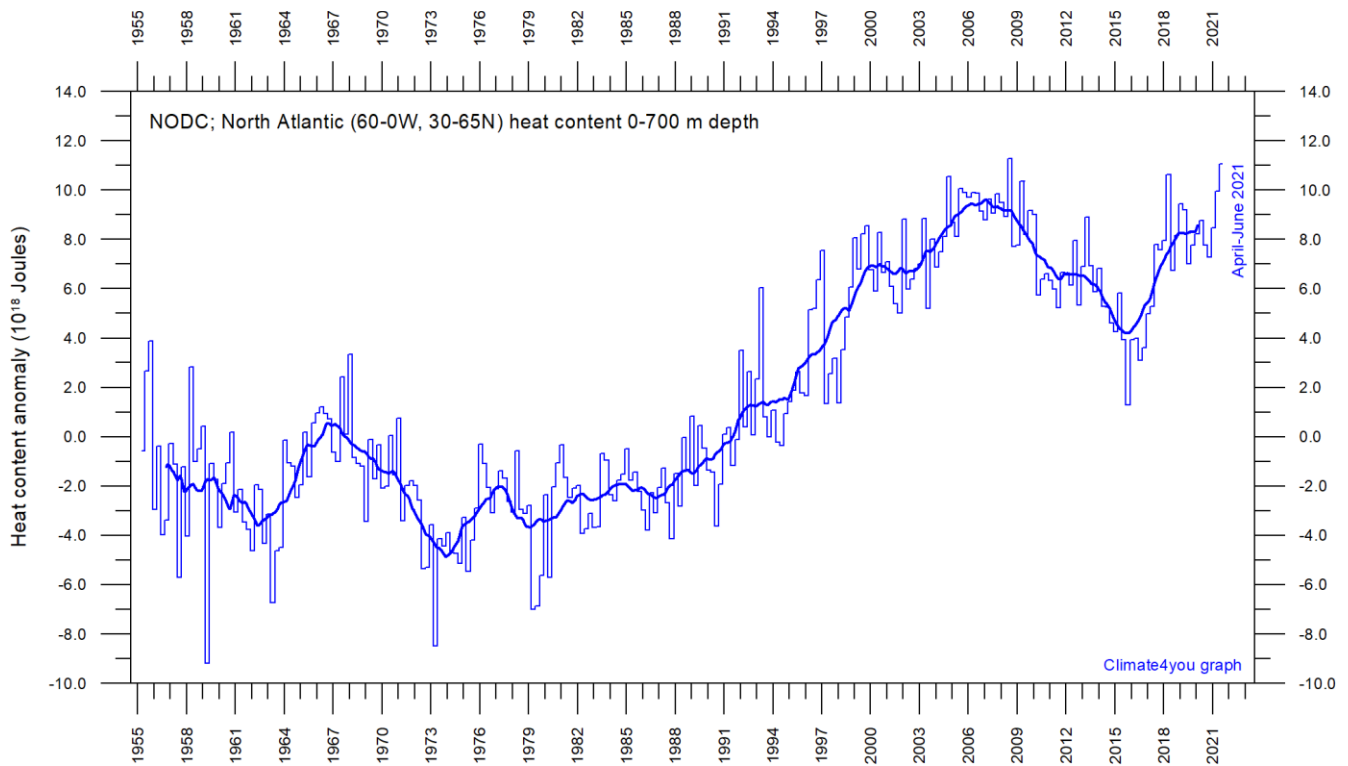
The PDO illustrates how global temperatures are tied to sea surface temperatures in the Pacific Ocean, the largest ocean on Earth. When sea surface temperatures are relatively low (negative phase PDO), as it was from 1945 to 1977, global air temperature often decreases. When Pacific Ocean surface temperatures are high (positive phase PDO), as from 1977 to 1998, global surface air temperature often increases.

A Fourier frequency analysis (not shown here) shows the entire PDO record since 1854 to be influenced by a 5.7-year cycle, and possibly also by a longer about 53-year long cycle.

North Atlantic heat content uppermost 700 m, updated to June 2021

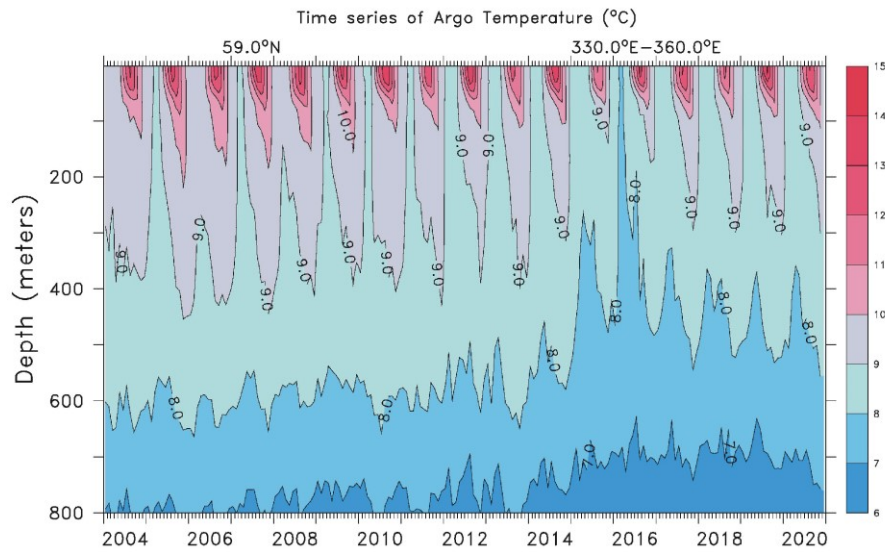


21



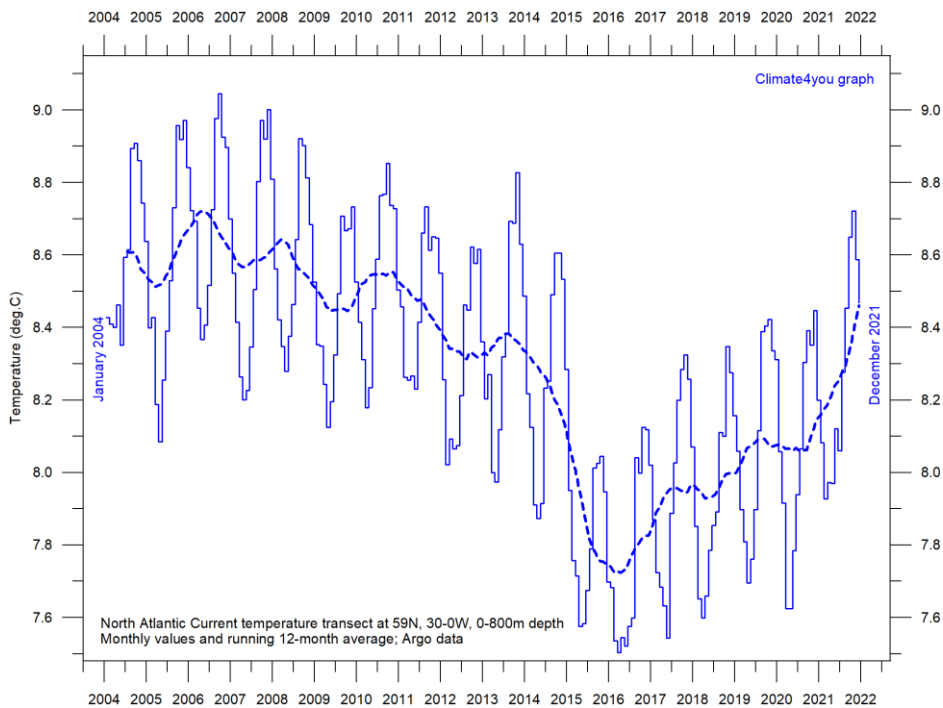
Global monthly heat content anomaly (10^{18} Joules) in the uppermost 700 m of the North Atlantic (60-0W, 30-65N; see map above) ocean since January 1955. The thin line indicates monthly values, and the thick line represents the simple running 37-month (c. 3 year) average. Data source: [National Oceanographic Data Center](https://www.nodc.noaa.gov/) (NODC).

North Atlantic temperatures 0-800 m depth along 59°N, 30-0W, updated to December 2021



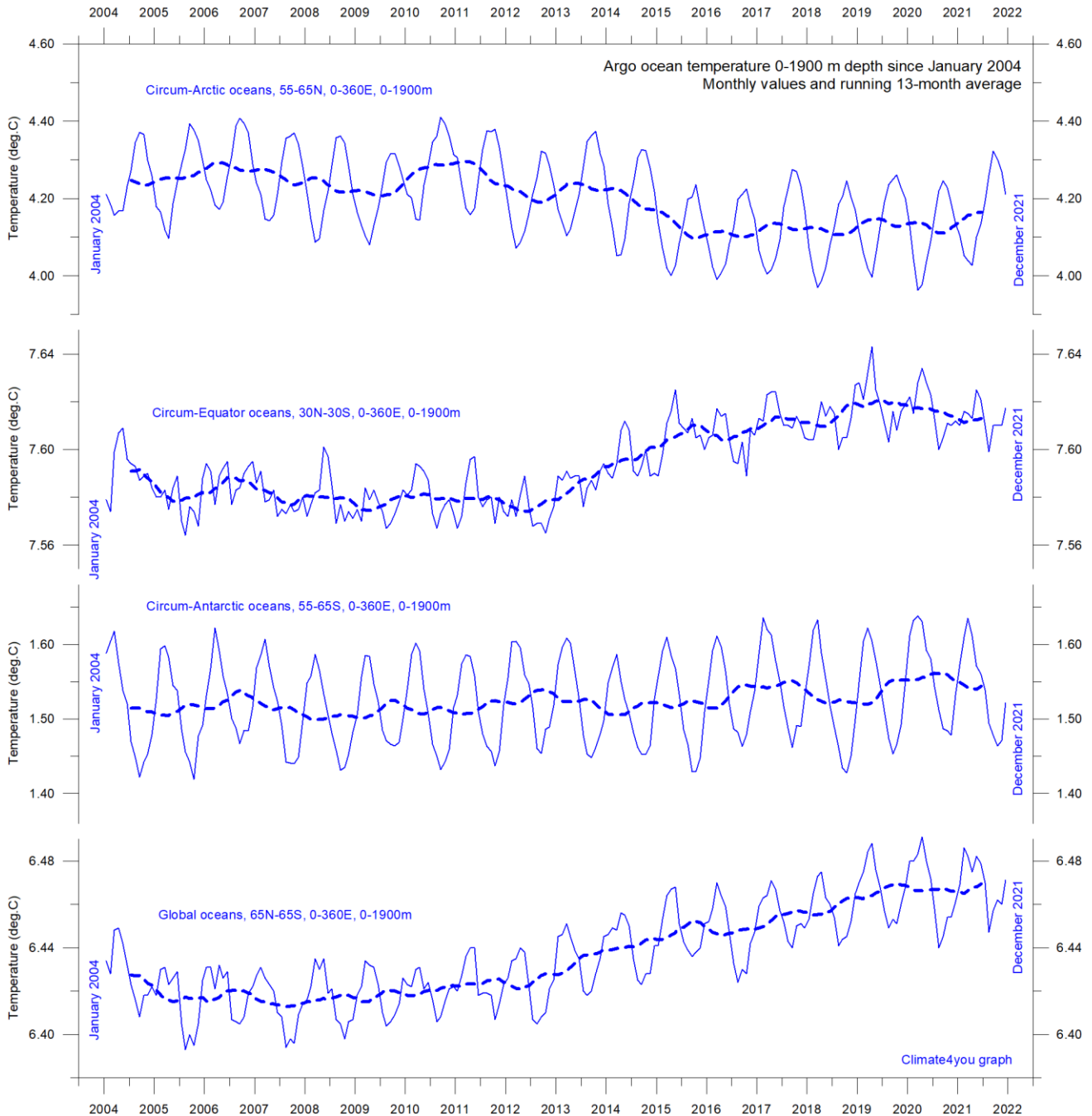
Time series depth-temperature diagram along 59 N across the North Atlantic Current from 30°W to 0°W, from surface to 800 m depth. Source: [Global Marine Argo Atlas](#). See also the diagram below.

22



Average temperature along 59 N, 30-0W, 0-800m depth, corresponding to the main part of the North Atlantic Current, using [Argo](#)-data. Source: [Global Marine Argo Atlas](#). Additional information can be found in: Roemmich, D. and J. Gilson, 2009. The 2004-2008 mean and annual cycle of temperature, salinity, and steric height in the global ocean from the Argo Program. [Progress in Oceanography](#), 82, 81-100.

Global ocean temperature 0-1900 m depth summary, updated to December 2021



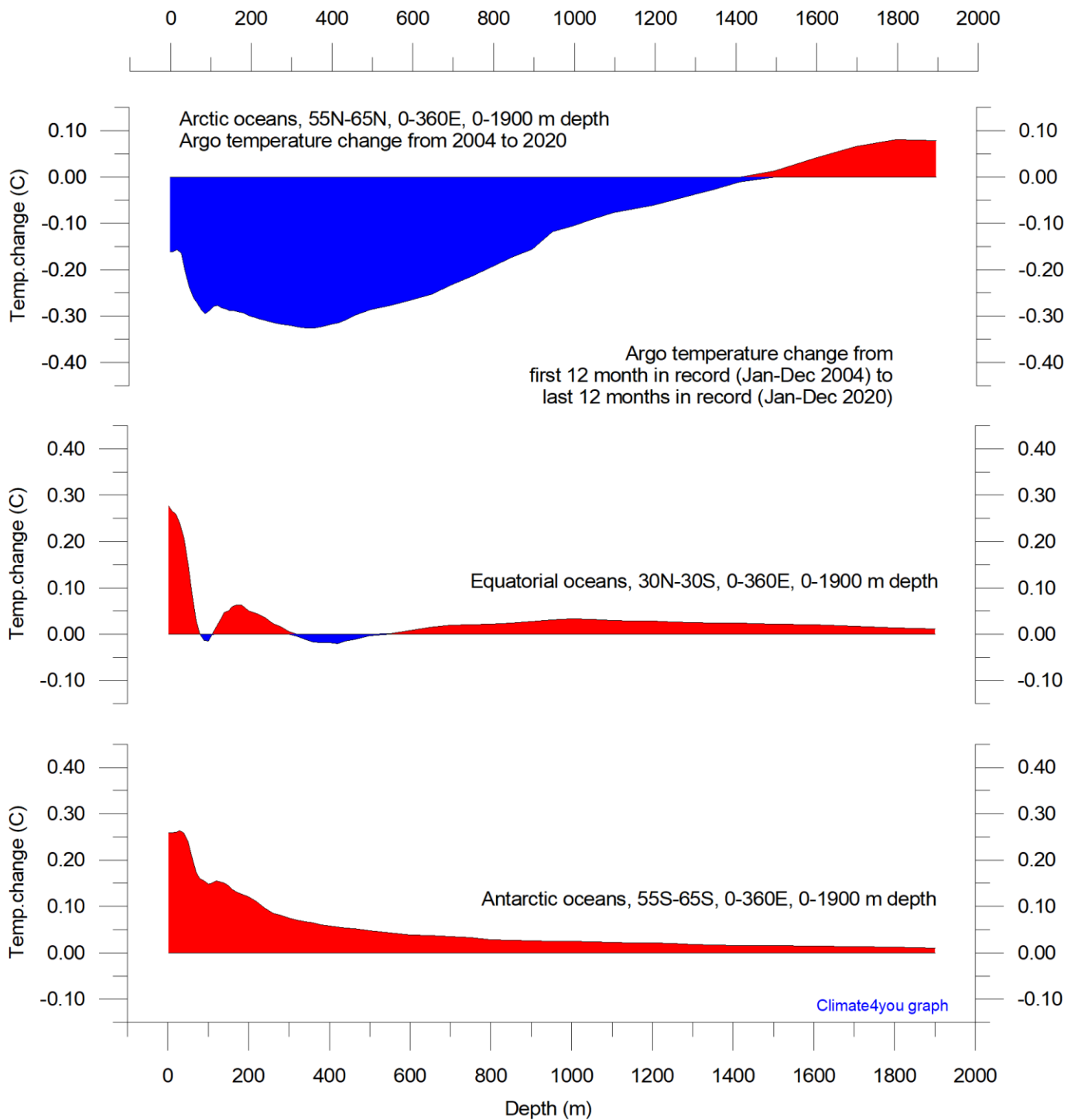
23

Summary of average temperature in uppermost 1900 m in different parts of the global oceans, using [Argo](#)-data. Source: [Global Marine Argo Atlas](#). Additional information can be found in: Roemmich, D. and J. Gilson, 2009. The 2004-2008 mean and annual cycle of temperature, salinity, and steric height in the global ocean from the Argo Program. [Progress in Oceanography](#), 82, 81-100.

The temperature of the global oceans down to 1900 m depth has been increasing since about 2011, but with a possible peak around 2020. The global increase since 2013 is mainly due to changes occurring near the Equator, between 30°N and 30°S. In contrast, for the circum-Arctic

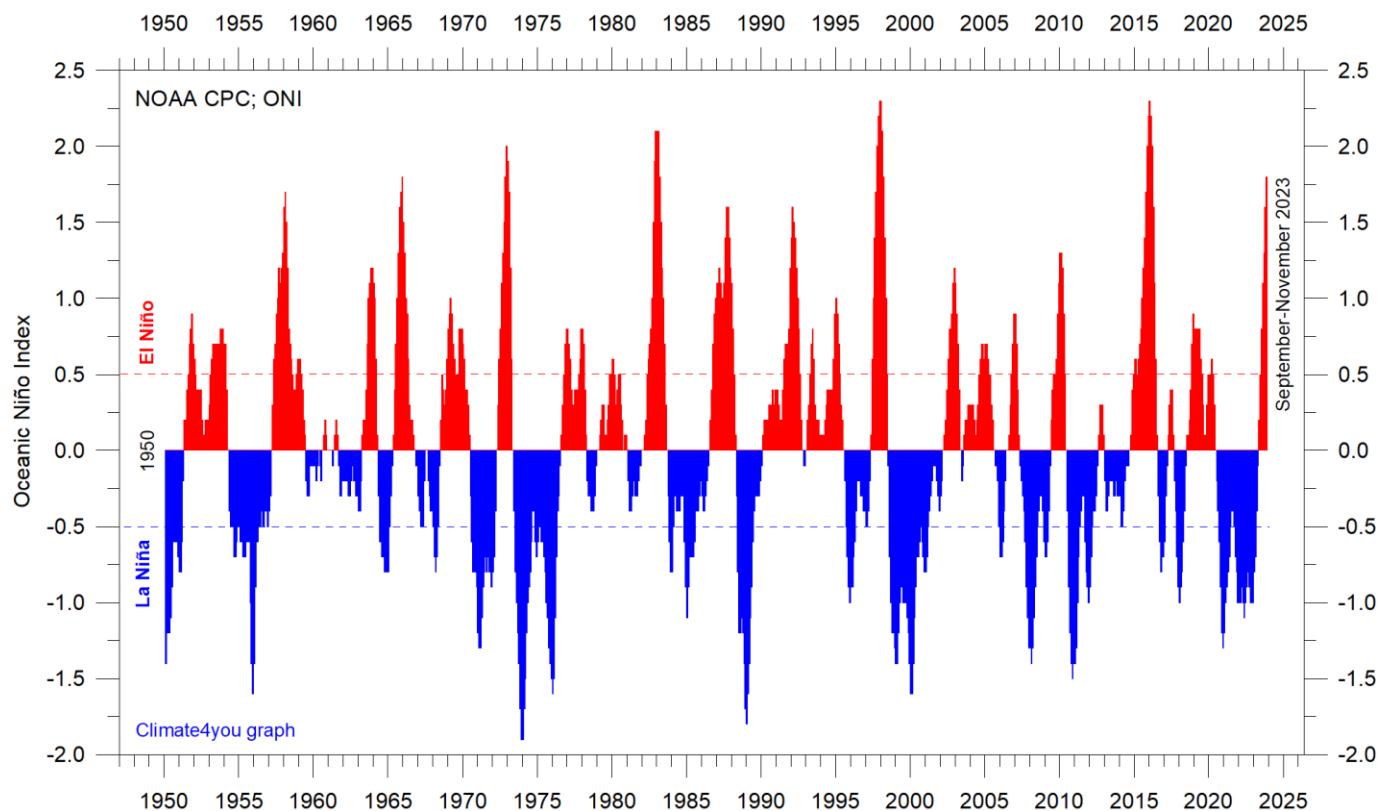
oceans north of 55°N, depth-integrated ocean temperatures have been decreasing since 2011, but with a possible low around 2019. Near the Antarctic, south of 55°S, temperatures have essentially been stable. At most latitudes, a clear annual rhythm is evident.

Global ocean net temperature change since 2004 at different depths, updated to December 2020



Net temperature change since 2004 from surface to 1900 m depth in different parts of the global oceans, using [Argo](#)-data. Source: [Global Marine Argo Atlas](#). Additional information can be found in: Roemmich, D. and J. Gilson, 2009. The 2004-2008 mean and annual cycle of temperature, salinity, and steric height in the global ocean from the Argo Program. [Progress in Oceanography](#), 82, 81-100. Please note that due to the spherical form of Earth, northern and southern latitudes represent only small ocean volumes, compared to latitudes near the Equator.

La Niña and El Niño episodes, Oceanic Niño Index (ONI), updated to November 2023



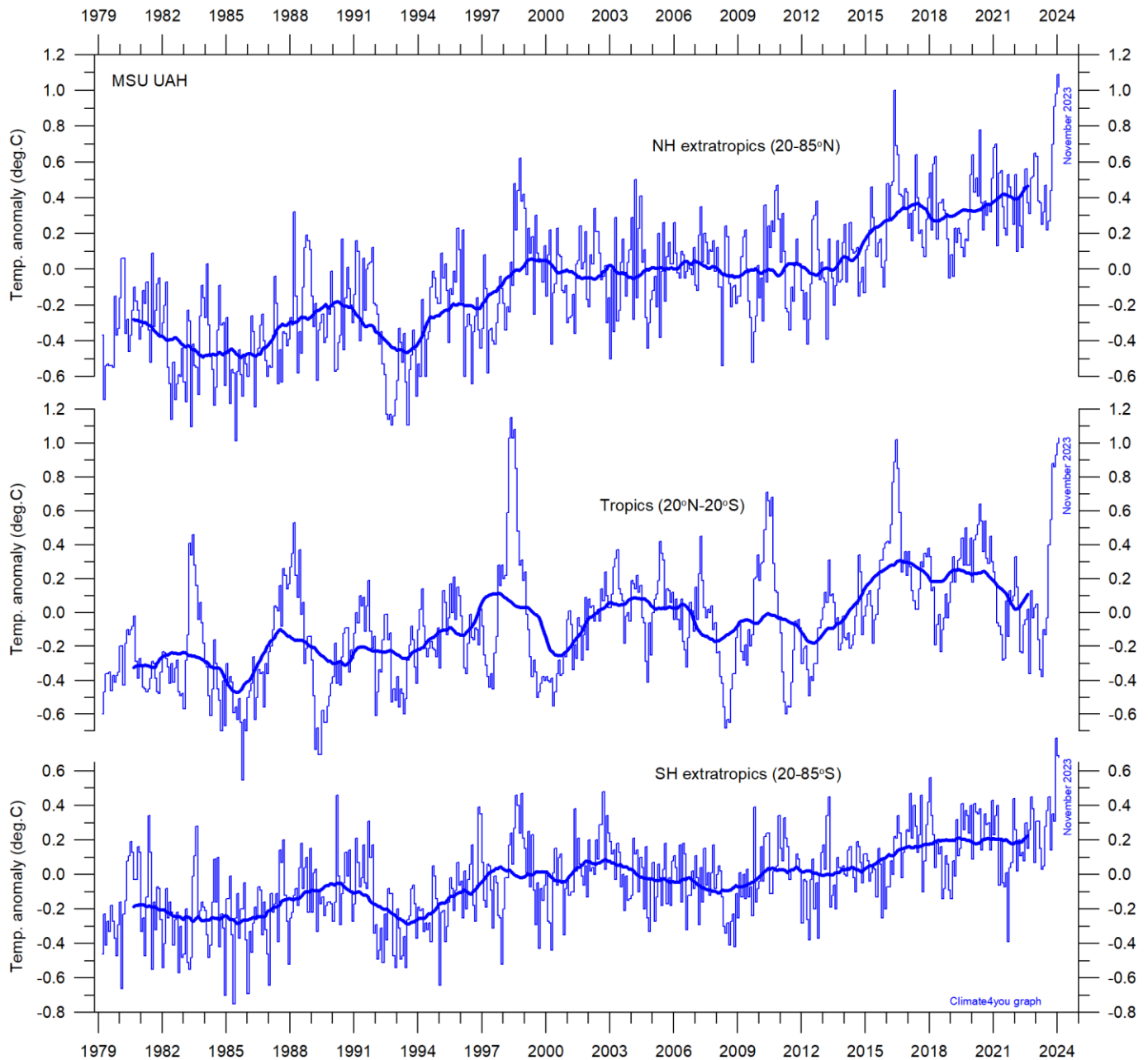
25

Warm ($>+0.5^{\circ}\text{C}$) and cold ($<-0.5^{\circ}\text{C}$) episodes for the [Oceanic Niño Index \(ONI\)](#), defined as 3 month running mean of ERSSTv4 SST anomalies in the Niño 3.4 region (5°N - 5°S , 120° - 170°W). For historical purposes cold and warm episodes are defined when the threshold is met for a minimum of 5 consecutive over-lapping seasons. Anomalies are centred on 30-yr base periods updated every 5 years.

The 2015-16 El Niño episode is among the strongest since the beginning of the record in 1950. Considering the entire record, however, recent variations

between El Niño and La Niña episodes do not appear abnormal in any way. See also diagrams on pages 44 and 53.

Zonal lower troposphere temperatures from satellites, updated to November 2023

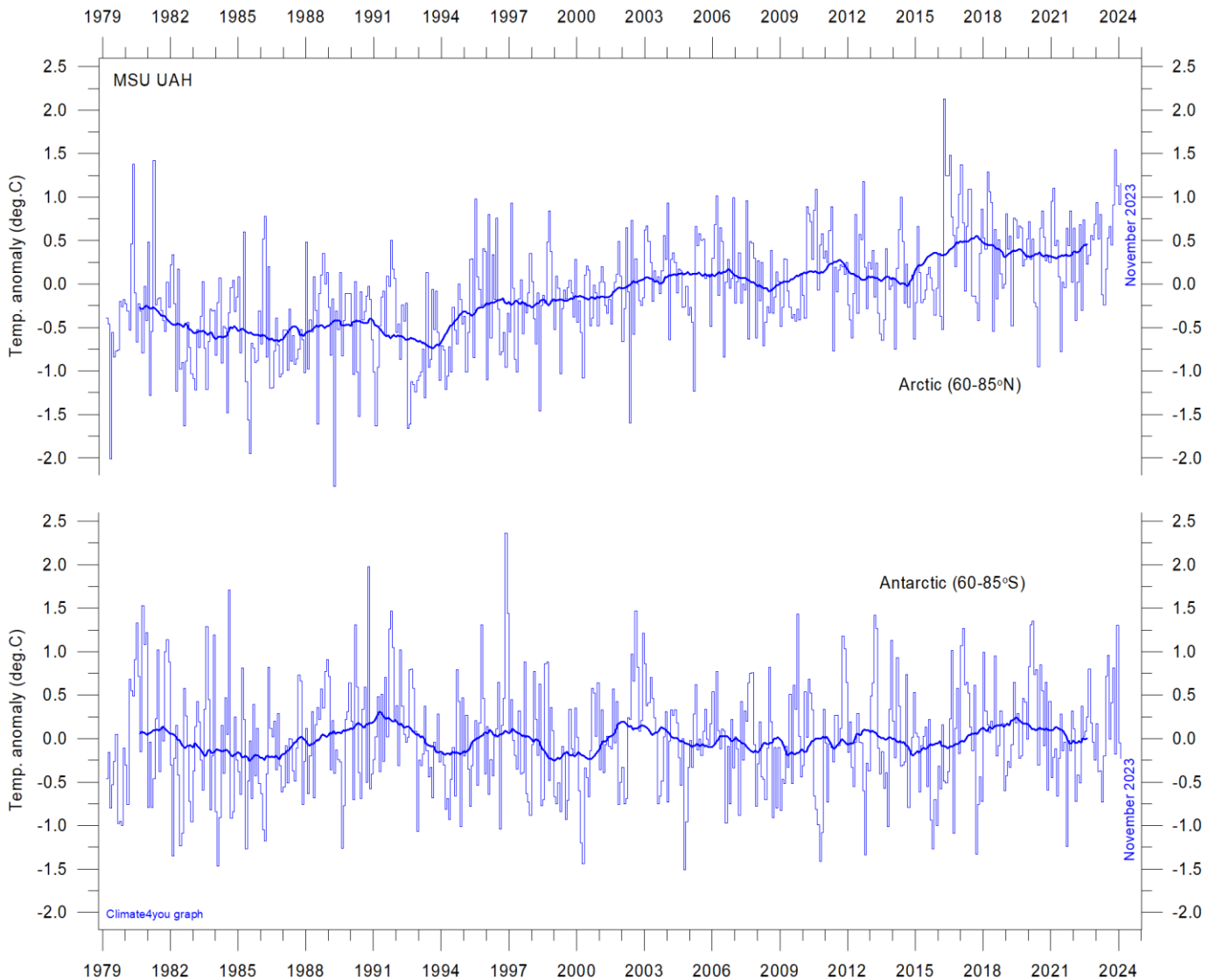


Global monthly average lower troposphere temperature since 1979 for the tropics and the northern and southern extratropics, according to University of Alabama at Huntsville, USA. Thin lines show the monthly temperature. Thick lines represent the simple running 37-month average, nearly corresponding to a running 3-year average. Reference period 1981-2010.

The overall warming since 1980 has dominantly been a northern hemisphere phenomenon, and mainly played out as a marked change between 1994 and 1999. However, this rather rapid temperature change is probably influenced by the Mt. Pinatubo eruption 1992-93 and the subsequent 1997 El Niño episode. The diagram also shows the

temperature effects of the strong Equatorial El Niño's in 1997 and 2015-16, as well as the moderate El Niño in 2019. Apparently, these effects were spreading to higher latitudes in both hemispheres with some delay. Just now a new El Niño has begun in the Pacific Ocean (p.25), as indicated by tropics surface air temperatures.

Arctic and Antarctic lower troposphere temperature, updated to November 2023



Global monthly average lower troposphere temperature since 1979 for the North Pole and South Pole regions, based on satellite observations ([University of Alabama](#) at Huntsville, USA). Thin lines show the monthly temperature. The thick line is the simple running 37-month average, nearly corresponding to a running 3-year average. Reference period 1991-2020.

In the Arctic region, warming mainly took place 1994-96, and less so subsequently. In 2016, however, temperatures peaked for several months, presumably because of oceanic heat given off to the atmosphere during the 2015-15 El Niño (see also diagram on page 25) and subsequently advected to higher latitudes.

This underscores how Arctic air temperatures may be affected not only by variations in local conditions but also by variations playing out in geographically remote regions.

A slight temperature decrease has characterised the Arctic since the marked 2016 El Niño peak. In contrast, the present (2023) El Niño episode is recorded by Arctic temperatures in a less pronounced way.

In the Antarctic region, temperatures have basically remained stable since the onset of the satellite record in 1979. In 2016-17 a small temperature peak visible in the monthly record may be interpreted as the subdued effect of the recent El Niño episode.

Arctic and Antarctic surface air temperature, updated to December 2021

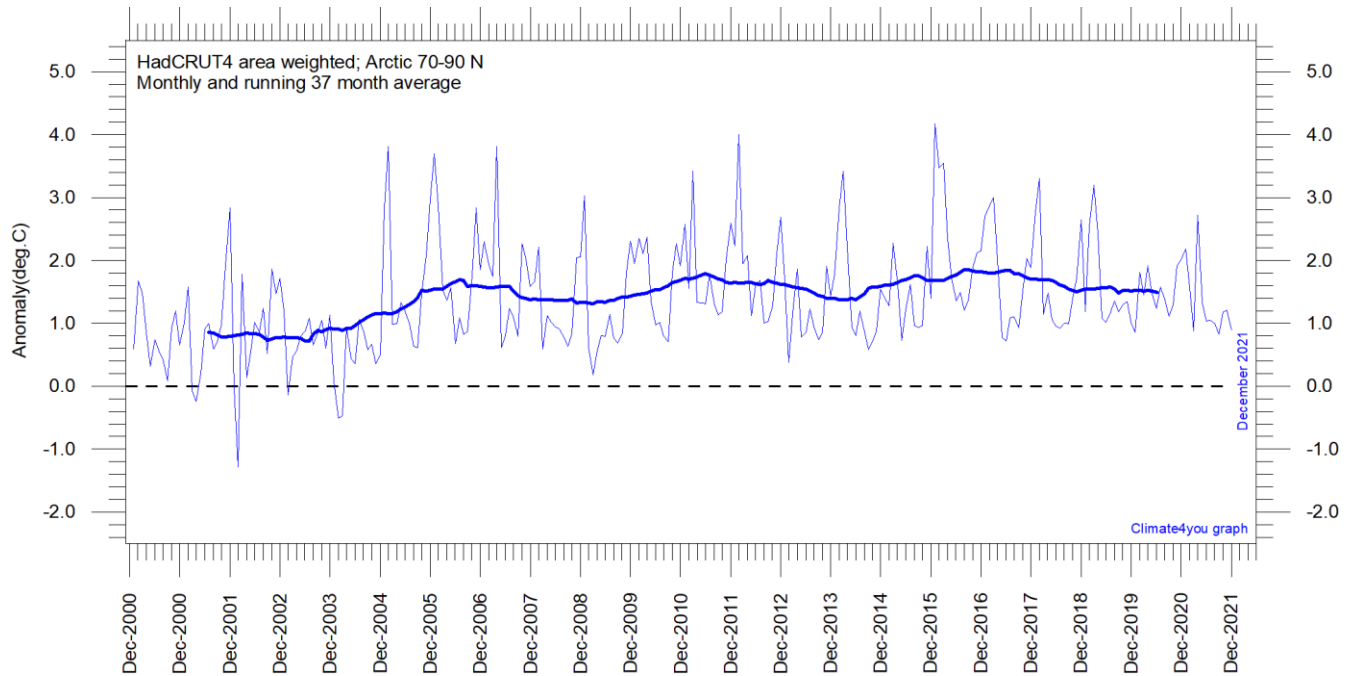


Diagram showing area weighted Arctic (70-90°N) monthly surface air temperature anomalies ([HadCRUT4](#)) since January 2000, in relation to the WMO [normal period](#) 1961-1990. The thin line shows the monthly temperature anomaly, while the thicker line shows the running 37-month (c. 3 year) average.

28

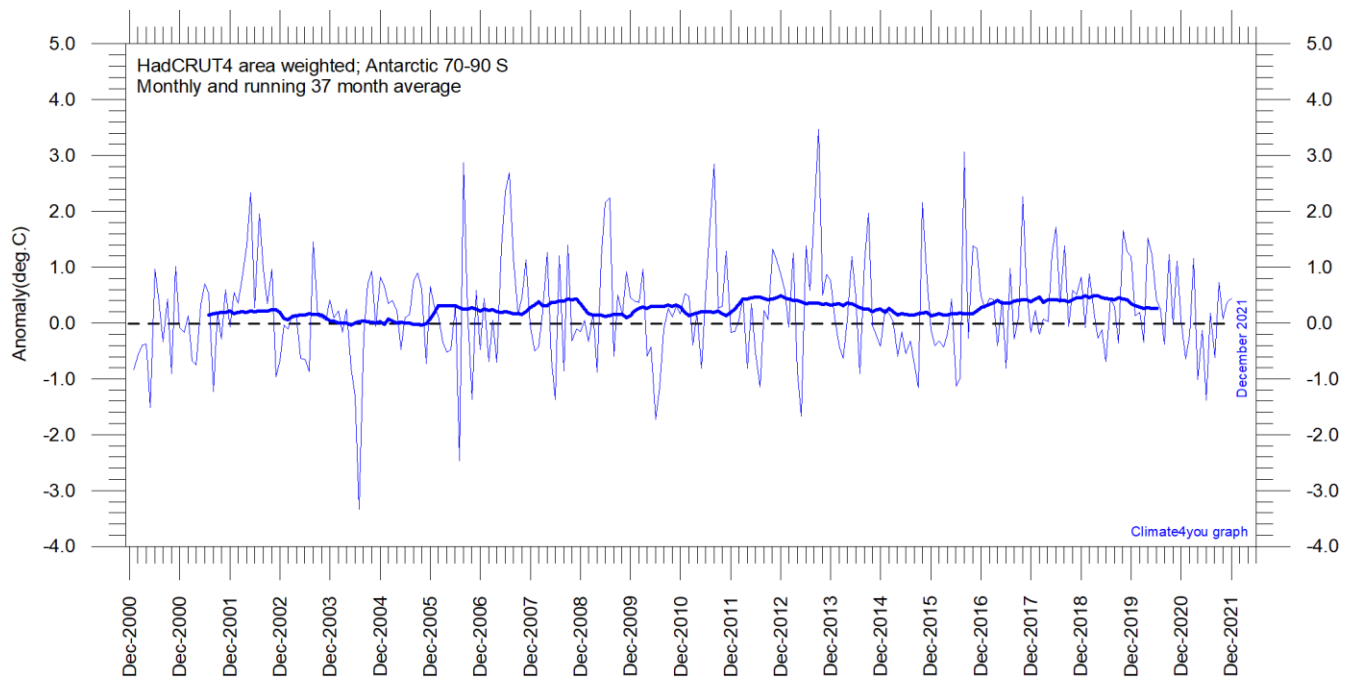


Diagram showing area weighted Antarctic (70-90°S) monthly surface air temperature anomalies ([HadCRUT4](#)) since January 2000, in relation to the WMO [normal period](#) 1961-1990. The thin line shows the monthly temperature anomaly, while the thicker line shows the running 37-month (c. 3 year) average.

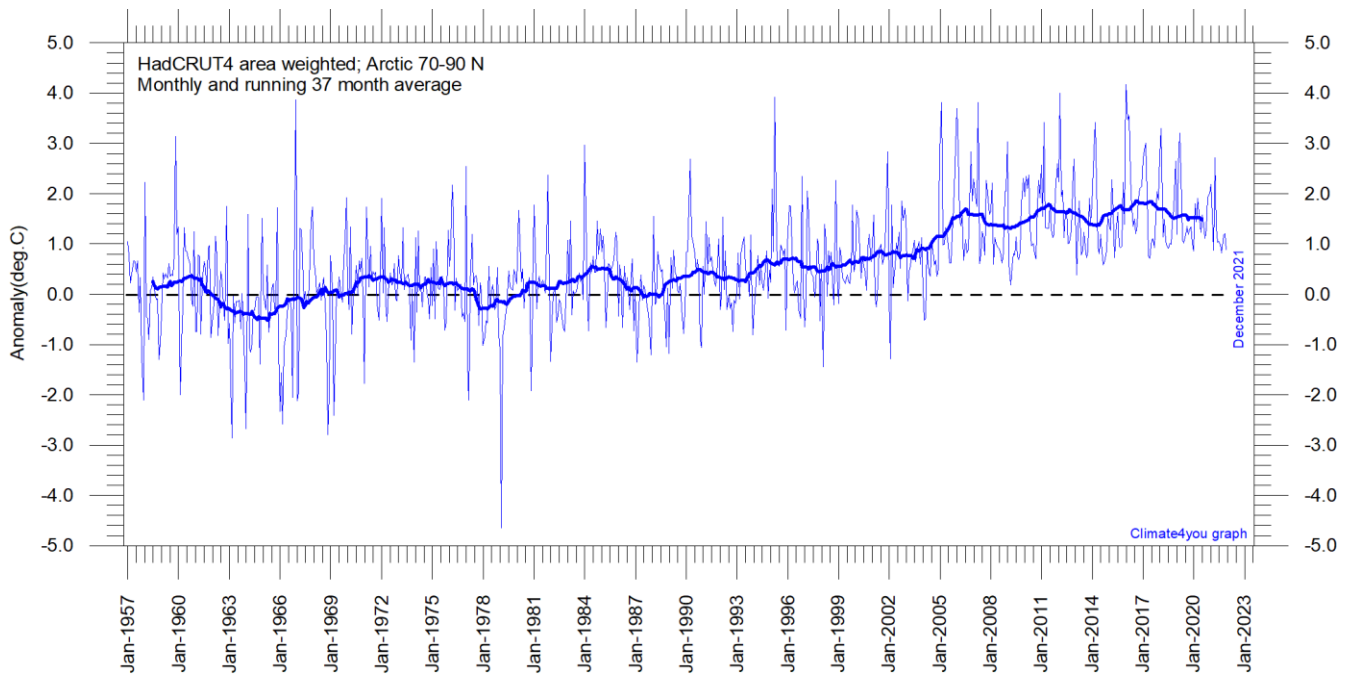


Diagram showing area weighted Arctic (70-90°N) monthly surface air temperature anomalies ([HadCRUT4](#)) since January 1957, in relation to the WMO [normal period](#) 1961-1990. The thin line shows the monthly temperature anomaly, while the thicker line shows the running 37-month (c. 3 year) average.

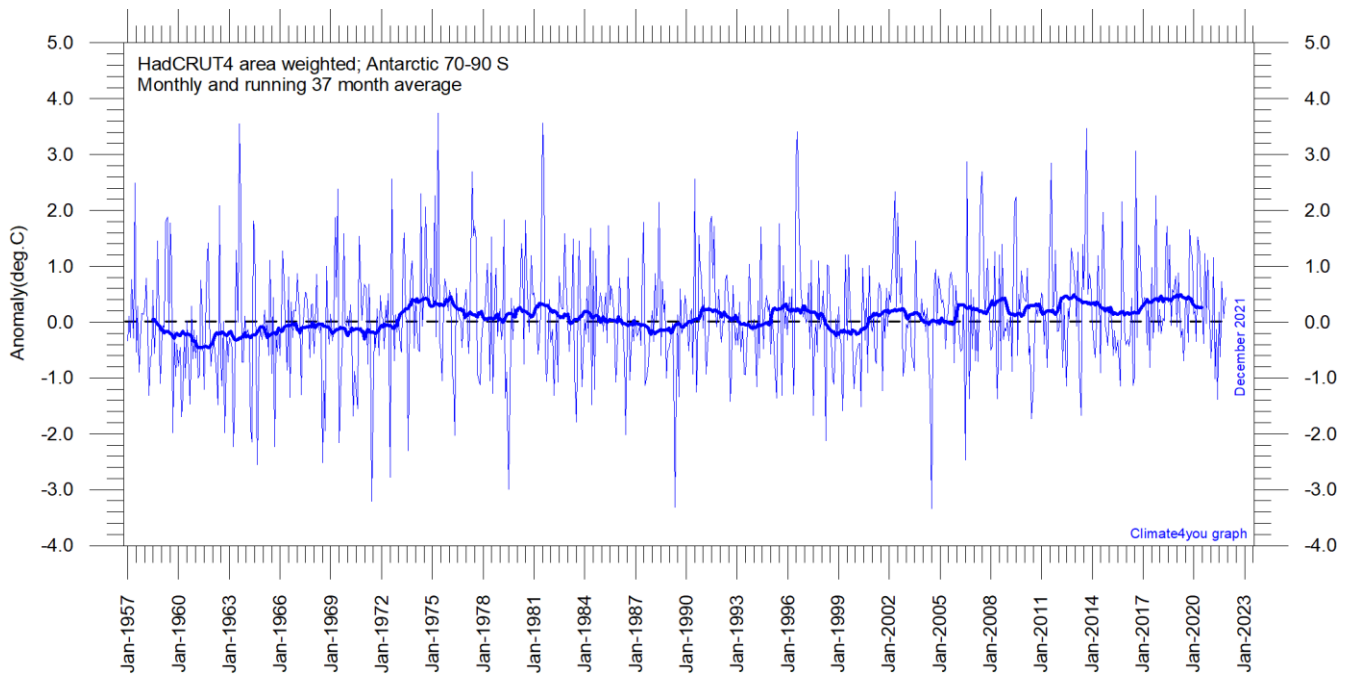


Diagram showing area weighted Antarctic (70-90°S) monthly surface air temperature anomalies ([HadCRUT4](#)) since January 1957, in relation to the WMO [normal period](#) 1961-1990. The thin line shows the monthly temperature anomaly, while the thicker line shows the running 37-month (c. 3 year) average.

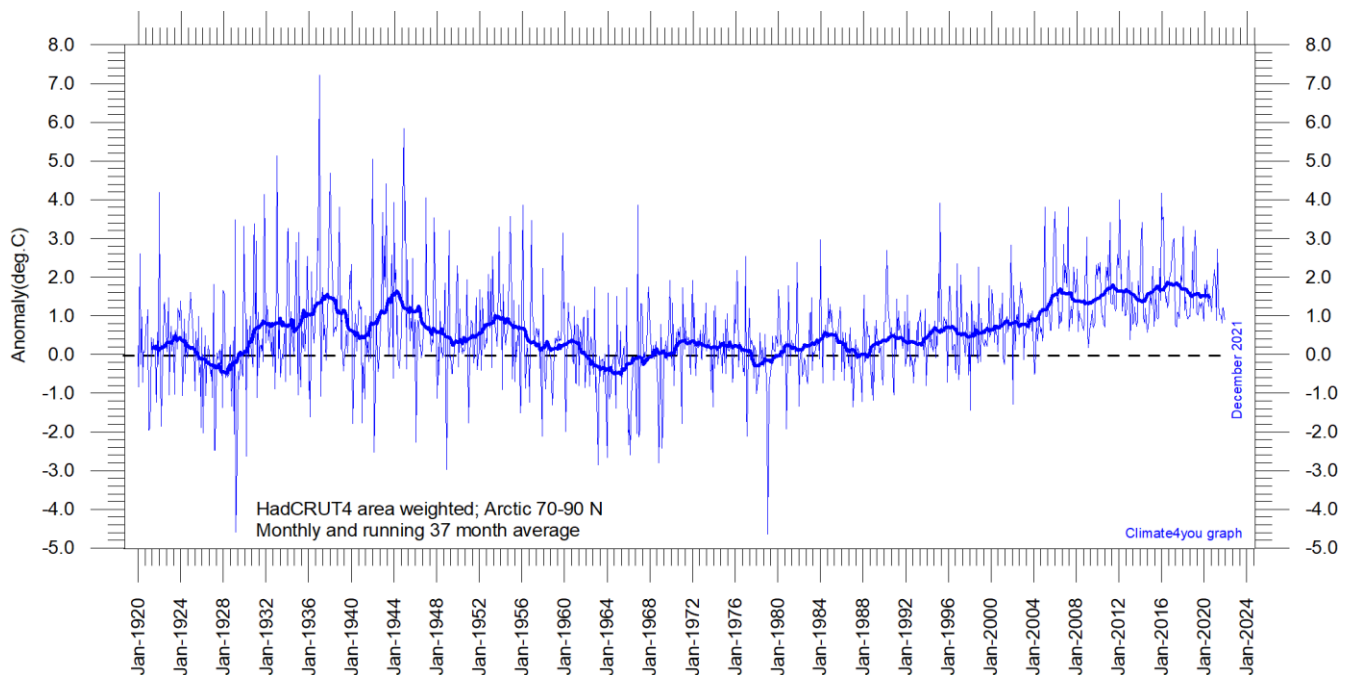


Diagram showing area-weighted Arctic (70-90°N) monthly surface air temperature anomalies ([HadCRUT4](#)) since January 1920, in relation to the WMO [normal period](#) 1961-1990. The thin line shows the monthly temperature anomaly, while the thicker line shows the running 37-month (c. 3 year) average.

Because of the relatively small number of Arctic stations before 1930, month-to-month variations in the early part of the Arctic temperature record 1920-2018 are higher than later (diagram above).

The period from about 1930 saw the establishment of many new Arctic meteorological stations, first in Russia and Siberia, and following the 2nd World War, also in North America, explaining the above difference.

The period since 2005 is warm, about as warm as the period 1930-1940.

As the HadCRUT4 data series has improved high latitude coverage data coverage (compared to the HadCRUT3 series), the individual 5°x5° grid cells have been weighted according to their surface area. This area correction is especially important for polar

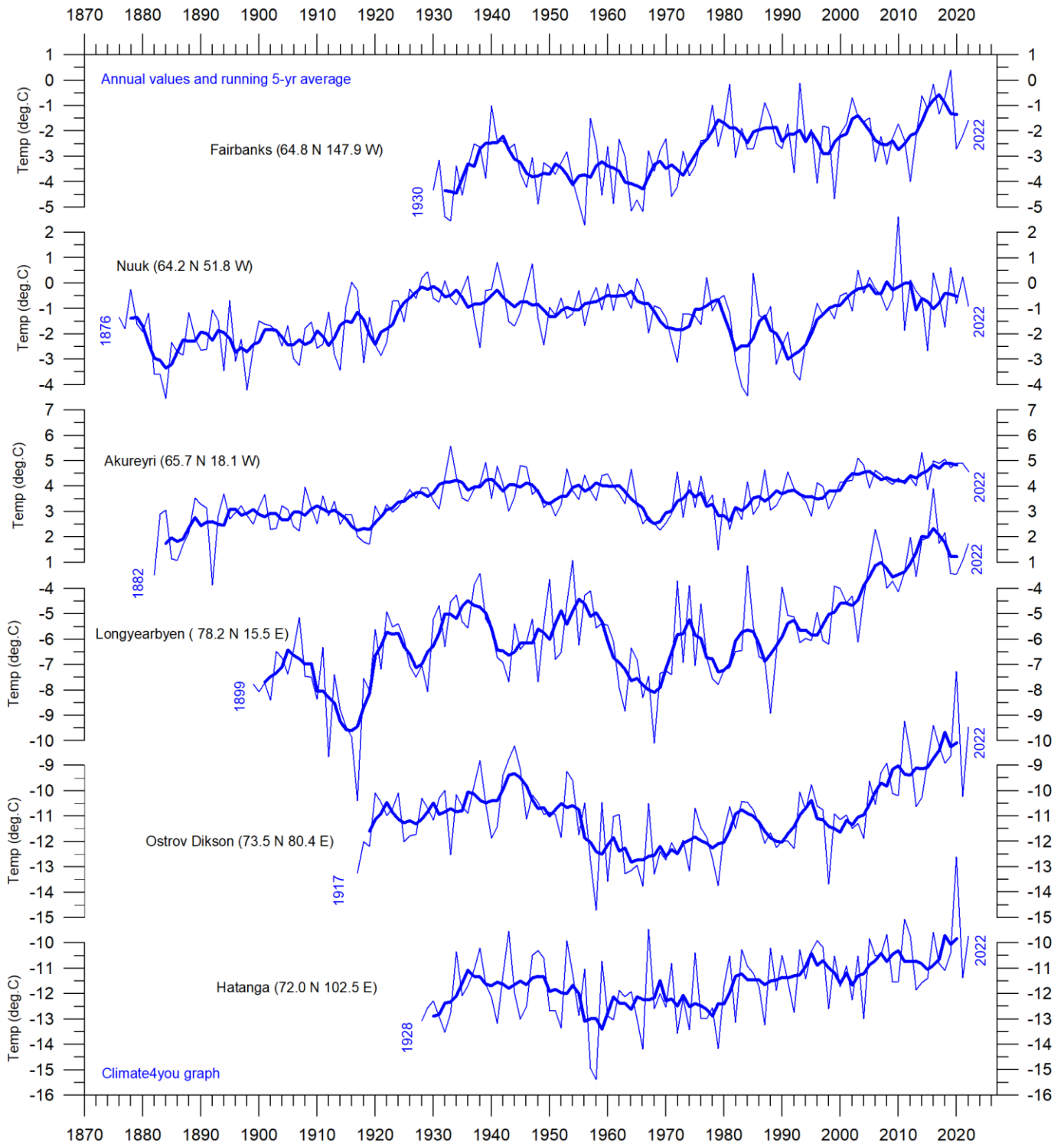
regions, where longitudes converge rapidly. This approach differs from the approach used by Gillett et al. 2008, which calculated a simple average, with no correction for the substantial latitudinal surface area effect in polar regions.

The area weighted Arctic HadCRUT4 surface air temperature anomalies (p.28-30) correspond rather well to the lower troposphere temperature anomalies recorded by satellites (p.27).

Literature:

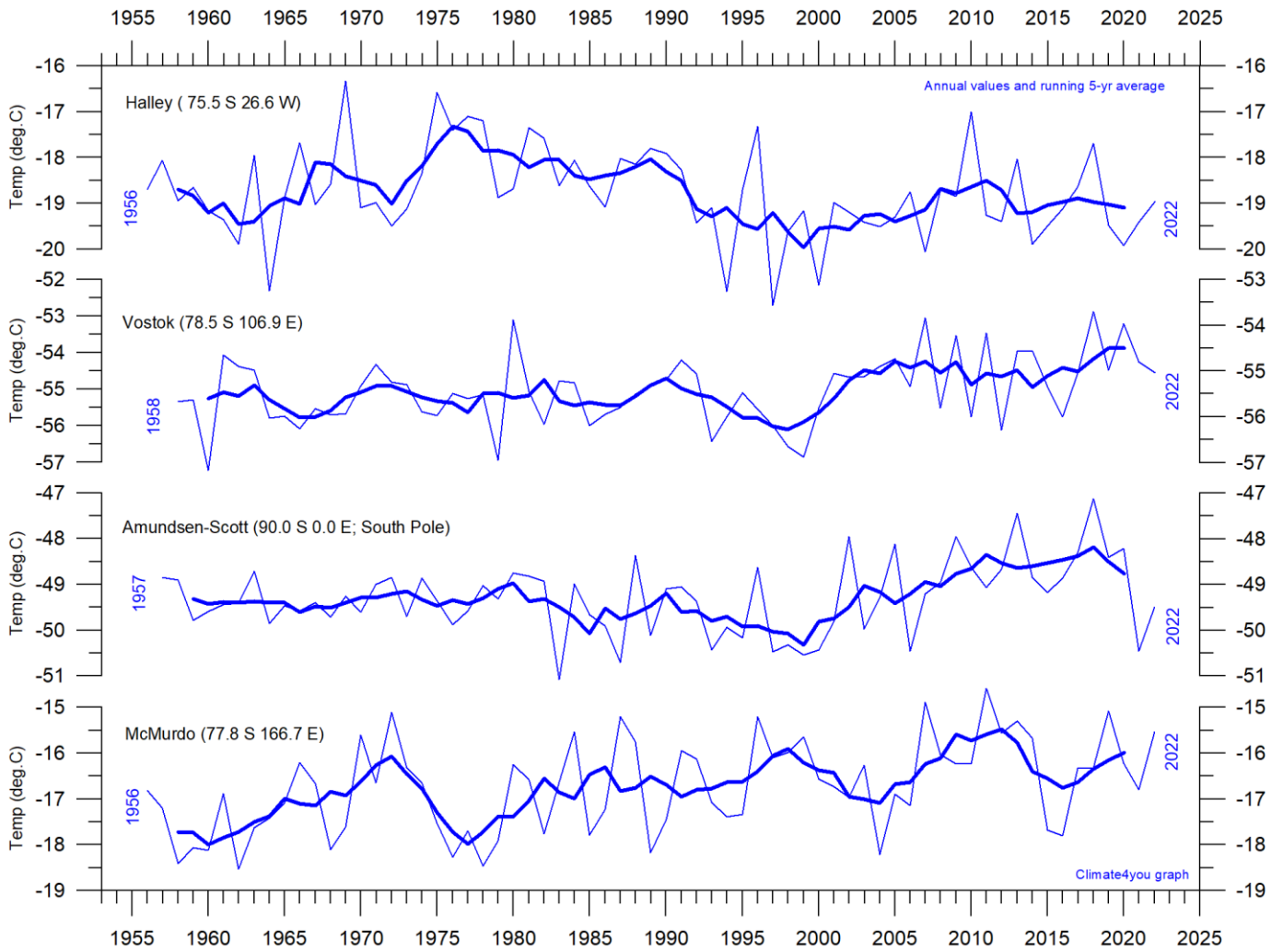
Gillett, N.P., Stone, D.A., Stott, P.A., Nozawa, T., Karpechko, A.Y.U., Hegerl, G.C., Wehner, M.F. and Jones, P.D. 2008. Attribution of polar warming to human influence. *Nature Geoscience* 1, 750-754.

Long Arctic annual surface air temperature series, updated to year 2022



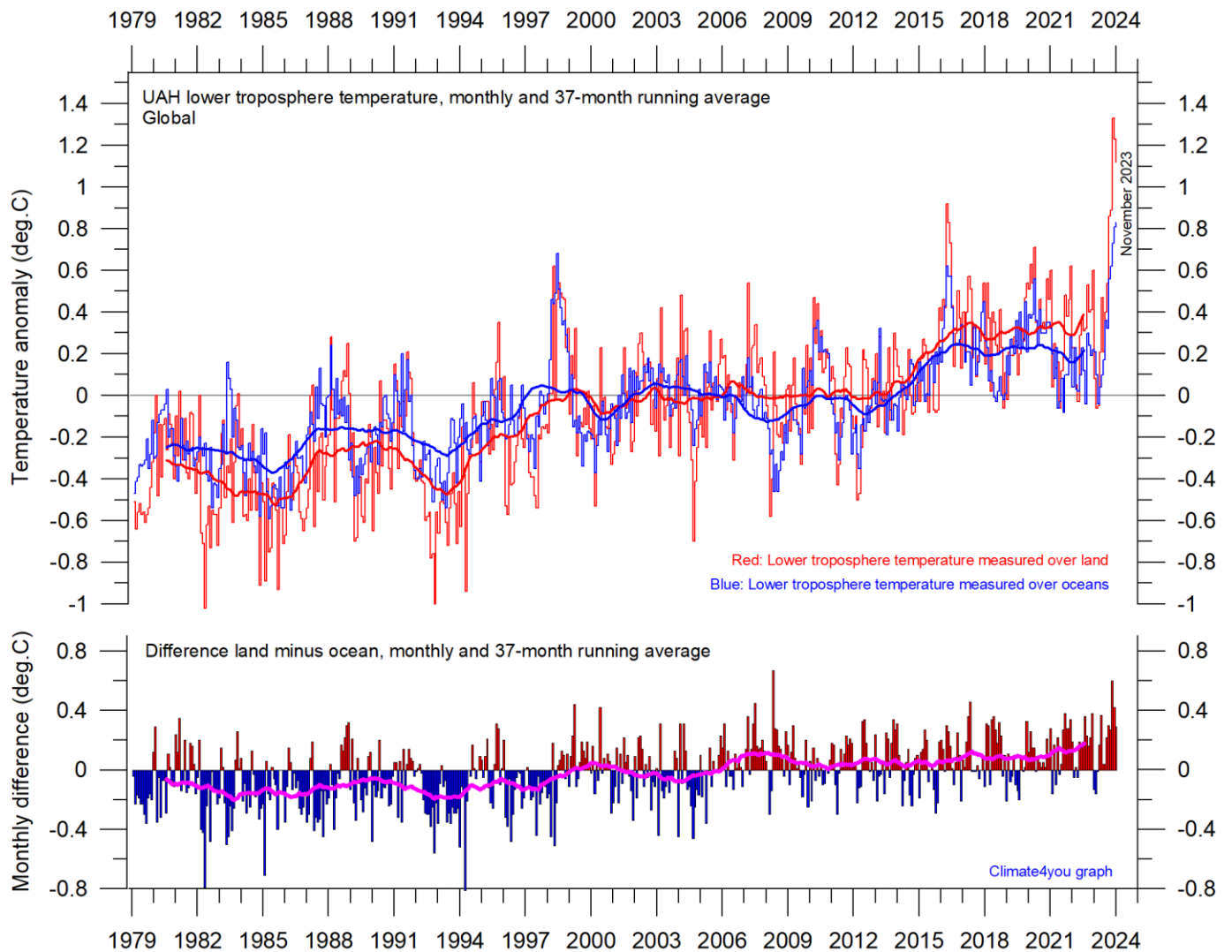
Arctic annual surface air temperature series, selected because of their length of observation time. The thin blue line represents the mean annual air temperature, and the thick blue line is the running 5-year average. Annual values were calculated from monthly average temperatures. More info on [Climate4you](#).

Long Antarctic annual surface air temperature series, updated to year 2022



Antarctic annual surface air temperature series, selected because of their length of observation time. The thin blue line represents the mean annual air temperature, and the thick blue line is the running 5-year average. Annual values were calculated from monthly average temperatures. More info on [Climate4you](https://climate4you.com).

Temperature over land versus over oceans, updated to November 2023

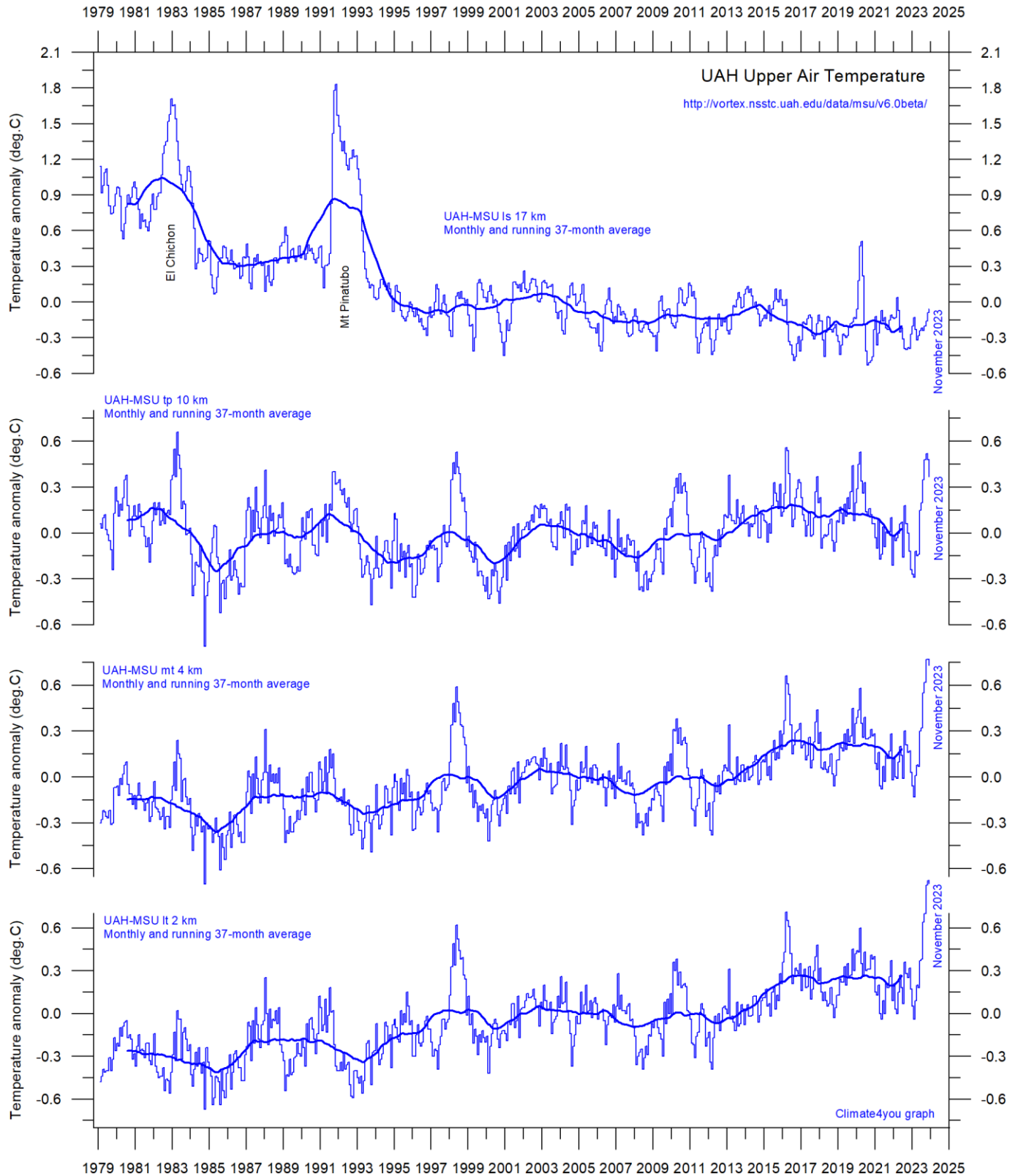


Global monthly average lower troposphere temperature since 1979 measured over land and oceans, respectively, according to [University of Alabama](#) at Huntsville, USA. Thick lines are the simple running 37-month average, nearly corresponding to a running 3-year average. Reference period 1991-2020.

Since 1979, the lower troposphere over land has warmed much more than over oceans, suggesting that the overall warming is derived mainly from incoming solar radiation. In addition, there may be supplementary reasons for this divergence, such as, e.g., variations in cloud cover and changes in land use.

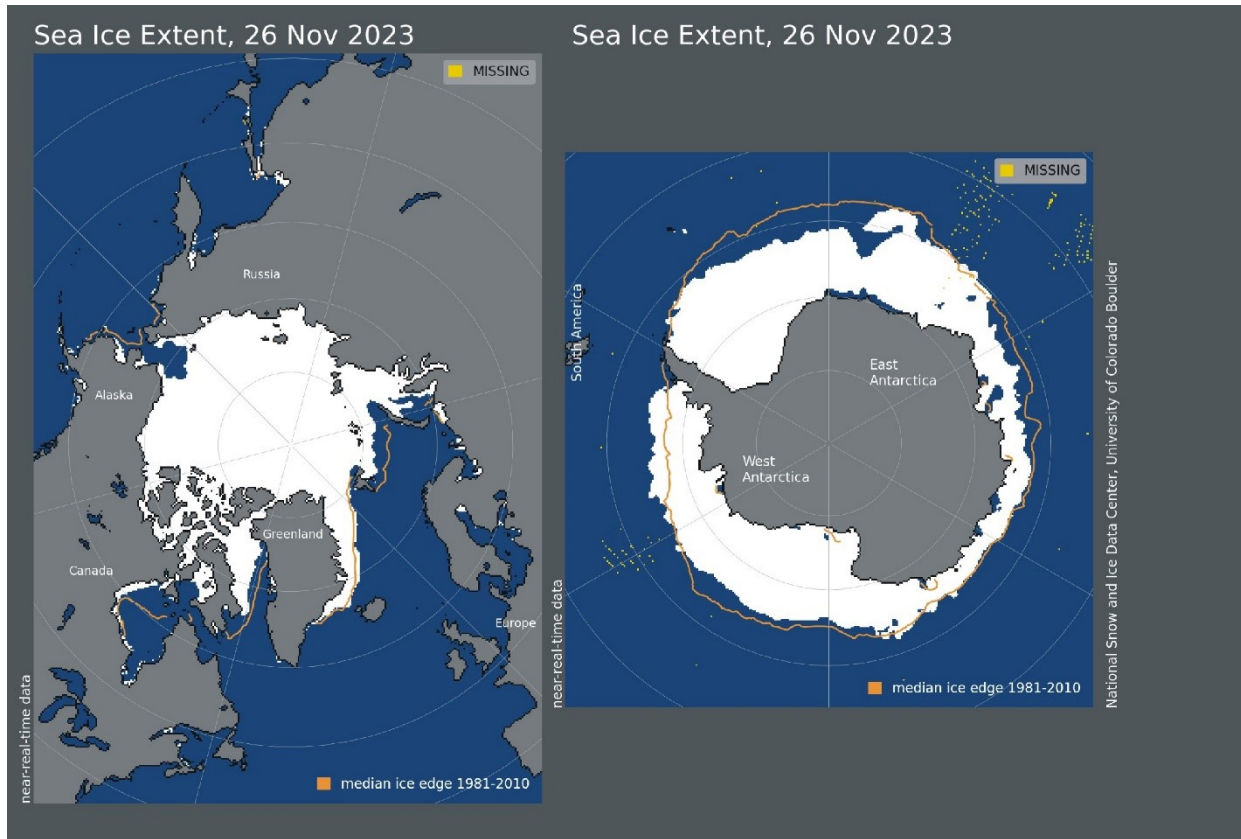
The present (2023) El Niño episode is recorded more pronounced over land regions, compared to ocean regions.

Troposphere and stratosphere temperatures from satellites, updated to November 2023



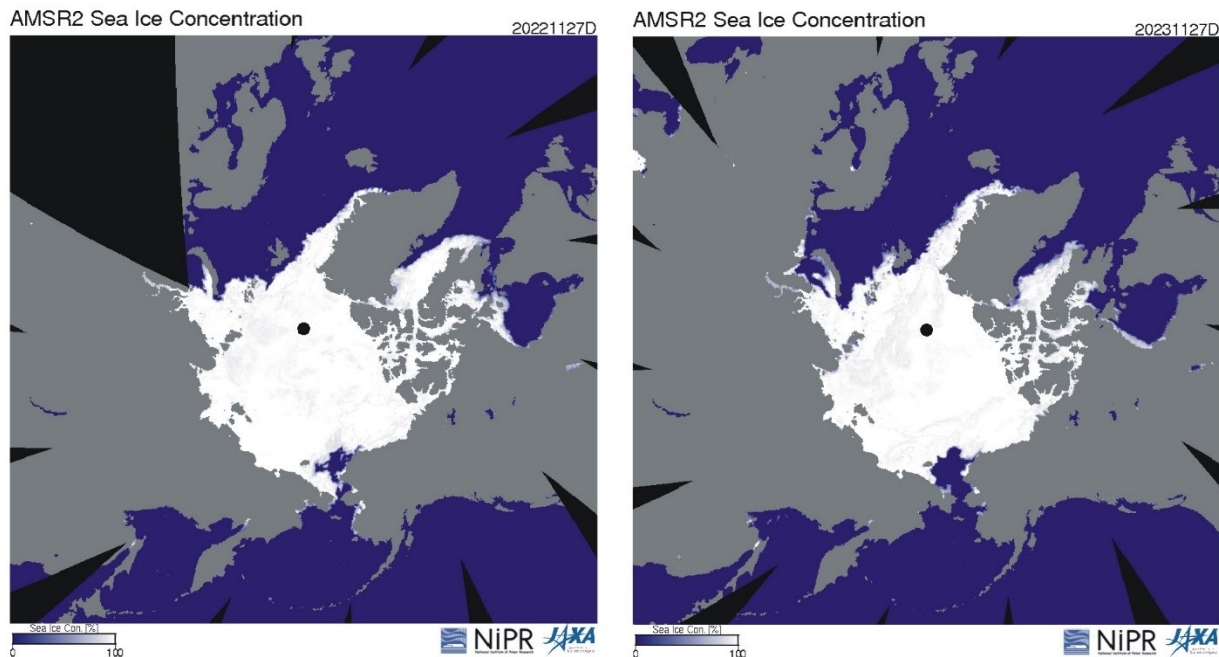
Global monthly average temperature in different according to University of Alabama at Huntsville, USA. The thin lines represent the monthly average, and the thick line the simple running 37-month average, nearly corresponding to a running 3-year average. Reference period 1991-2020.

Arctic and Antarctic sea ice, updated to November 2023

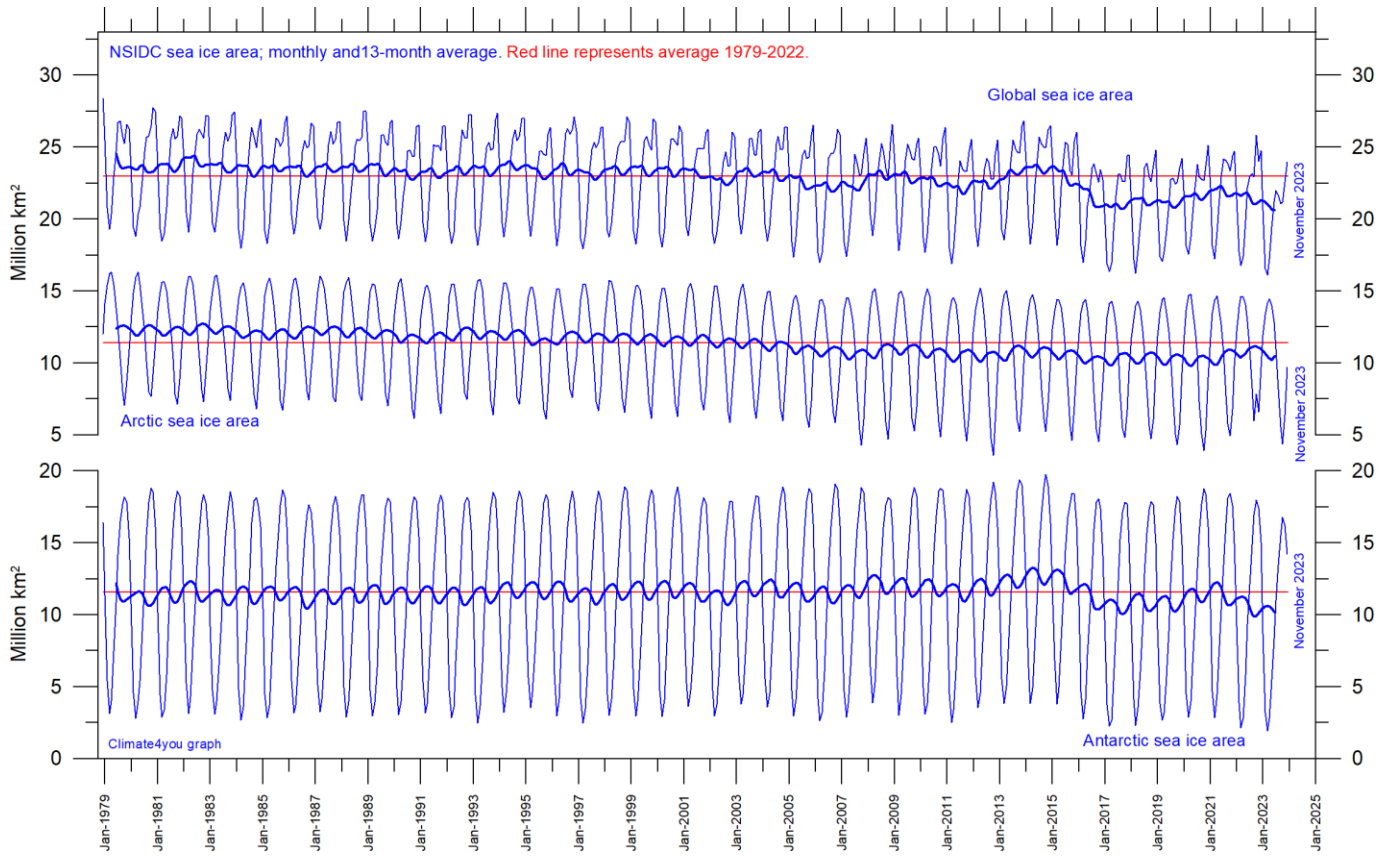


35

Sea ice extent 26 November 2023. The median limit of sea ice (orange line) is defined as 15% sea ice cover, according to the average of satellite observations 1981-2010 (both years included). Sea ice may therefore well be encountered outside and open water areas inside the limit shown in the diagrams above. Map source: National Snow and Ice Data Center (NSIDC).



Diagrams showing Arctic sea ice extent and concentration 27 November 2022 (left) and 2023 (right), according to the Japan Aerospace Exploration Agency (JAXA).



Graphs showing monthly Antarctic, Arctic, and global sea ice extent since November 1978, according to the [National Snow and Ice data Center \(NSIDC\)](#).

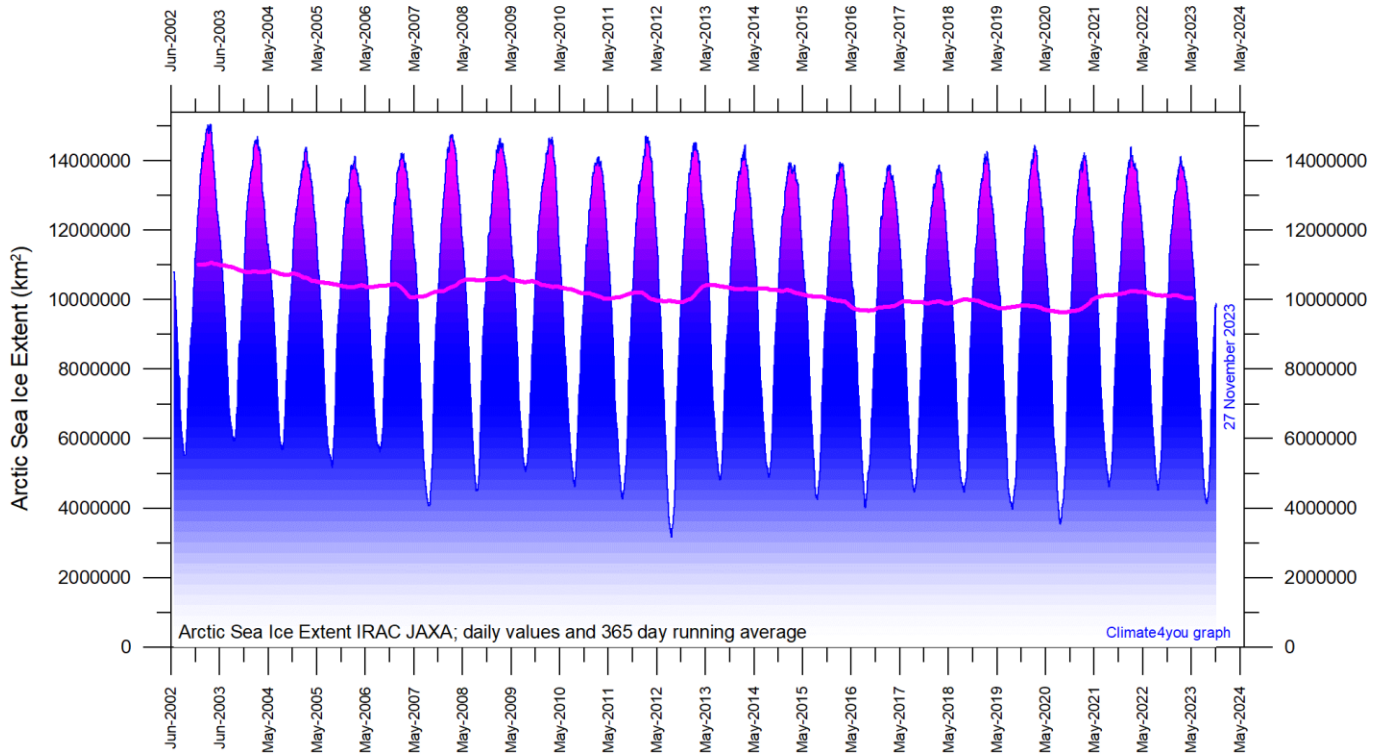
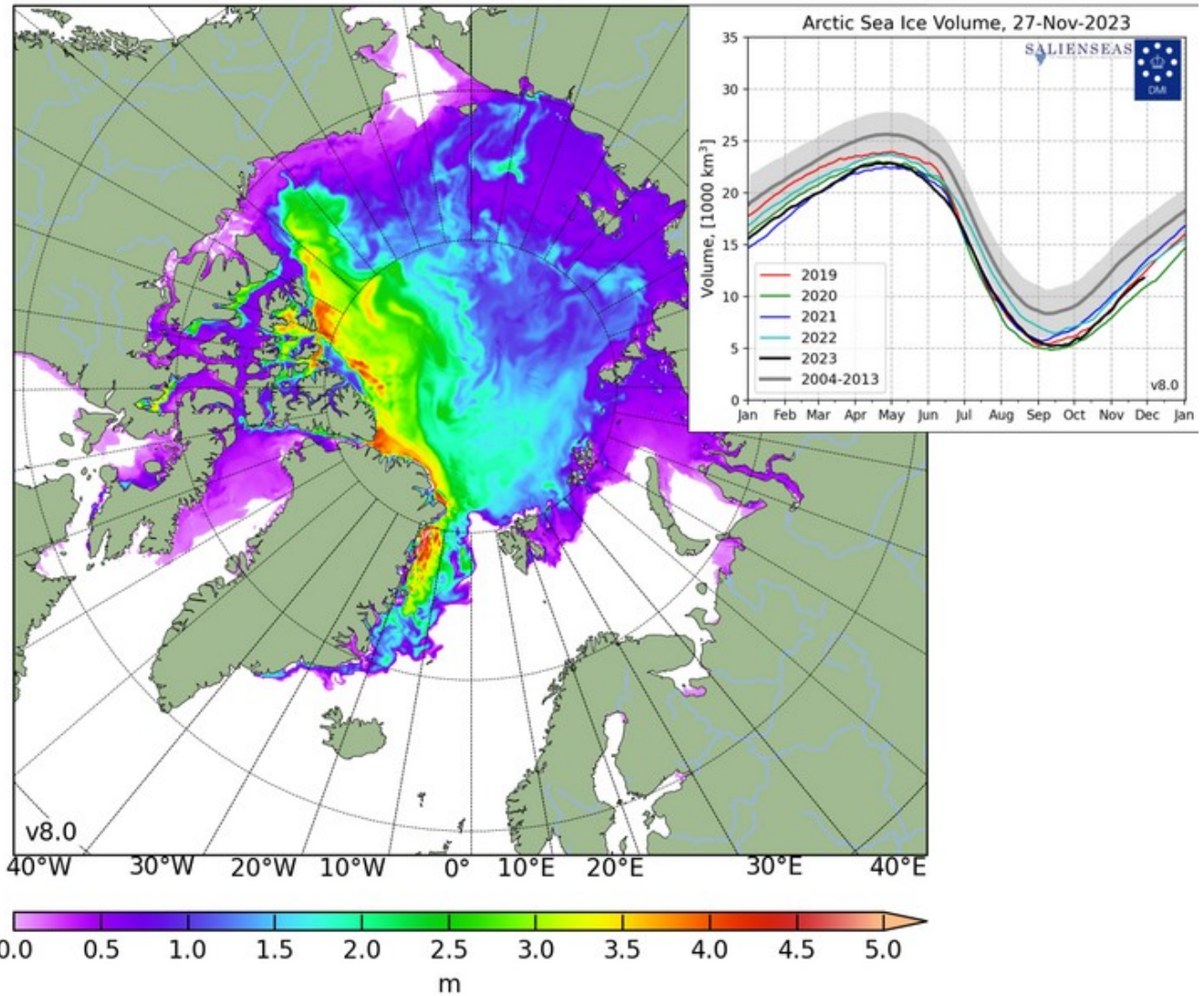
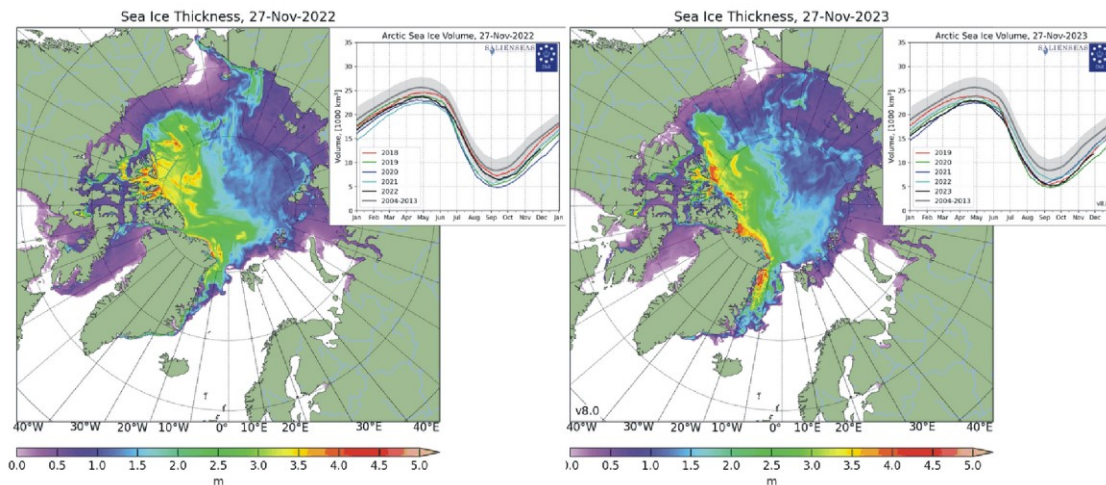


Diagram showing daily Arctic sea ice extent since June 2002, to 27 November 2023, data courtesy of [Japan Aerospace Exploration Agency \(JAXA\)](#).

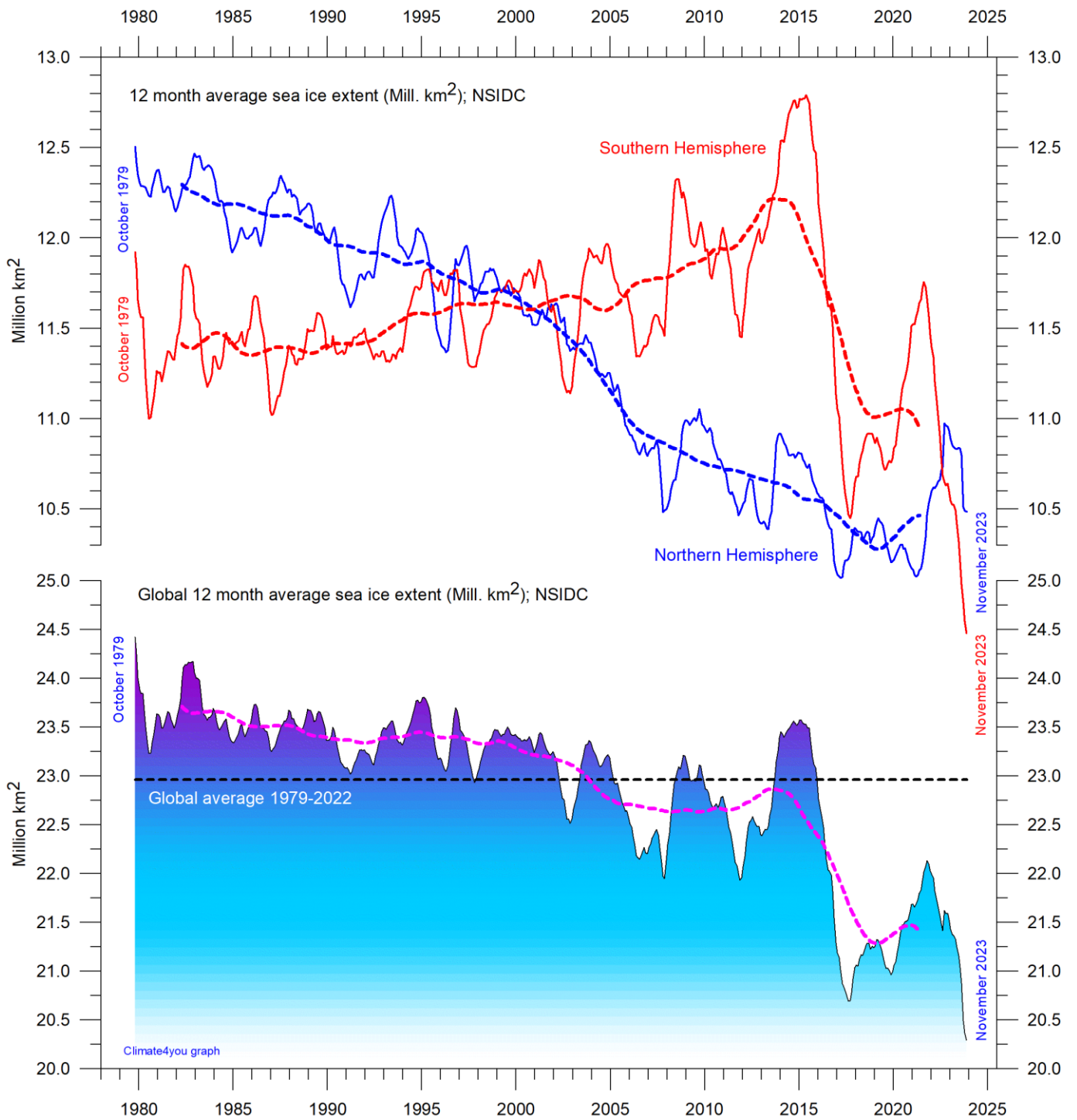
Sea Ice Thickness, 27-Nov-2023



37



Diagrams showing Arctic sea ice extent and thickness 27 November 2022 (left) and 2023 (right and above) and the seasonal cycles of the calculated total arctic sea ice volume, according to [The Danish Meteorological Institute \(DMI\)](http://www.dmi.dk/). The mean sea ice volume and standard deviation for the period 2004-2013 are shown by grey shading. Please note that DMI on 7 December 2021 changed their sea ice calculation model. DMI's description of the model version change can be read here: <http://polarportal.dk/en/sea-ice-and-icebergs/sea-ice-thickness-and-volume/>



12 month running average sea ice extension, global and in both hemispheres since 1979, the satellite-era. The October 1979 value represents the monthly 12-month average of November 1978 - October 1979, the November 1979 value represents the average of December 1978 - November 1979, etc. The stippled lines represent a 61-month (ca. 5 years) average. Data source: National Snow and Ice Data Center (NSIDC).

Sea level in general

Global (or eustatic) sea-level change is measured relative to an idealised reference level, the geoid, which is a mathematical model of planet Earth's surface (Carter et al. 2014). Global sea-level is a function of the volume of the ocean basins and the volume of water they contain. Changes in global sea-level are caused by – but not limited to - four main mechanisms:

1. Changes in local and regional air pressure and wind, and tidal changes introduced by the Moon.
2. Changes in ocean basin volume by tectonic (geological) forces.
3. Changes in ocean water density caused by variations in currents, water temperature and salinity.
4. Changes in the volume of water caused by changes in the mass balance of terrestrial glaciers.

In addition to these there are other mechanisms influencing sea-level, such as storage of ground water, storage in lakes and rivers, evaporation, etc.

Mechanism 1 is controlling sea-level at many sites on a time scale from months to several years. As an example, many coastal stations show a pronounced annual variation reflecting seasonal changes in air pressures and wind speed. Longer-term climatic changes playing out over decades or centuries will also affect measurements of sea-level changes. Hansen et al. (2011, 2015) provide excellent analyses of sea-level changes caused by recurrent changes of the orbit of the Moon and other phenomena.

Mechanism 2 – with the important exception of earthquakes and tsunamis - typically operates over long (geological) time scales and is not significant on human time scales. It may relate to variations in the seafloor spreading rate, causing volume changes in mid-ocean mountain ridges, and to the slowly changing configuration of land and oceans. Another effect may be the slow rise of basins due to isostatic offloading by deglaciation after an ice age. The floor of the Baltic Sea and the Hudson Bay are

presently rising, causing a slow net transfer of water from these basins into the adjoining oceans. Slow changes of excessively big glaciers (ice sheets) and movements in the mantle will affect the gravity field and thereby the vertical position of the ocean surface. Any increase of the total water mass as well as sediment deposition into oceans increase the load on their bottom, generating sinking by viscoelastic flow in the mantle below. The mantle flow is directed towards the surrounding land areas, which will rise, thereby partly compensating for the initial sea level increase induced by the increased water mass in the ocean.

Mechanism 3 (temperature-driven expansion) only affects the uppermost part of the oceans on human time scales. Usually, temperature-driven changes in density are more important than salinity-driven changes. Seawater is characterised by a relatively small coefficient of expansion, but the effect should however not be overlooked, especially when interpreting satellite altimetry data. Temperature-driven expansion of a column of seawater will not affect the total mass of water within the column considered and will therefore not affect the potential at the top of the water column. Temperature-driven ocean water expansion will therefore not in itself lead to any lateral displacement of water, but only locally lift the ocean surface. Near the coast, where people are living, the depth of water approaches zero, so no measurable temperature-driven expansion will take place here (Mörner 2015). Mechanism 3 is for that reason not important for coastal regions.

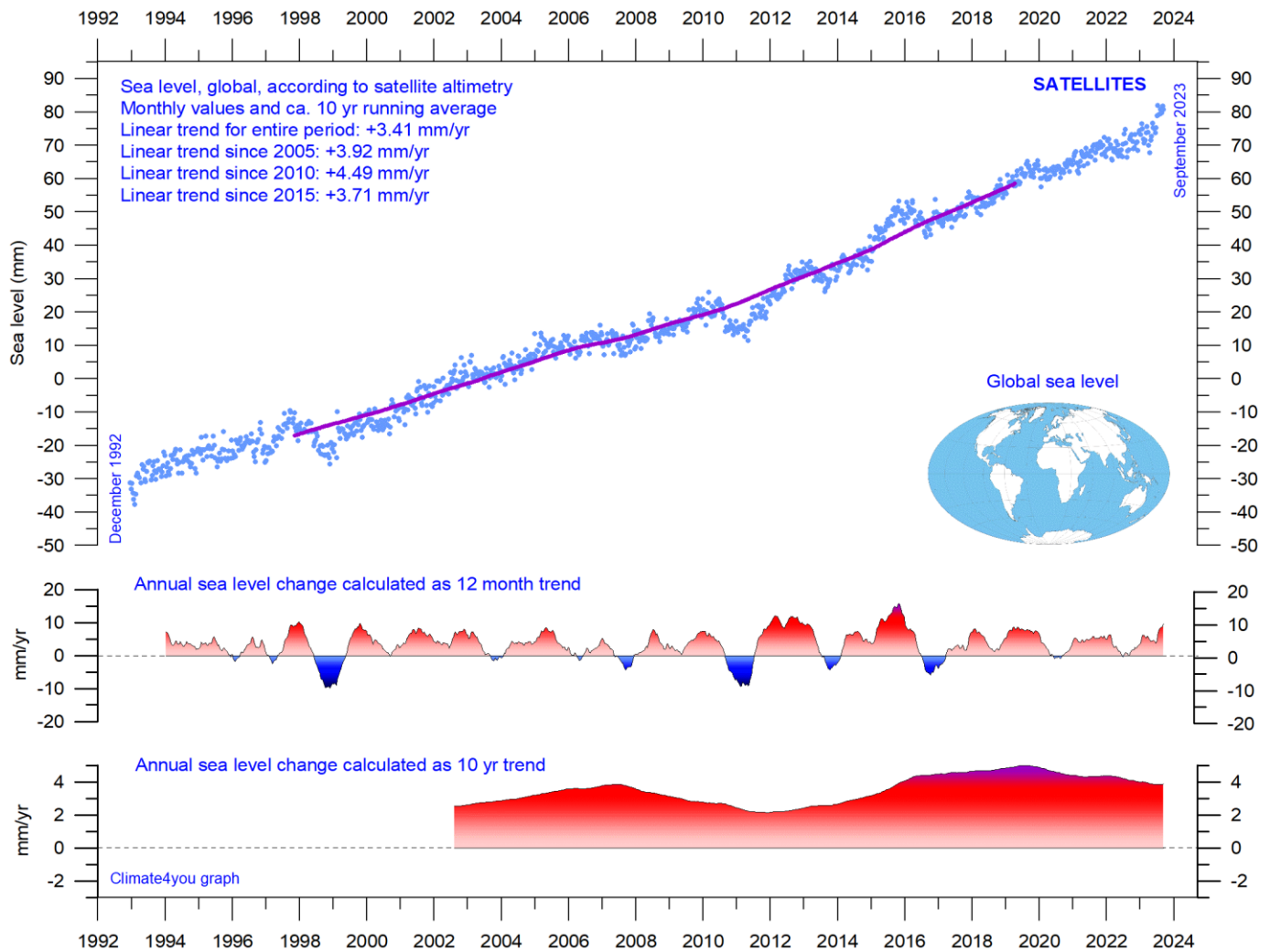
Mechanism 4 (changes in glacier mass balance) is an important driver for global sea-level changes along coasts, for human time scales. Volume changes of floating glaciers – ice shelves – has no influence on the global sea-level, just like volume changes of floating sea ice has no influence. Only the mass-balance of grounded or land-based glaciers is important for the global sea-level along coasts.

Summing up: Presumably, mechanism 1 and 4 are the most important for understanding sea-level changes along coasts.

References:

- Carter R.M., de Lange W., Hansen, J.M., Humlum O., Idso C., Kear, D., Legates, D., Mörner, N.A., Ollier C., Singer F. & Soon W. 2014. Commentary and Analysis on the Whitehead& Associates 2014 NSW Sea-Level Report. Policy Brief, NIPCC, 24. September 2014, 44 pp. <http://climatechangereconsidered.org/wp-content/uploads/2014/09/NIPCC-Report-on-NSW-Coastal-SL-9z-corrected.pdf>
- Hansen, J.-M., Aagaard, T. and Binderup, M. 2011. Absolute sea levels and isostatic changes of the eastern North Sea to central Baltic region during the last 900 years. *Boreas*, 10.1111/j.1502-3885.2011.00229.x. ISSN 0300–9483.
- Hansen, J.-M., Aagaard, T. and Huijpers, A. 2015. Sea-Level Forcing by Synchronization of 56- and 74-Year Oscillations with the Moon's Nodal Tide on the Northwest European Shelf (Eastern North Sea to Central Baltic Sea). *Journ. Coastal Research*, 16 pp.
- Mörner, Nils-Axel 2015. Sea Level Changes as recorded in nature itself. *Journal of Engineering Research and Applications*, Vol.5, 1, 124-129.

Global sea level from satellite altimetry, updated to September 2023



Global sea level since December 1992 according to the Colorado Center for Astrodynamics Research at University of Colorado at Boulder. The blue dots are the individual observations, and the purple line represents the running 121-month (ca. 10 year) average. The two lower panels show the annual sea level change, calculated for 1 and 10-year time windows, respectively. These values are plotted at the end of the interval considered. Compare with tide-gauge diagram on page 41.

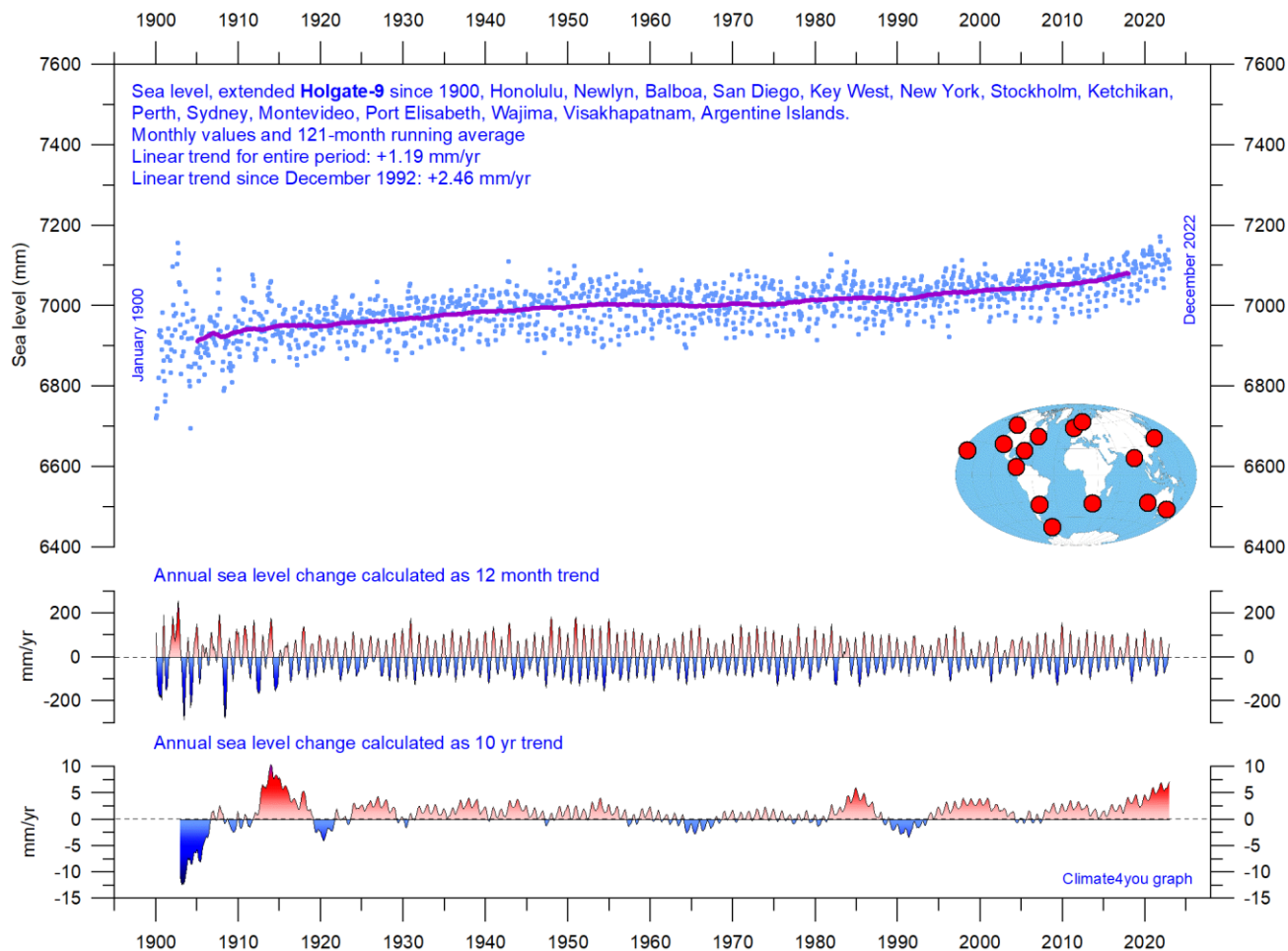
Ground truth is a term used in various fields to refer to information provided by direct observation as opposed to information provided by inference, such as, e.g., by satellite observations.

In remote sensing using satellite observations, ground truth data refers to information collected on location. Ground truth allows the satellite data to be related to real features observed on the planet surface. The collection of ground truth data enables calibration of remote-sensing data, and

aids in the interpretation and analysis of what is being sensed or recorded by satellites. Ground truth sites allow the remote sensor operator to correct and improve the interpretation of satellite data.

For satellite observations on sea level ground true data are provided by the classical tide gauges (example diagram on next page), that directly measures the local sea level many places distributed along the coastlines on the surface of the planet.

Global sea level from tide-gauges, extended Holgate-9, updated to December 2022



Extended Holgate-9 monthly tide-gauge data from PSMSL Data Explorer. Holgate (2007) suggested 9 stations to capture the global variability found in a larger number of stations over the last half century studied previously. However, some of the stations suggested by Holgate has not reported values for several years, leading to the southern hemisphere now being seriously underrepresented in his original data set. Therefore, in the above diagram several other long tide-gauge series have been included, to provide a more balanced representation of both hemispheres (15 stations in total). The blue dots are the individual average monthly observations, and the purple line represents the running 121-month (ca. 10 year) average. The two lower panels show the average annual sea level change, calculated for moving 1 and 10-year windows, respectively. These values are plotted at the end of the time window considered, month by month.

Data from tide-gauges all over the world suggest an average global sea-level rise of 1-2 mm/year, while the modern satellite-derived record (since 1992, page 40) suggest a rise of about 3.4 mm/year, or more. The difference between the two data sets is remarkable. It is however known that satellite observations are facing

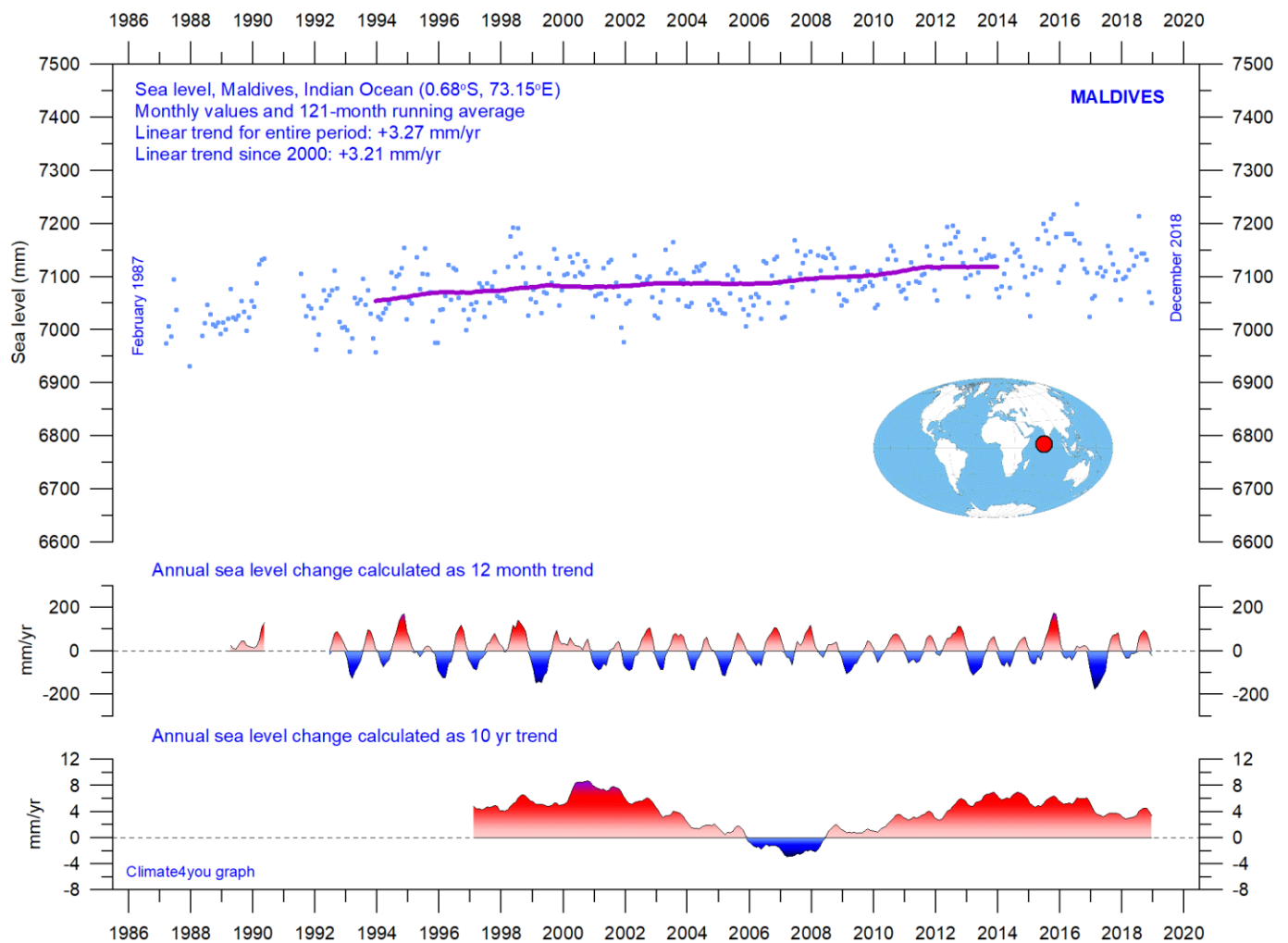
References:

Holgate, S.J. 2007. On the decadal rates of sea level change during the twentieth century. *Geophys. Res. Letters*, 34, L01602, doi:10.1029/2006GL028492

Vignudelli et al. 2019. Satellite Altimetry Measurements of Sea Level in the Coastal Zone. *Surveys in Geophysics*, Vol. 40, p. 1319–1349. <https://link.springer.com/article/10.1007/s10712-019-09569-1>

several complications in areas near the coast. Vignudelli et al. (2019) provide an updated overview of the current limitations of classical satellite altimetry in coastal regions. Since 2015 a sea level increase rate may be suggested by the above composite record.

This month's selected sea level station (tide-gauge) with long record, updated to December 2018



Maldives (Indian Ocean) monthly tide gauge data from [PSMSL Data Explorer](#). The blue dots are the individual monthly observations, and the purple line represents the running 121-month (ca. 10 yr) average. The two lower panels show the annual sea level change, calculated for 1 and 10 yr time windows, respectively. These values are plotted at the end of the interval considered. Last month shown: December 2022.

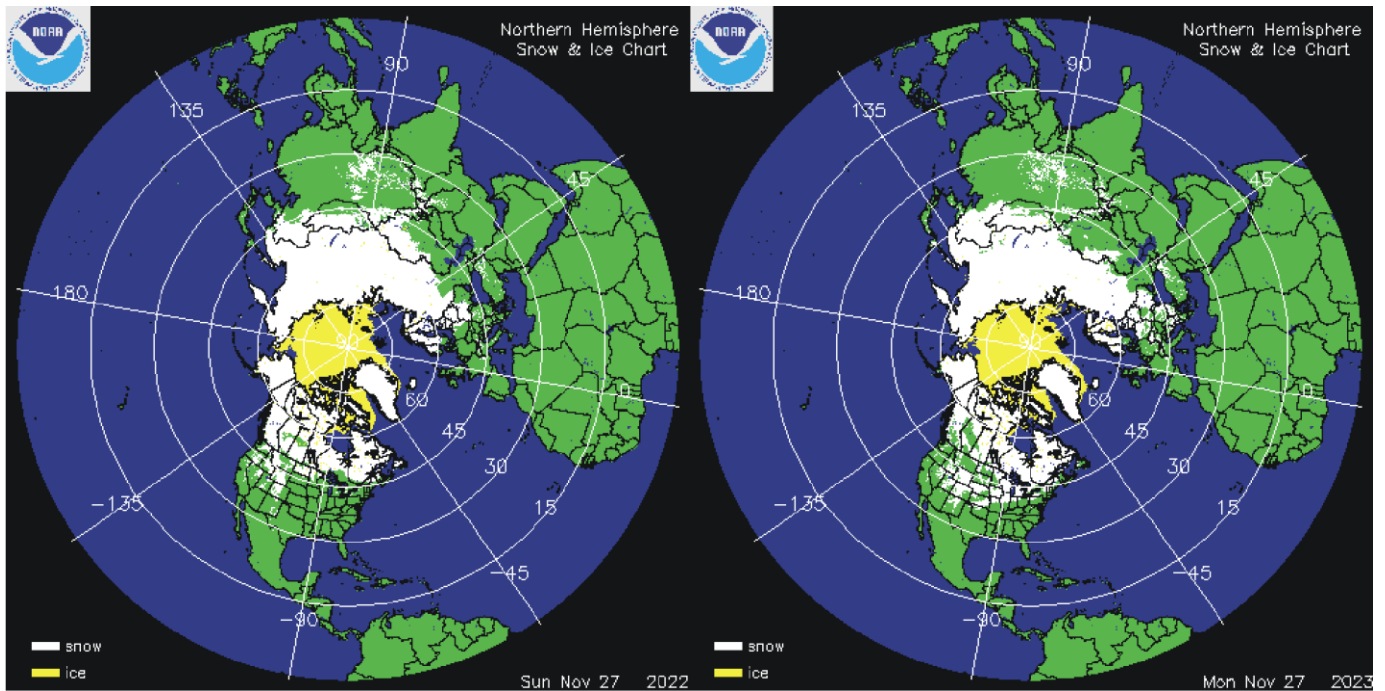
Maldives (the Republic of Maldives) is a small archipelagic island country in the northern part of the Indian Ocean.

The Maldives archipelago (coral islands) is located on a vast submarine mountain range. With an average ground-level elevation of 1.5 metres above sea level, Maldives is said to be the world's lowest-lying country, with its highest natural point being only 5.1 metres above sea level. This low maximum elevation is, however, not surprising considering the type of island (a coral island).

The UN's environmental panel has warned that, at current rates, sea-level rise would be high enough to make the Maldives uninhabitable by 2100.

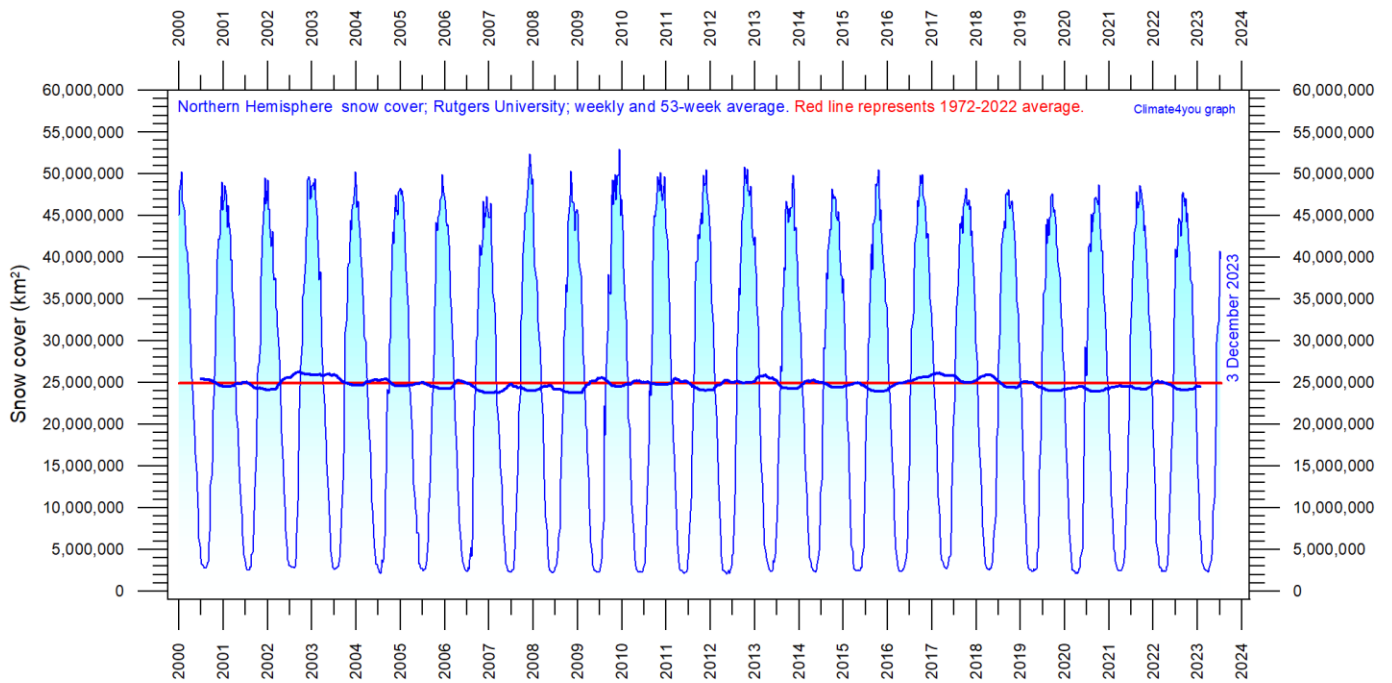
This dire forecast, however, appears not to be supported by observations; if the observed relative sea level rise at the Maldives since 1987 continues, relative sea level will have increased only about 26 cm by year 2100. Additional good news is that the observed relative sea level increase appears to be stable or slightly decelerating since year 2000.

Northern Hemisphere weekly and seasonal snow cover, updated to November 2023

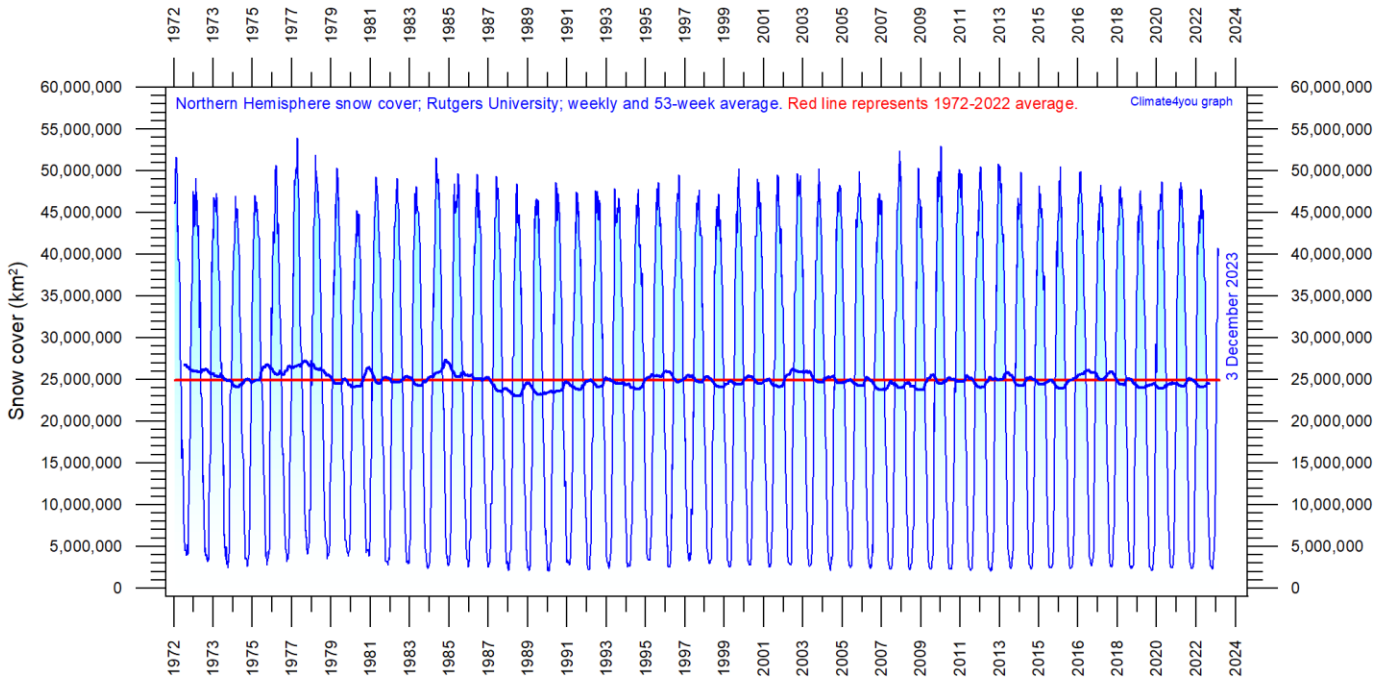


Northern hemisphere snow cover (white) and sea ice (yellow) 27 November 2022 (left) and 2023 (right). Map source: [National Ice Center \(NIC\)](#).

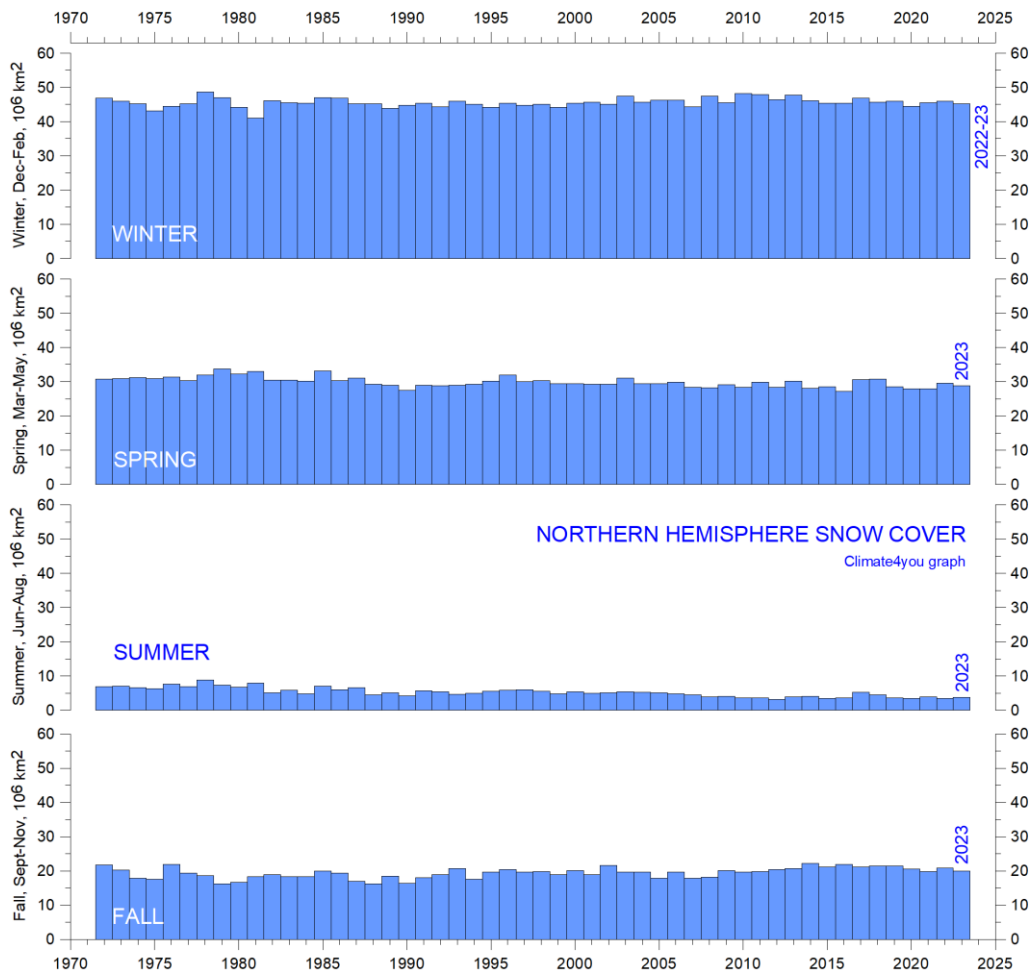
43



Northern hemisphere weekly snow cover since January 2000 according to Rutgers University Global Snow Laboratory. The thin blue line is the weekly data, and the thick blue line is the running 53-week average (approximately 1 year). The horizontal red line is the 1972-2022 average.



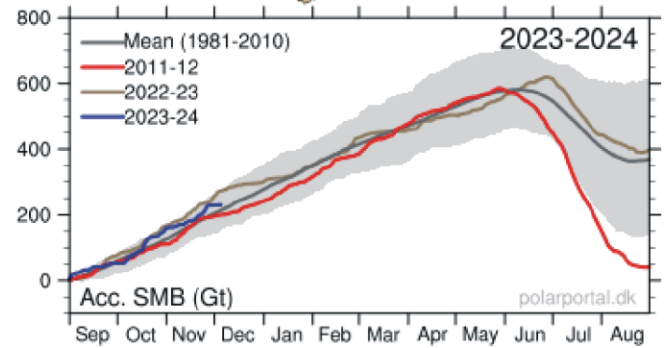
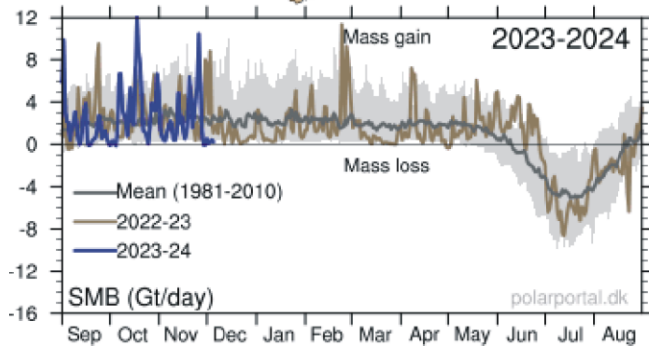
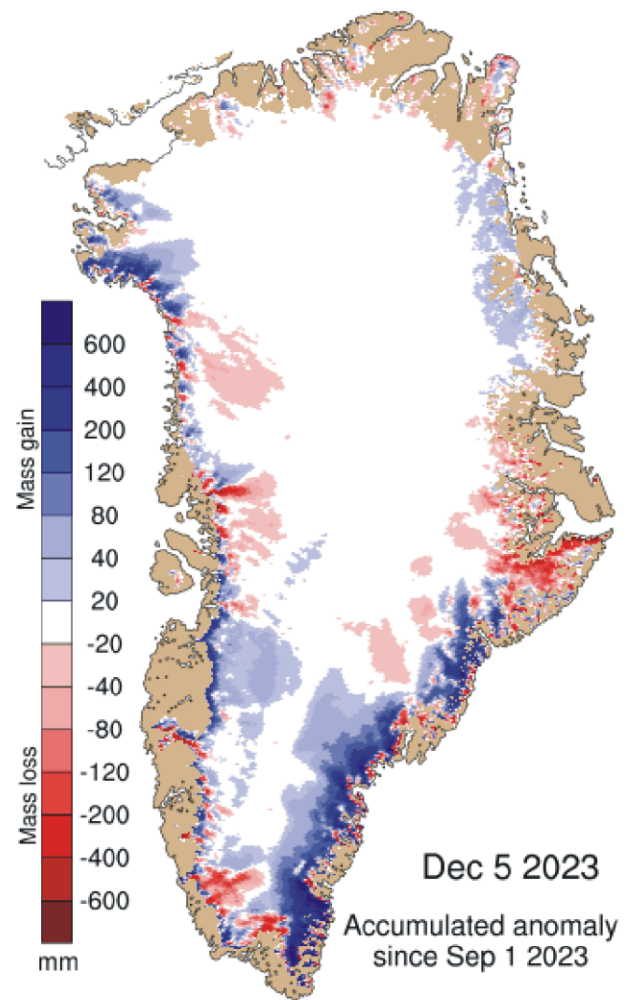
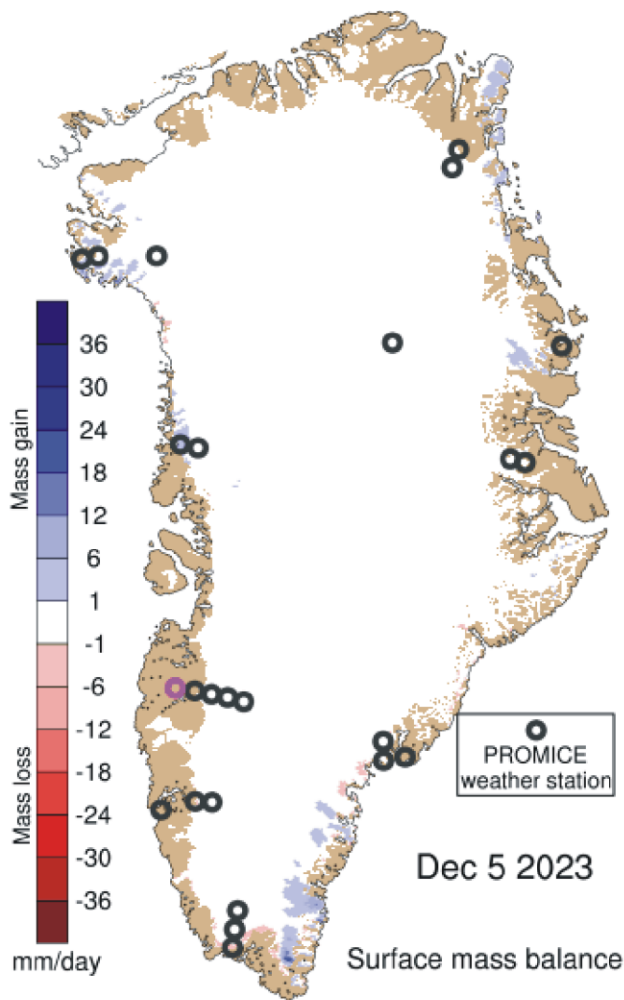
Northern hemisphere weekly snow cover since January 1972 according to Rutgers University Global Snow Laboratory. The thin blue line is the weekly data, and the thick blue line is the running 53-week average (approximately 1 year). The horizontal red line is the 1972-2022 average.



Northern hemisphere seasonal snow cover since January 1972 according to Rutgers University Global Snow Laboratory.

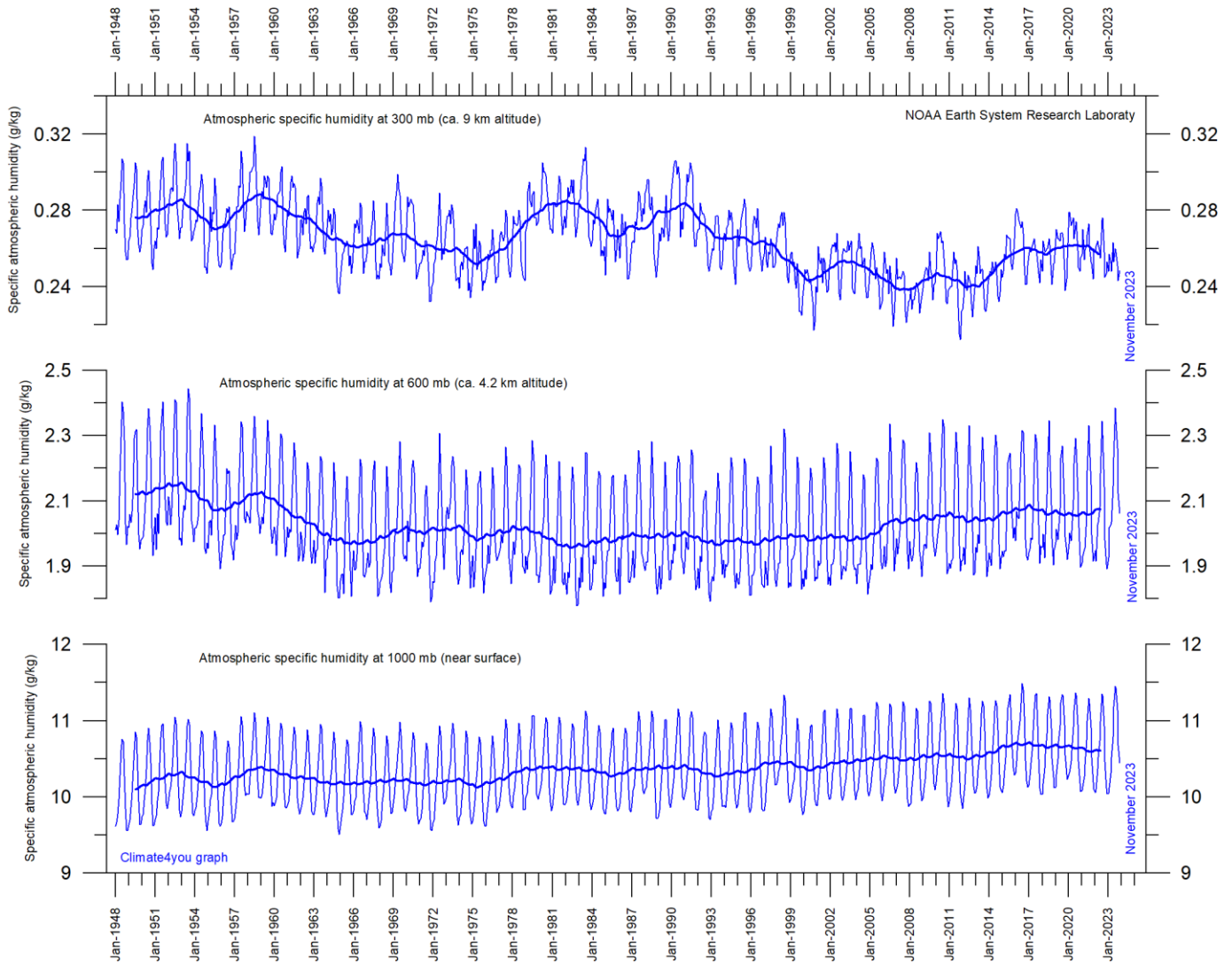
Greenland Ice Sheet net surface mass balance, updated to November 2023

45



Left: Surface mass balance 5 December 2023. Right: Net surface mass balance anomaly since September 1, 2023. Courtesy of Danish Meteorological Institute (DMI).

Atmospheric specific humidity, updated to November 2023



Specific atmospheric humidity (g/kg) at three different altitudes in the lower part of the atmosphere ([the Troposphere](#)) since January 1948 ([Kalnay et al. 1996](#)). The thin blue lines show monthly values, while the thick blue lines show the running 37-month average (about 3 years). Data source: [Earth System Research Laboratory \(NOAA\)](#).

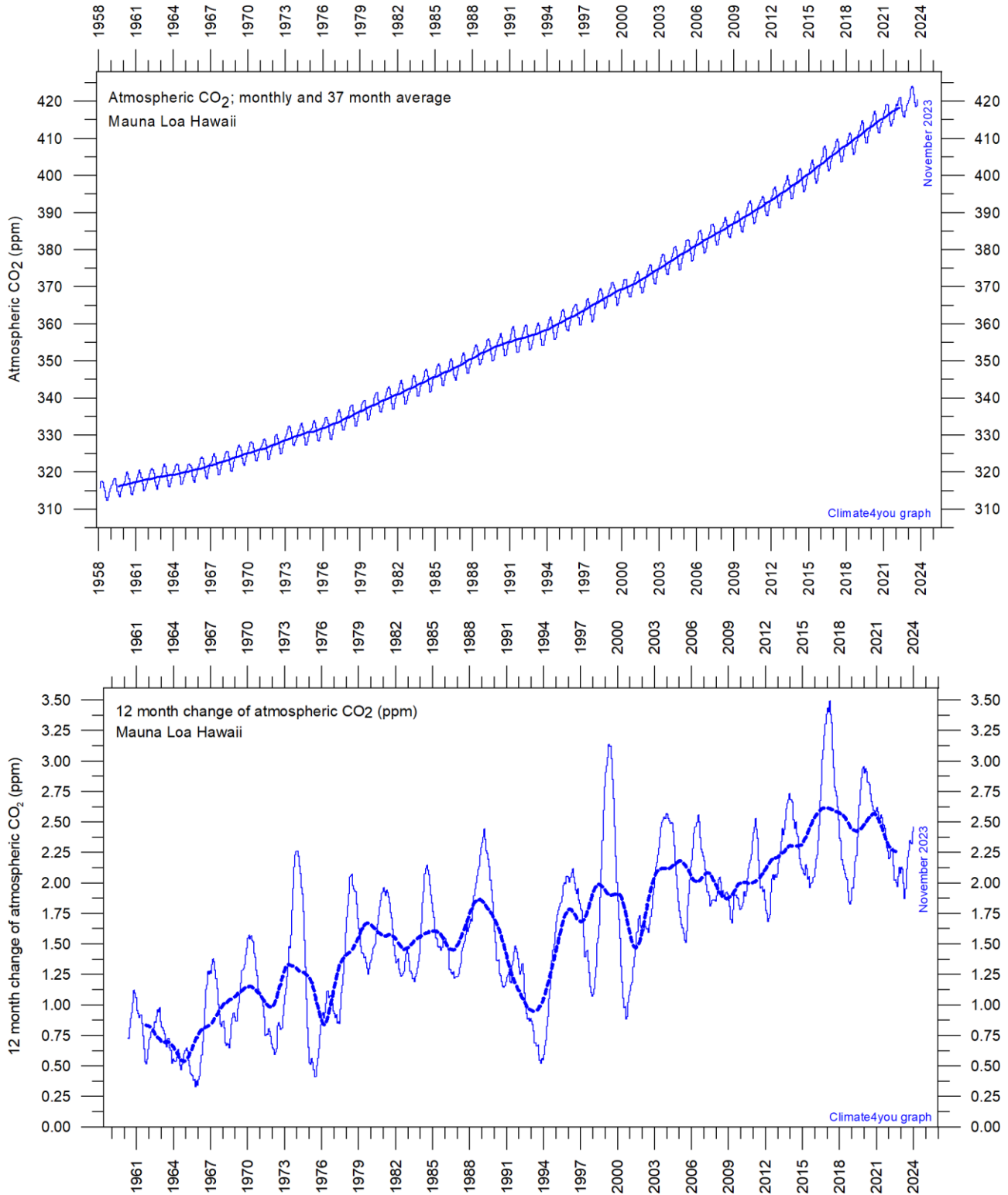
Water vapor is the most important greenhouse gas in the Troposphere. The highest concentration is found within a latitudinal range from 50°N to 60°S. The two polar regions of the Troposphere are comparatively dry.

The diagram above shows the specific atmospheric humidity to be stable or slightly increasing up to about 4-5 km altitude. At higher levels in the Troposphere (about 9 km), the specific humidity has been decreasing for the duration of the record (since 1948), but with shorter

variations superimposed on the falling trend. A Fourier frequency analysis (not shown here) shows these variations to be influenced especially by a periodic variation of about 3.7-year duration.

The persistent decrease in specific humidity at about 9 km altitude is particularly noteworthy, as this altitude roughly corresponds to the level where the theoretical temperature effect of increased atmospheric CO₂ is expected initially to play out.

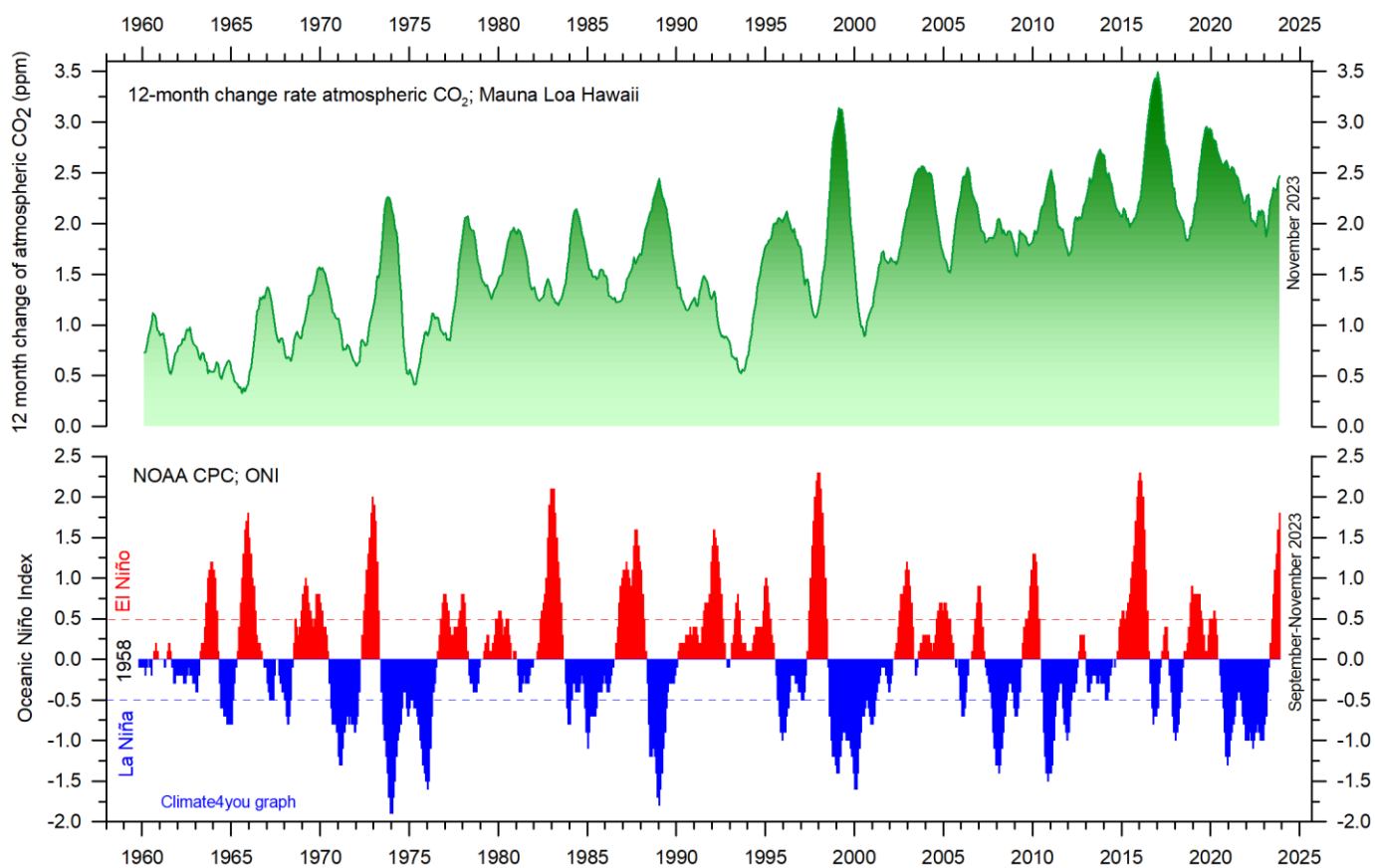
Atmospheric CO₂, updated to November 2023



47

Monthly amount of atmospheric CO₂ (upper diagram) and annual growth rate (lower diagram); average last 12 months minus average preceding 12 months, thin line) of atmospheric CO₂ since 1959, according to data provided by the [Mauna Loa Observatory](#), Hawaii, USA. The thick, stippled line is the simple running 37-observation average, nearly corresponding to a running 3-year average. A Fourier frequency analysis (not shown here) shows the 12-month change of Tropospheric CO₂ to be influenced especially by periodic variations of 2.5- and 3.8-years' duration.

The relation between annual change of atmospheric CO₂ and La Niña and El Niño episodes, updated to November 2023



Visual association between annual growth rate of atmospheric CO₂ (upper panel) and Oceanic Niño Index (lower panel). See also diagrams on page 40 and 22, respectively.

Changes in the global atmospheric CO₂ is seen to vary roughly in concert with changes in the Oceanic Niño Index. The typical sequence of events is that changes in the global atmospheric CO₂ to a certain degree follows changes in the Oceanic Niño Index, but clearly not in all details. Many processes, natural as well as anthropogenic, controls the amount of atmospheric CO₂, but oceanographic processes are clearly particularly important (see also diagram on next page).

Atmospheric CO₂ and the present coronavirus pandemic

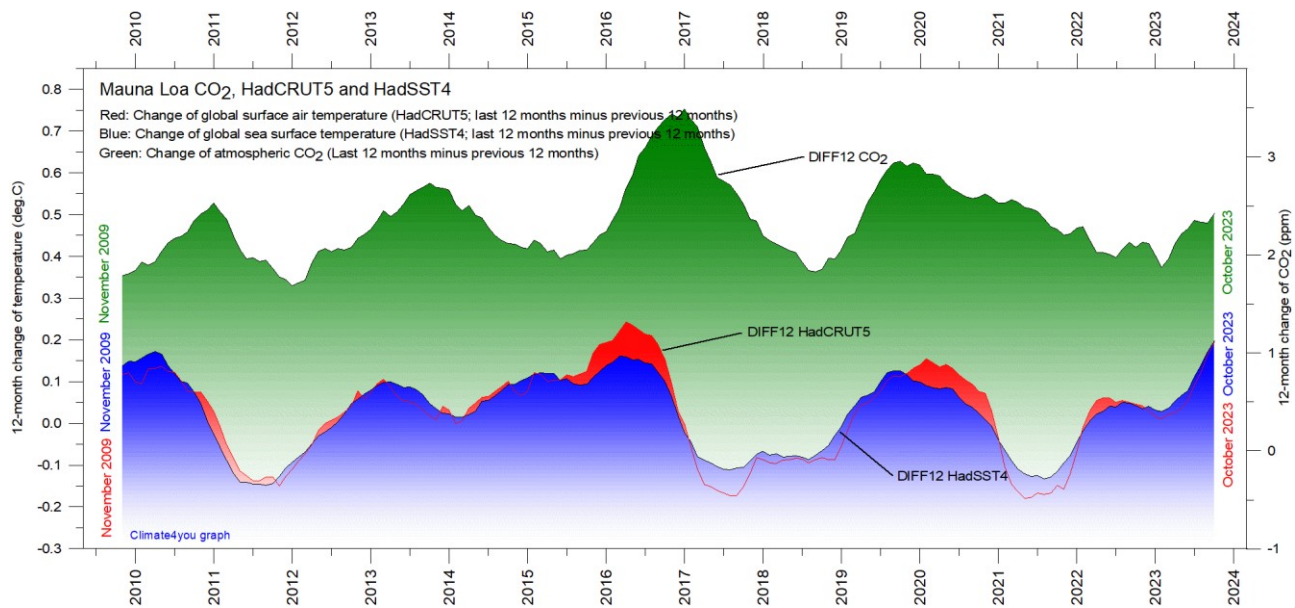
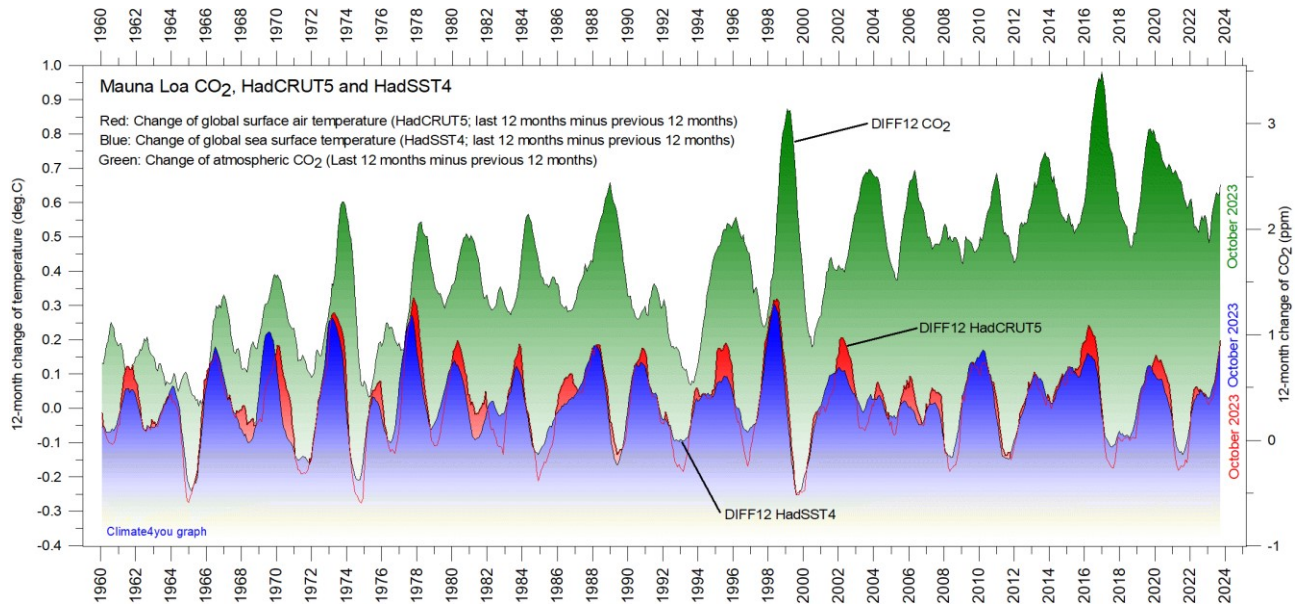
Modern political initiatives usually assume the human influence (mainly the burning of fossil fuels) to represent

the core reason for the observed increase in atmospheric CO₂ since 1958 (diagrams on page 44).

The coronavirus pandemic since January 2020 resulted in a marked reduction in the global consumption of fossil fuels. It is therefore enlightening to follow the effect of this reduction on the amount of atmospheric CO₂.

However, there is still no clear effect to be seen of the above reduction in release of CO₂ from fossil fuels. Presumably, the main explanation for this is that the human contribution is too small compared to the numerous natural sources and sinks for atmospheric CO₂ to appear in diagrams showing the amount of atmospheric CO₂ (see, e.g., diagrams on p. 47-49).

The phase relation between atmospheric CO₂ and global temperature, updated to October 2023



12-month change of global atmospheric CO₂ concentration ([Mauna Loa](#); green), global sea surface temperature ([HadSST4](#); blue) and global surface air temperature ([HadCRUT5](#); red dotted). Entire data series since 1958 in upper figure, and last 15 years in lower figure, to enhance modern dynamics. All graphs are showing monthly values of DIFF12, the difference between the average of the last 12 months and the average for the previous 12 months for each data series.

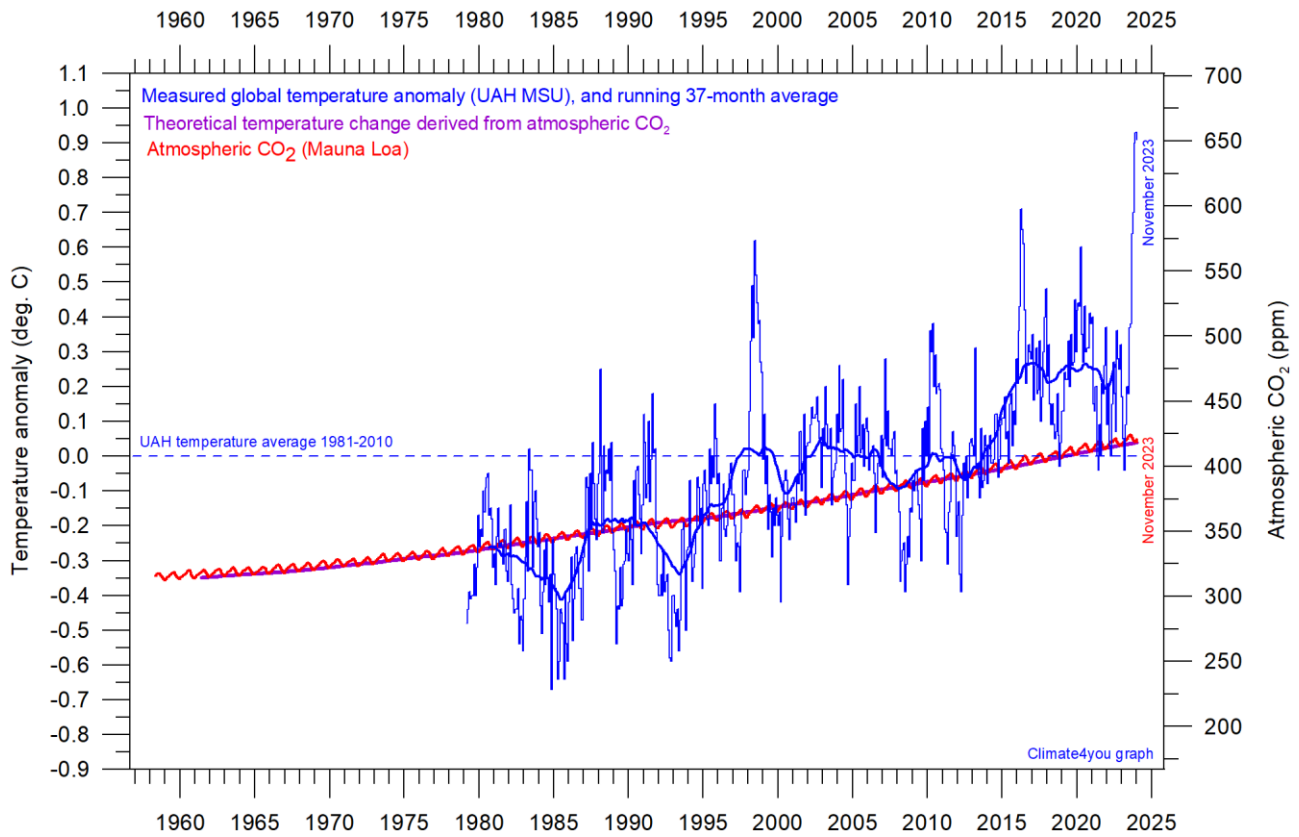
The typical sequence of events is seen to be that changes in the global atmospheric CO₂ follow changes in global surface air temperature, which again follow changes in global ocean surface temperatures. Thus, changes in global

atmospheric CO₂ usually are lagging 9.5–10 months behind changes in global air surface temperature, and 11–12 months behind changes in global sea surface temperature.

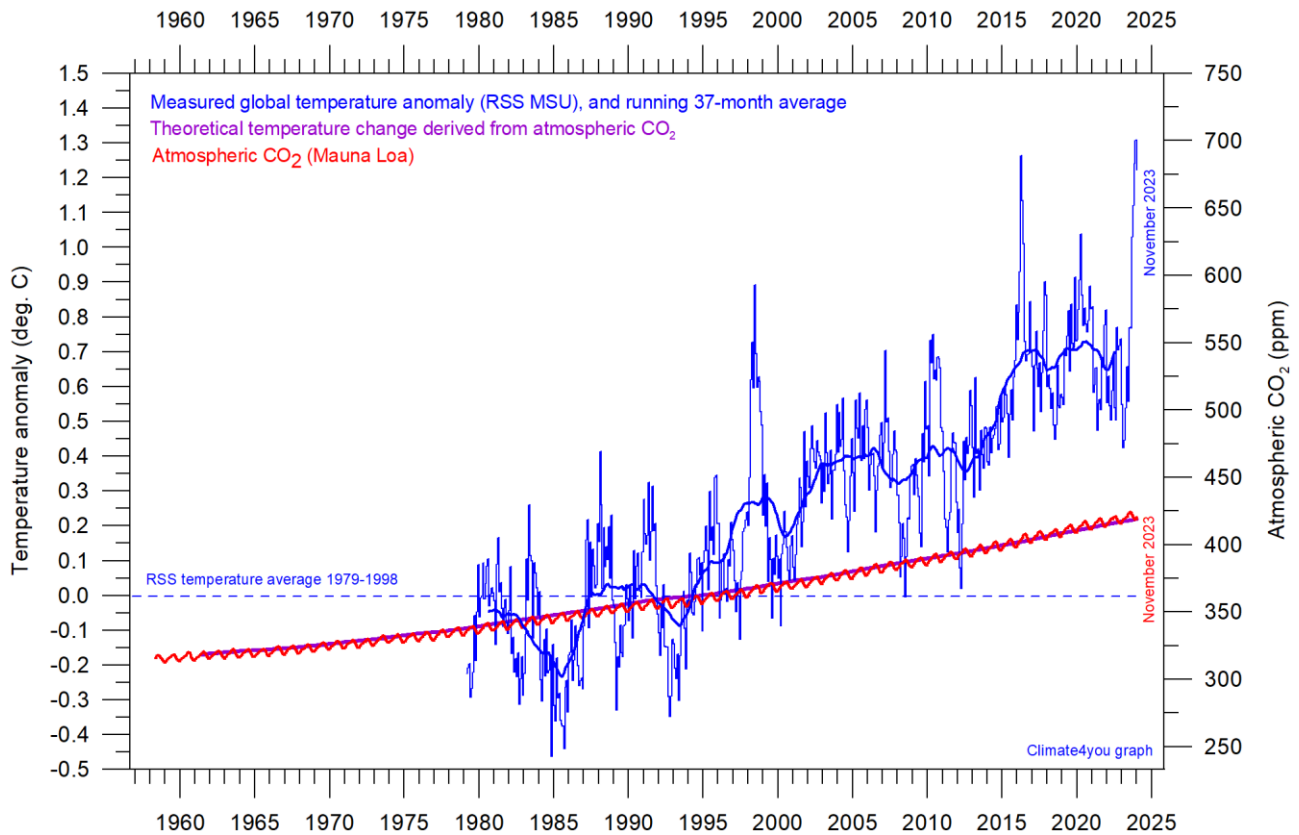
Reference: Humlum, O., Stordahl, K. and Solheim, J-E. 2012. The phase relation between atmospheric carbon dioxide and global temperature. *Global and Planetary Change*, August 30, 2012.

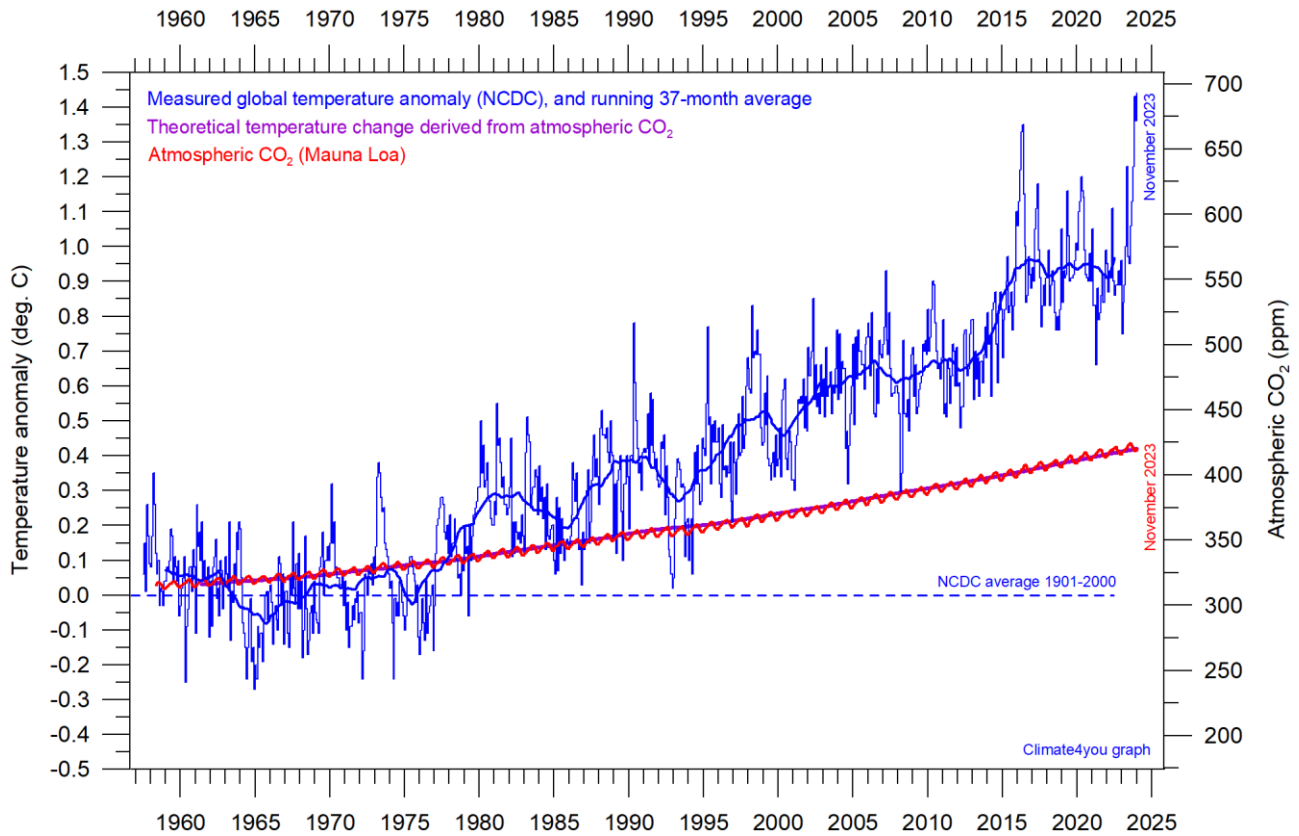
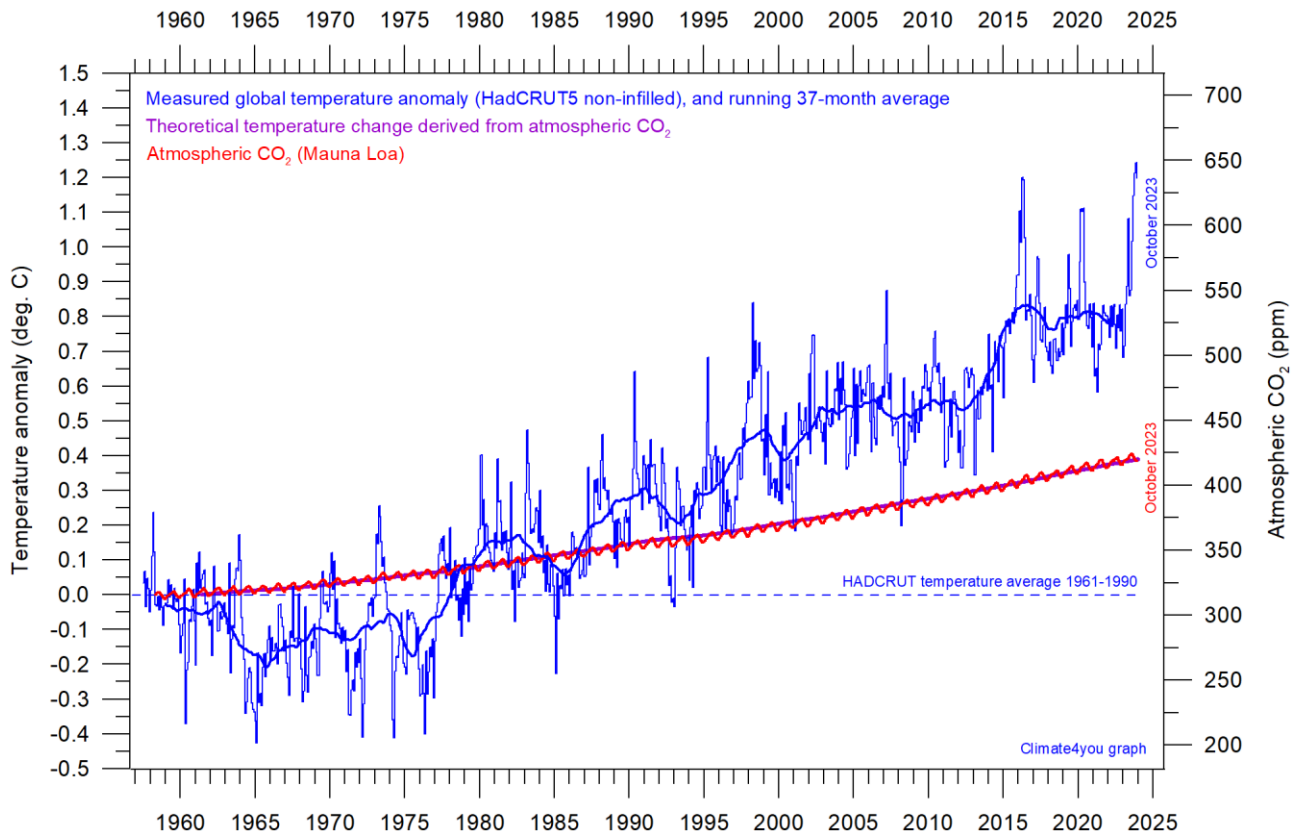
<http://www.sciencedirect.com/science/article/pii/S0921818112001658?v=s5>

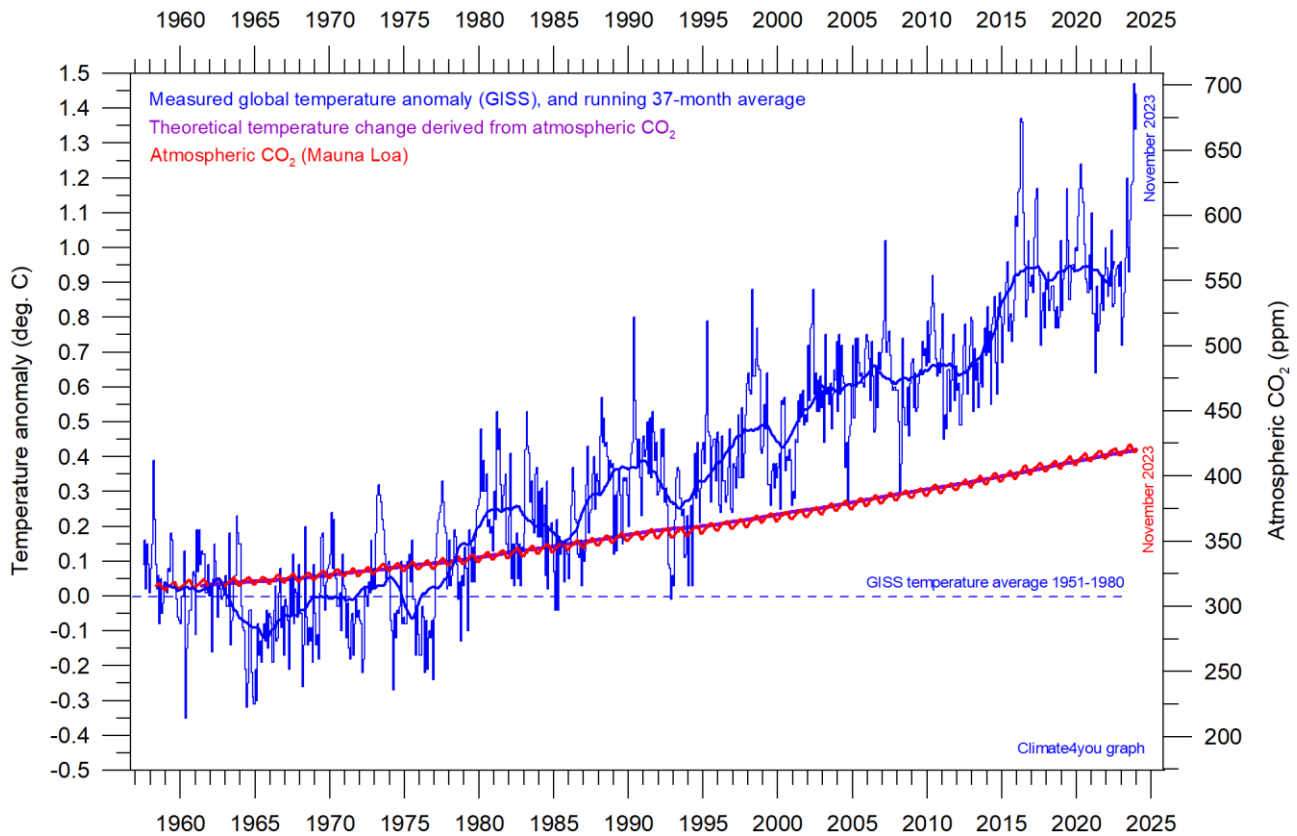
Global air temperature and atmospheric CO₂, updated to November 2023



50







Diagrams showing UAH, RSS, HadCRUT5, NCD and GISS monthly global air temperature estimates (blue) and the monthly atmospheric CO₂ content (red) according to the [Mauna Loa Observatory](#), Hawaii. Purple line (running along red CO₂ curve) shows theoretical temperature change due to changing atmospheric CO₂. The Mauna Loa data series begins in March 1958, and 1958 was therefore chosen as starting year for all diagrams above. Reconstructions of past atmospheric CO₂ concentrations (before 1958) are not incorporated in this diagram, as such past CO₂ values are derived by other means (ice cores, stomata, or older measurements using different methodology), and therefore are not directly comparable with direct atmospheric measurements.

It is generally agreed that, from a theoretical point of view, the temperature effect ΔT of increasing atmospheric CO₂ may be expressed as (see, e.g. Myhre et al. 1998 and IPCC Third Assessment Report, section 6.1):

$$\Delta T = \Delta F * \lambda$$

where $\Delta F = 5,35 \ln(C1/Co)$ W/m², and where Co and C1 indicates the concentration of atmospheric CO₂ at the beginning and end of the time interval considered. The factor λ is a so-called climate sensitivity parameter (expressing the global mean surface temperature response to the imposed radiative CO₂ forcing). This factor has been determined to about 0,26°CW⁻¹m². The relation shows that as the concentration of atmospheric CO₂ increases, its

theoretical greenhouse effect increases in a logarithmic fashion, not linear. Therefore, for each increase in CO₂ concentration, the effect on temperature is smaller and smaller.

If all other effects in the real world are ignored, the above relation shows that any doubling of atmospheric CO₂ concentration produces a temperature increase of nearly 1°C (0.96°C), no matter how high the initial concentration of CO₂.

The purple line in the above diagrams (p.50-52) is calculated using the observed concentration of atmospheric CO₂ since March 1958. The axis for CO₂ is adjusted to show overlap between CO₂ (red) and the

calculated accumulated temperature effect (purple). In all graphs, the temperature anomaly axis has been adjusted to position the initial calculated effect of CO₂ roughly at the average for the beginning of the observed temperature graph (blue). This is done to make it possible to compare the theoretical CO₂ temperature development (purple) with the observed development (blue).

All these diagrams show the observed temperature development to be much more complicated than the theoretical development from atmospheric CO₂ alone. With exception of the UAH diagram, the overall observed temperature increases since 1958 is much larger than calculated from CO₂ alone. In addition, the observed temperature development is characterised by recurrent intervals characterised by increasing and decreasing temperatures, respectively, a development extremely different from the calculated temperature (purple graph). Clearly many other factors than only CO₂ is in control of the real-world atmospheric temperature.

In contrast to this real-world observation, climate models are programmed to give the greenhouse gas carbon dioxide CO₂ a leading role on control on the global air temperature.

The fact that the observed real-world temperature has been changing much more than expected just from CO₂, is usually ascribed to an added greenhouse effect of atmospheric water vapour in the upper Troposphere, the concentration of which by the models is expected to increase along with CO₂ (see, e.g. Schneider et. al. 1999).

However, measurements of water vapour in the upper Troposphere apparently show this assumption to be mistaken (see, e.g., diagram on p.46). Therefore, the quite substantial difference between modelled and observed atmospheric temperature must be caused by other factors. In addition, the very dynamic change pattern displayed by the observed temperature also needs to be explained before a sound understanding of global climate dynamics can be claimed.

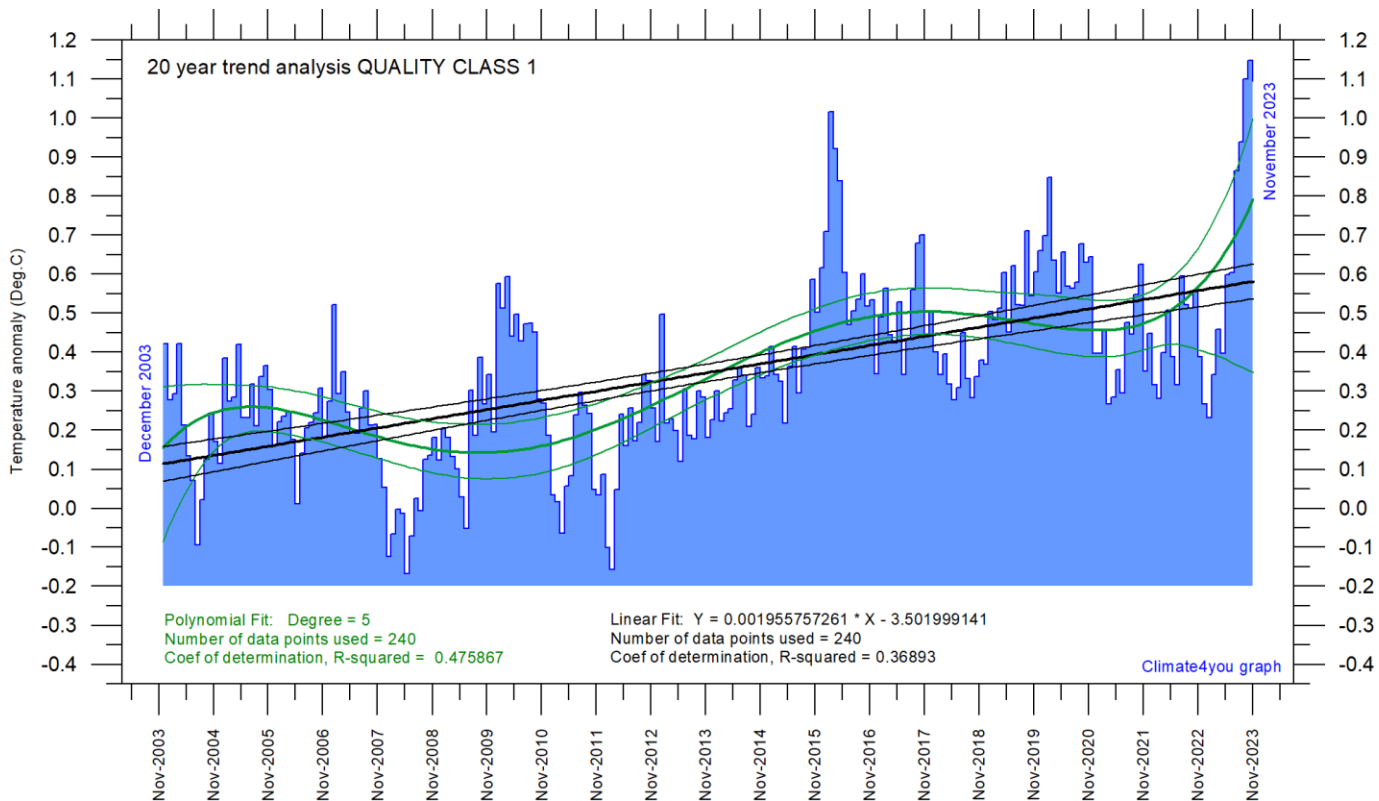
All temperature-CO₂ diagrams (p.50-52) shows both atmospheric temperature and atmospheric CO₂ to be increasing since 1959. However, this fact does not demonstrate that temperature is controlled by CO₂. In fact, it might just as well demonstrate the opposite relation (temperature controlling CO₂), or, that both temperature and CO₂ is controlled by a third factor.

Litterature:

Myhre, G., E. Highwood, K. Shine, and F. Stordal 1998. *New estimates of radiative forcing due to well mixed greenhouse gases*, Geophys. Res. Lett., 25(14), 2715–2718, doi:10.1029/98GL0190

Schneider, E.K., Kirtman, B.P., and Lindzen, R.S. 1999. *Tropospheric Water Vapor and Climate Sensitivity*. Journal of the Atmospheric Sciences, 56, 1649-1658.

Latest 20-year QC1 global monthly air temperature changes, updated to November 2023



Last 20 years' global monthly average air temperature according to Quality Class 1 (UAH and RSS; see p.6 and 9) global monthly temperature estimates. The thin blue line represents the monthly values. The thick black line is the linear fit, with 95% confidence intervals indicated by the two thin black lines. The thick green line represents a 5-degree polynomial fit, with 95% confidence intervals indicated by the two thin green lines. A few key statistics are given in the lower part of the diagram (please note that the linear trend is the monthly trend).

In the enduring scientific climate debate, the following question is often put forward: Is the surface air temperature still increasing or has it basically remained without significant changes during the last 15-16 years?

The diagram above may be useful in this context and demonstrates the differences between two often used statistical approaches to determine recent temperature trends. Please also note that such fits only attempt to describe the past, and usually have small, if any, predictive power.

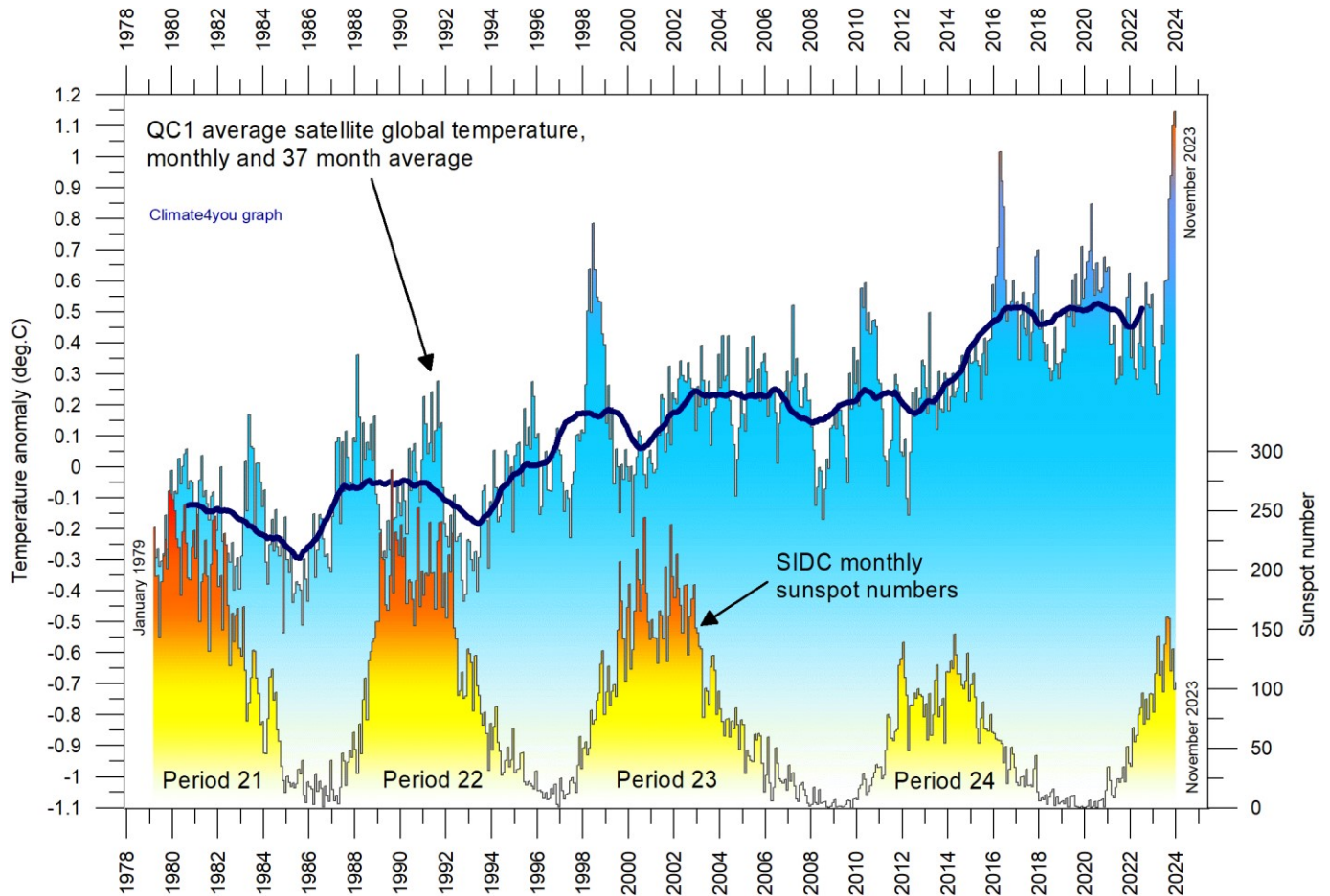
In addition, before using any linear trend (or other) analysis of time series a proper statistical model should be chosen, based on statistical justification.

For global temperature time series, there is no *a priori* physical reason why the long-term trend should be linear in time. In fact, climatic time series often have trends for which a straight line is not a good approximation, as is clearly demonstrated by several of the diagrams shown in the present report.

For an commendable description of problems often encountered by analyses of temperature time series analyses, please see [Keenan, D.J. 2014: Statistical Analyses of Surface Temperatures in the IPCC Fifth Assessment Report.](#)

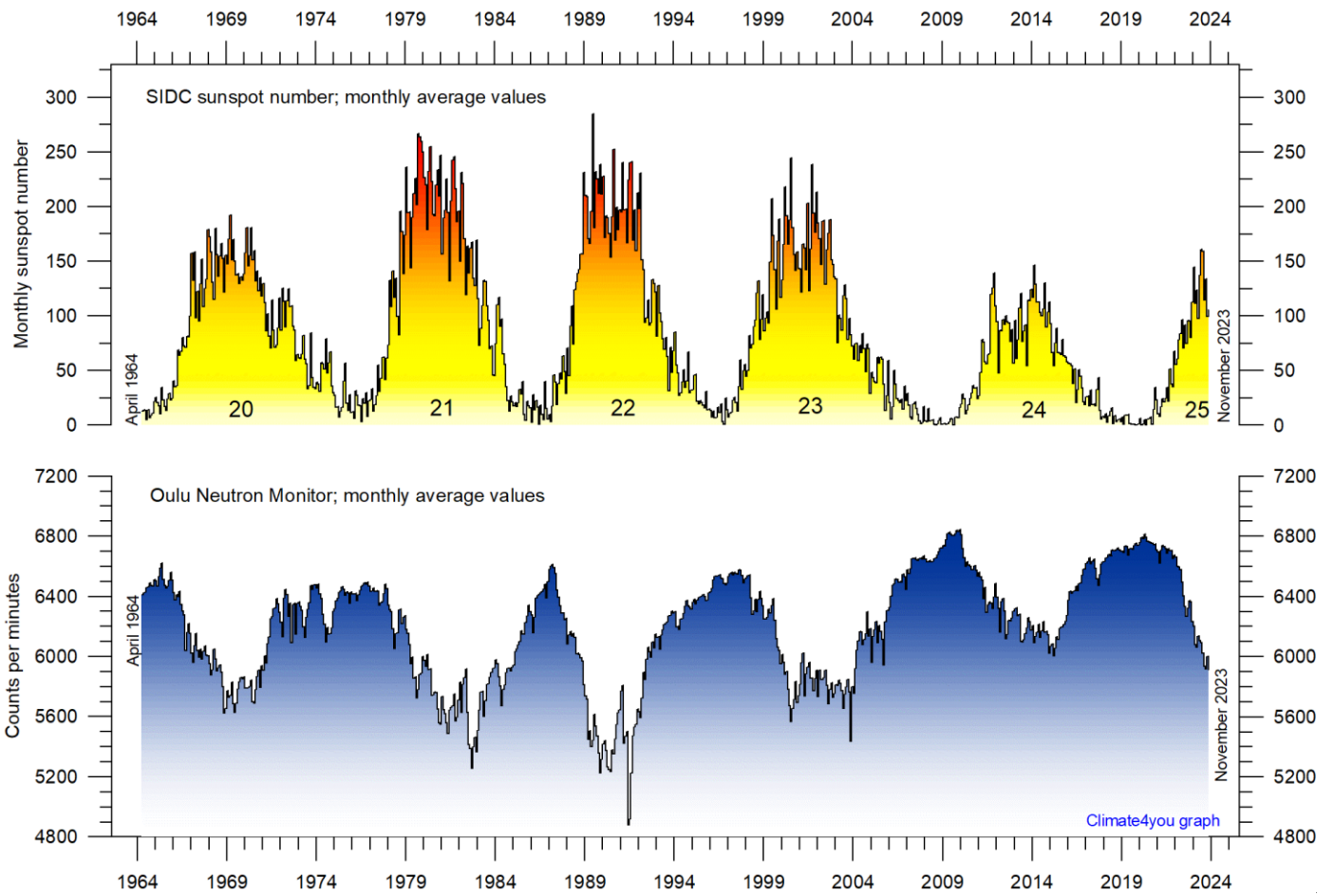
See also diagrams on page 12.

Sunspot activity (SIDC) and QC1 average satellite global air temperature, updated to November 2023



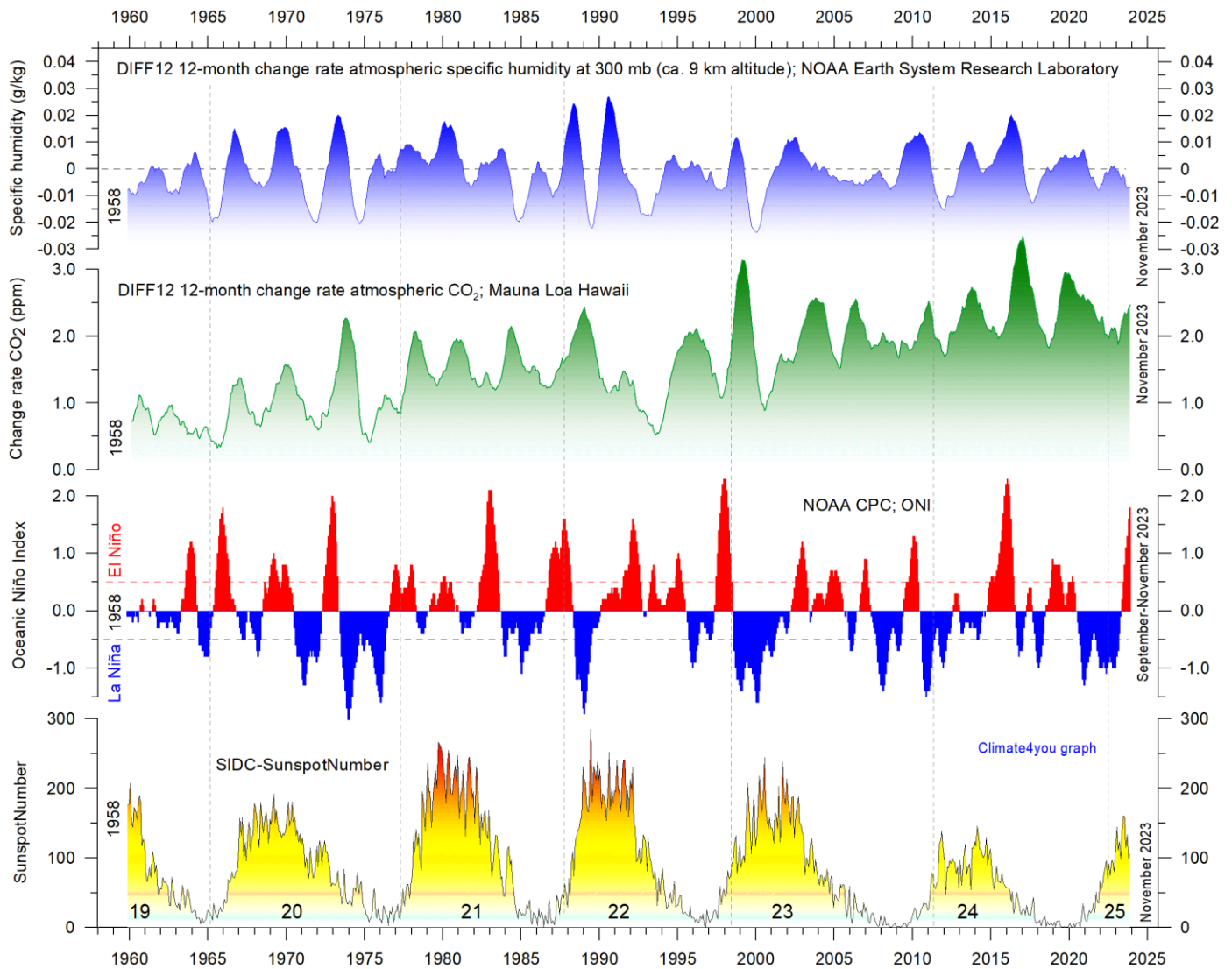
Variation of global monthly air temperature according to Quality Class 1 (UAH and RSS; see p.4) and observed sunspot number as provided by the Solar Influences Data Analysis Center (SIDC), since 1979. The thin lines represent the monthly values, while the thick line is the simple running 37-month average, nearly corresponding to a running 3-year average. The asymmetrical temperature 'bump' around 1998 is influenced by the oceanographic El Niño phenomenon in 1998, as is the case also for 2015-16. Temperatures in year 2019-20 was influenced by a moderate El Niño. In summer 2023 a new El Niño episode has begun (see diagram on p.25).

Monthly sunspot activity (SIDC) and average neutron counts (Oulu, Finland), updated to November 2023



Observed monthly sunspot number (Solar Influences Data Analysis Center (SIDC) since April 1964, and (lower panel) monthly average counts of the Oulu (Finland) neutron monitor, adjusted for barometric pressure and efficiency.

Monthly sunspot activity (SIDC), Oceanic Niño Index (ONI), and change rates of atmospheric CO2 and specific humidity, updated to November 2023

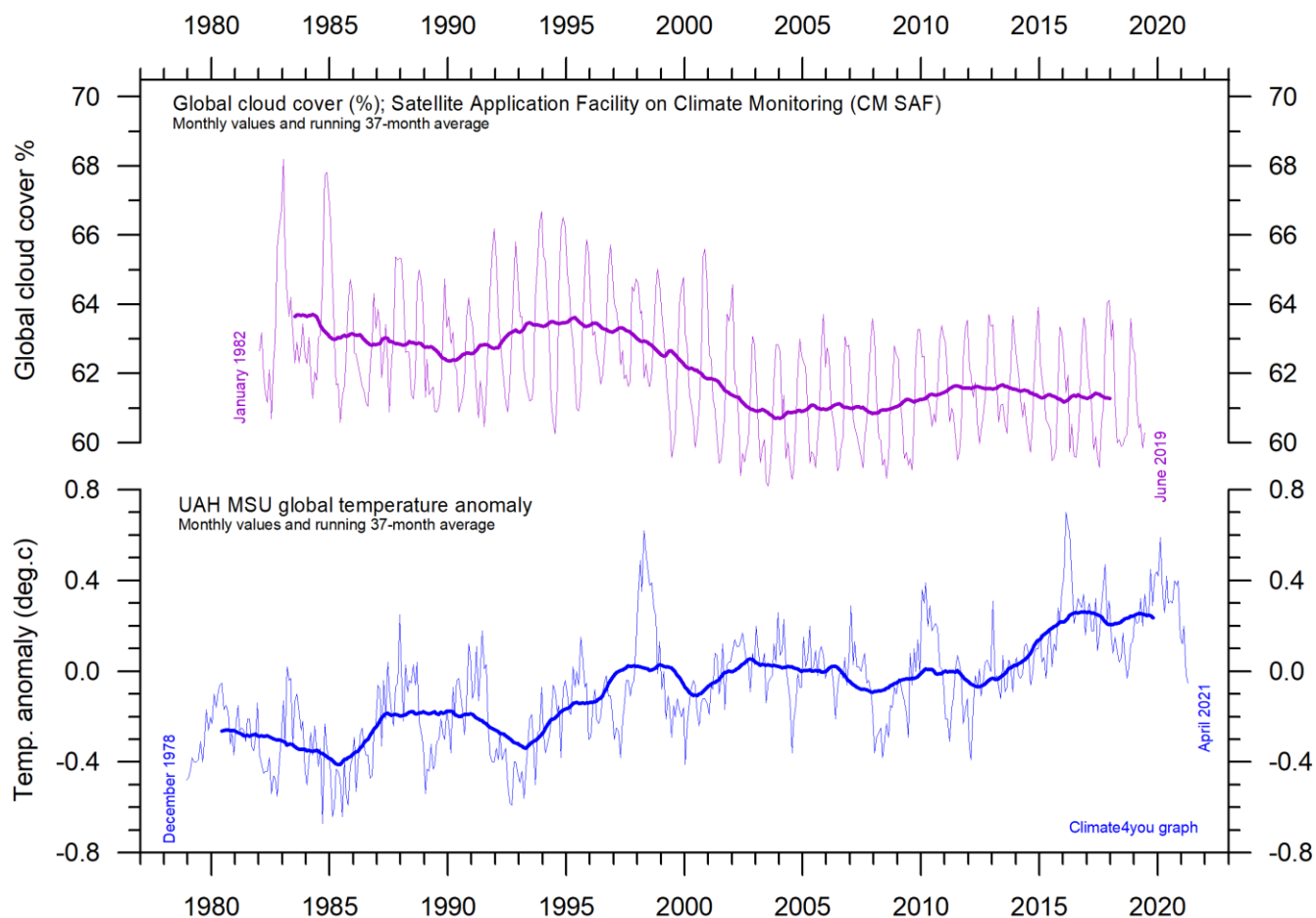


57

Visual association since 1958 between (from bottom to top) Sunspot Number, Oceanic Niño Index (ONI) and annual change rate of atmospheric CO₂ and specific humidity at 300 mb (ca. 9 km altitude). Upper two panels: Annual (12 month) change rate of atmospheric CO₂ and specific humidity at 300 mb since 1959, calculated as the average amount of atmospheric CO₂/humidity during the last 12 months, minus the average for the preceding 12 months (see also diagrams on page 43+44). Niño index panel: Warm (>+0.5°C) and cold (<0.5°C) episodes for the Oceanic Niño Index (ONI), defined as 3 month running mean of ERSSTv4 SST anomalies in the Niño 3.4 region (5°N-5°S, 120°-170°W)]. For historical purposes cold and warm episodes are defined when the threshold is met for a minimum of 5 consecutive over-lapping seasons. Anomalies are centred on 30-yr base periods updated every 5 years. Thin vertical stippled lines indicate the visually estimated timing of sunspot minima. The typically sequence following a sunspot minimum appears to be a warm El Niño episode followed by a cold La Niña episode. Effects on change rates of atmospheric CO₂ and atmospheric specific humidity are visually apparent, with ONI variations being followed by changes in first humidity, and then (last) by CO₂.

The above diagram is inspired by the Leamon et al. 2021 publication: Robert J. Leamon, Scott W. McIntosh, Daniel R. Marsh. Termination of Solar Cycles and Correlated Tropospheric Variability. Earth and Space Science, 2021; 8 (4) DOI: [10.1029/2020EA001223](https://doi.org/10.1029/2020EA001223)

Monthly lower troposphere temperature (UAH) and global cloud cover, updated to April 2021



Lower tropospheric air temperature and global cloud cover. Upper panel: Global cloud cover according to Satellite Application Facility on Climate Monitoring. Lower panel: Global monthly average lower troposphere temperature (thin line) since 1979 according to [University of Alabama at Huntsville, USA](#). The thick lines represent the simple running 37-month average. Reference period for UAH is 1991-2020.

Cloud cover data citation: Karlsson, Karl-Göran; Anttila, Kati; Trentmann, Jörg; Stengel, Martin; Solodovnik, Irina; Meirink, Jan Fokke; Devasthale, Abhay; Kothe, Steffen; Jääskeläinen, Emmihenna; Sedlar, Joseph; Benas, Nikos; van Zadelhoff, Gerd-Jan; Stein, Diana; Finkensieper, Stephan; Håkansson, Nina; Hollmann, Rainer; Kaiser, Johannes; Werscheck, Martin (2020): CLARA-A2.1: CM SAF cCloud, Albedo and surface RAdiation dataset from AVHRR data - Edition 2.1, Satellite Application Facility on Climate Monitoring,

DOI:10.5676/EUM_SAF_CM/CLARA_AVHRR/V002_01, https://doi.org/10.5676/EUM_SAF_CM/CLARA_AVHRR/V002_01.

Climate and history; one example among many

1812: Napoleon's retreat from Moscow



Napoleon and his army retreating in western Russia early November 1812.

As Napoleon left Moscow on 20 October 1812, the actual armed forces at his disposal numbered no more than 95,000, and probably less. Marshal Kutuzov was still camping passively SW of Moscow, reinforcing his army to about 97,000 men. He was, however, still in no hurry to engage in regular warfare. So, while Napoleon was retreating west towards Smolensk along the Moscow Road, Kutuzov did not seriously attempt to cut across their line of retreat, even though he from a tactical point of view was excellently placed to do so.

The French retreat was slow, mainly due to lack of horsepower. The shortage of fodder had debilitated the horses, and they were growing too weak to pull the guns and wagons. Part of the problem was that Napoleon saw himself carrying out a tactical withdrawal rather than a true retreat. Therefore, not to lose face, he refused to abandon a proportion of their guns to liberate horses and thereby save time. This resolve would

later cost him dear. As well as slowing their progress, the choice of retreat route had a demoralising effect on the French troops, marching down a devastated road, seeing only abandoned equipment, human and animal corpses. Kutuzov was still following at a safe distance south of the French army, remaining resolutely opposed to any suggestions from his generals to make an offensive move by striking north.

The good news for the French was that the weather was superb. Apparently, the early snow in Moscow presumably only was a short-lived meteorological mishap. On 31 October, at Viazma, Napoleon therefore ridiculed those of his personal staff who had been attempting to scare him with unpleasant stories of the Russian winter. The weather remained fine during the first days of November 1812, until 3 November, which turned out to be the last warm day in western Russia this year.

During the night between 4 and 5 November the wind turned north, bringing with it a rapid drop in air temperature. On 6 November the French retreat was entering an utterly new phase. It began to snow, and in short time it lay half a meter thick on the ground. The drop in temperature had not been that great, probably not exceeding -10°C , but the French army was not used to or dressed for cold and windy weather. There was no such thing as a winter uniform, since in those days armies were not trained for or even supposed to fight during winter. Usually, they spend the time in peaceful winter quarters. The Russian cold also provided the last straw for many of the remaining French horses. The meteorological change early November 1812 quickly had a profound effect on the whole French army.

The French army reached Smolensk on 9 November. The wind was still northerly, and the air temperature was now down to -15°C . On 14

November it dropped even more to -28°C . Napoleon's army was now down to 35,000 soldiers. In concert with the reduction of the French Army General Kutuzov gained courage and launched a few attempts to cut across the French line of retreat, but without much success.

On 22 November Napoleon entered the town Tolochin (in today's Belarus), where he received intelligence that other Russian troops from north had occupied the city Minsk further to the west. Napoleon and the remaining parts of his Grande Armée were now surrounded deep into enemy country. However, Napoleon was far from beaten on the tactical level. He indicated preparations for an attack towards south, while his engineers constructed a bridge across the partly frozen river Berezina. By this the French Army escaped from the Russian encirclement 27-28 November, in westerly direction.



Retreat of the French army in western Russia, mid- and late November 1812. Oil paintings by Vereschagin

The following two days were probably the worst during the entire French retreat. When Napoleon on 30 November entered the town Pleshchenitse,

Dr. Louis Lagneau recorded an air temperature of -30°C . Many of the hungry French soldiers had serious frostbite, a high number were dying, and

the military organisation began to fall apart. However, on the Russian side conditions were not much better. During November the cold had reduced Kutuzov's army from 97,000 to only 27,000 soldiers. Under such circumstances there was no possibility for an organised attack on the remaining French troops. The winter conditions in November 1812 had reduced both armies to two groups of freezing and hungry men, slowly walking in westerly direction.

On the evening of 5 December, at Smorgonie, about 100 km NW of Minsk, Napoleon decided that it was time for him to go back to Paris and take control from there. He called together his marshals and apparently apologised for his mistake of having remained in Moscow for too long. He then set off into the night. The Imperial Mameluke, Roustam, later reported that the wine in Napoleon's carriage froze that night, causing the bottles to shatter. On 6 December the temperature fell even more, reaching -37.5°C according to Dr. Louis Lagneau.

For the French army this was the end. On 9 December the remains of the Grande Armée turned up at the gates of Vilnia. The city, however, could not be held with the forces available, and the retreat had to continue towards the campaign's starting point at the river Niemen. The weather continued bitterly cold, with daytime temperatures around -35°C . The French commander Murat realised that a defensive line along Niemen could not be held either. The French army therefore had to retreat all the way to first Königsberg, and later Danzig and Küstrin much longer to the west. Eventually, the

remnants of the French army were driven all the way back to Dresden, in today's Germany.

It was only when the French retreat finally came to a stop towards the end of January 1813 that the true scale of the disaster began to emerge. In June 1812 somewhere between 550,000 and 600,000 French and allied troops have been assembled along river Niemen. Only about 120,000 came out of Russia in December 1812, including all the substantial reinforcements received after the invasion was launched 22 June 1812. Presumably at least 400,000 French and allied troops died during the campaign, but less than 100,000 in battle. On the Russian side it has been estimated that up to 400,000 soldiers and militia died, about 110,000 of them in battle.

The extremely cold winter November-December 1812, in combination with the previous warm summer July-August 1812, had been devastating for the whole military operation on both French and Russian side and were to have lasting effects on Europe's political future.

The catastrophic outcome of the Russian campaign sealed Napoleon's fate. Not only did it cost him 300,000 of his best French soldiers, but it also destroyed the aura of superiority and being invincible that has been surrounding Napoleon's person. Few saw this more clearly than the German patriots in Prussia, who had been suffering under the humiliation of French dominion. On 28 February 1813 an alliance was concluded between Russia and Prussia, and two weeks later the latter declared war on France.

References cited:

Zamoyski, A. 2005. *1812 - Napoleon's Fatal March on Moscow*. Harper Perennial, London, 644 pp.

All diagrams in this report, along with any supplementary information, including links to data sources and previous issues of this newsletter, are freely available for download on www.climate4you.com

Season's Greetings, yours sincerely,

Ole Humlum (Ole.Humlum@gmail.com)

Arctic Historical Evaluation and Research Organisation, Longyearbyen, Svalbard

20 December 2023.

Planned publication of next newsletter: around 20 January 2024.